Ghent University
Faculty of Sciences

Linkage Engineering of Imine Covalent Organic Frameworks for Enhanced Adsorption Properties

Gilles Matthys

Dissertation to obtain the degree of
Doctor of Science: Chemistry
Academic year 2025–2026

Promotor	Affiliation
Prof. Dr. Pascal Van Der Voort	Ghent University

Chair	Affiliation
Prof. Dr. Laszlo Vincze	Ghent University

Members of the jury	Affiliation
Prof. Dr. Gijs Du Laing	Ghent University
Prof. Dr. Klaartje De Buyser	Ghent University
Dr. Roy Lavendomme	Université Libre de Bruxelles
Dr. Andreas Laemont	Ghent University
Dr. Maojun Deng	Ghent University

Ghent University
Faculty of Sciences

Department of Chemistry
Krijgslaan 281 Building S3, 9000 Gent, Belgium

This work was realized with the support of
FWO (Research Foundation Flanders)

Acknowledgements

When I began this PhD four years ago, I never imagined I would learn so much on both an academic and personal level. My journey into the vast world of COFs started as a learning experience, but it quickly became the defining part of my PhD. This interest was originally sparked during my master's degree, where I worked on CTFs and their applications in catalysis for CO_2 conversion, not knowing that this subject would shape the next 4 years of my life . Along this path, I had the privilege of meeting remarkable people who made the experience truly worthwhile.

First and foremost, I must thank my promoter and experienced guide, Prof. Pascal Van Der Voort. Thank you for believing in me, supporting me from the very beginning, and giving me the freedom to pursue the topics that interested me most. I am sincerely grateful for the opportunity to work in the COMOC lab and to grow as a researcher under your mentorship. I would also like to extend my gratitude to the members of the thesis committee for your time, effort, and the insightful feedback that helped improve this dissertation.

I have met so many people over the past few years, but I must first thank my (ex-)COMOC colleagues: Roy, Karen, Andreas, Geert, Yoran, Laurens, Chidharth, Himanshu, Diem, Eline, Parviz, Sara, Wafaa, Linyang, Maojun, Hui, Chunhui, Kobe, Tijs, Rundong, Zhongliang, Meng, Matteus, Tingting, Jiamin, Jeet, Ipsita, and Joanna.

I would like to highlight a few people from this list. Andreas: starting as your "mere" master's student (willingly or not), you showed me the ropes of the COF world while you were in the first year of your own PhD. After my master's, I joined as a PhD student, and we shared the majority of

this road together. I will always cherish our discussions, both the serious scientific ones and the unserious ones, inside and outside the lab. Roy: you are the most knowledgeable chemist I know. You had an answer for almost every question I asked. I truly enjoyed our (non-)scientific discussions and trying to solve the mysteries within COMOC together.

In the last two years, Diem and Eline joined the group. I really enjoyed our talks and the fact that you could convince me to join you for lunch outside the office. I hope I have contributed a little bit to the expansion of your knowledge in the research field, and I know for a fact that you will lead the lab to a prosperous future. I can convincingly say that all of you transitioned from being colleagues to being friends.

I must also thank the technical staff of our department; Kathleen, Pierre, Pat, Bram, Grim, and Katrien for always being the daily support system for everyone in the building.

Next, I would like to thank the friends I made during my chemistry degree: Emiel, Sigo, Chemiel, Vincent, Ruben, Daria, Ben, Laure, Lobke, Ellen, and Marre. I look forward to our future yearly trips, drinks, Secret Santas, and quizzes. I also want to thank Pieter and Emmeran from my short "physics era", we don't see each other often, but I appreciate it every time we meet. Also, the "gymbros": Gilles, Arthur, and Jerome certainly deserve a shout-out because you guys are motivational for me in every way of life.

I cannot forget to thank "ma boi" Thibaut, with whom I have shared many ups and downs in every aspect of life. Together with Maarten and Thijs, I enjoyed our yearly holidays and meetups, which gave me the space to disconnect from the PhD for a while.

Last but not least, I need to thank my parents (especially my mother) and family for their unwavering support throughout my whole life. Without them, none of this would have been possible.

Contents

Summary

Covalent organic frameworks (COFs), discovered in 2005, are crystalline porous materials that hold promise for many applications. Their inherent porosity and tunable adsorption properties make them up-and-coming candidates for environmental remediation and resource recovery. However, many current industrial methods for capturing specific pollutants or recovering precious metals rely on materials that are either prohibitively expensive or unsustainable. This thesis addresses this challenge by developing and applying tailor-made COFs for two demanding separation processes. We investigate their efficacy for the selective capture of radioactive iodine from nuclear gaseous waste and for the recovery of gold from electronic waste, aiming to provide more cost-effective and robust alternatives to current technologies.

In **chapter 1**, we introduce the fundamental principles of covalent organic frameworks (COFs), covering key aspects of their synthesis, including linker design, linkage chemistry, and topology. Special attention is given to post-synthetic modification strategies relevant to the scope of this thesis. The discussion then transitions to the application of COFs as versatile adsorbents, exploring their potential within the pressing challenges of environmental remediation and resource recovery. Specifically, the chapter examines the state-of-the-art for radioactive iodine capture from nuclear waste and gold recovery from electronic waste, highlighting the need for more efficient materials by reviewing current industrial and academic solutions. Finally, the chapter outlines the research objectives of this dissertation, which focus on enhancing the adsorptive performance of imine-based COFs through post-synthetic linkage modification, yielding

novel imidazopyridinium and thiazole-functionalized frameworks for the targeted applications.

Chapter 2 describes the development of a robust, cationic covalent organic framework for iodine capture, designed to overcome the chemical instability of traditional imine-linked COFs. We present a two-step, post-synthetic modification strategy to convert a crystalline picolinaldehyde-based imine COF into a stable imidazopyridinium-linked framework. This modification introduces permanent positive charges and halide counter-anions, creating powerful and specific binding sites for iodine. The resulting materials demonstrate exceptional performance, exhibiting ultra-fast adsorption kinetics and high gravimetric capacities (up to 4.66 $g\,g^{-1}$) for iodine vapor. Under industrially relevant dynamic conditions (150°C, 50% relative humidity), the framework shows an uptake of 21 wt%, outperforming the current industrial benchmark (silver-mordenite zeolites). Furthermore, the material proves highly effective in aqueous environments, removing 98% of triiodide from solution in one minute and purifying spiked seawater to natural background levels. Spectroscopic analysis reveals a synergistic capture mechanism involving strong halogen bonding and electrostatic interactions, confirming these materials as a highly versatile and effective platform for nuclear waste remediation and water purification.

In **chapter 3**, we present a simple post-synthetic conversion of 2 imine-linked covalent organic frameworks (COFs) to their thiazole-linked analogues, creating highly efficient adsorbents for gold recovery. This modification provides multiple benefits: it enhances chemical stability and recyclability, introduces sulfur binding sites to increase adsorption capacity, maintains high selectivity, and significantly improves the material's photophysical properties. Under dark conditions, the thiazole-linked TTT-TAPB-S COF achieved an exceptional gold adsorption capacity of 3533 $mg\,g^{-1}$. Moreover, leveraging the materials' enhanced photophysical properties, we demonstrated a significant light-induced enhancement of gold uptake. The thiazole-linked Tfpy-PDA-S COF reached a record-high

capacity of 7980 mg g^{-1} under irradiation. Both imine and thiazole COFs exhibited high selectivity and practical efficacy, removing up to 98% of gold from a complex CPU waste leachate, which validates their potential for sustainable resource recovery.

Finally, in **chapter 4**, we discuss the general conclusions of this work and give an outlook within the research field.

Samenvatting

Covalent organische roosters (COF's), ontdekt in 2005, zijn kristallijne poreuze materialen die veelbelovend zijn voor tal van toepassingen. Hun inherente porositeit en afstembare adsorptie-eigenschappen maken hen bijzonder veelbelovende kandidaten voor milieusanering en het terugwinnen van grondstoffen. Veel huidige industriële methoden voor het afvangen van specifieke vervuilende stoffen of het terugwinnen van edelmetalen zijn echter gebaseerd op materialen die ofwel onbetaalbaar duur ofwel niet-duurzaam zijn. Dit proefschrift pakt deze uitdaging aan door op maat gemaakte COF's te ontwikkelen en toe te passen voor twee veeleisende scheidingsprocessen. We onderzoeken hun doeltreffendheid voor de selectieve adsorptie van radioactief jodium uit nucleaire gasvormige afvalstromen en voor de terugwinning van goud uit elektronisch afval, met als doel kosteneffectievere en robuustere alternatieven voor de huidige technologieën te bieden.

In **hoofdstuk 1** introduceren we de fundamentele principes van covalente organische roosters (COF's), waarbij we de belangrijkste aspecten van hun synthese behandelen, inclusief het ontwerp van linkers, de chemie van de bindingen en de topologie. Speciale aandacht wordt besteed aan post-synthetische modificatiestrategieën die relevant zijn voor de opzet van dit proefschrift. Vervolgens gaat de discussie over op de toepassing van COF's als veelzijdige adsorbentia, waarbij hun potentieel wordt gekaderd binnen de dringende uitdagingen van milieusanering en het terugwinnen van grondstoffen. Specifiek onderzoekt het hoofdstuk de stand van de techniek voor de afvangst van radioactief jodium uit kernafval en de scheiding van goud uit elektronisch afval, en wordt de

noodzaak voor efficiëntere adsorbentia benadrukt door een overzicht te geven van de materialen die in de industrie worden gebruikt en in de academische wereld worden onderzocht. Aan het einde van het hoofdstuk schetsen we wat er in dit proefschrift zal worden gedaan om de adsorptie-eigenschappen van imine-COF's en vervolgens de post-gemodificeerde imidazopyridinium- en thiazool-COF's te verbeteren om hun gebruik bij respectievelijk de afvangst van jodium en de terugwinning van goud uit elektronisch afval te bevorderen.

Hoofdstuk 2 beschrijft de ontwikkeling van een robuust, kationisch covalent organisch rooster voor de afvangst van jodium, ontworpen om de chemische instabiliteit van traditionele imine-gebonden COF's te overwinnen. We presenteren een tweestaps post-synthetische modificatiestrategie om een kristallijn, op picolinaldehyde gebaseerd imine-COF om te zetten in een stabiel imidazopyridinium-gebonden rooster. Deze modificatie introduceert permanente positieve ladingen en halogenide-tegenionen, waardoor krachtige en specifieke bindingsplaatsen voor jodium worden gecreëerd. De resulterende materialen vertonen uitzonderlijke prestaties, met ultrasnelle adsorptiekinetiek en hoge gravimetrische capaciteiten (tot 4.66 g g^{-1}) voor jodiumdamp. Onder industrieel relevante dynamische omstandigheden (150°C, 50% RH) vertoont het rooster een opname van 21 gew.%, waarmee het de huidige industriële benchmark overtreft. Bovendien blijkt het materiaal zeer effectief in waterige milieus, waarbij het 98% van het trijodide uit de oplossing verwijdert in één minuut en verontreinigd zeewater zuivert tot natuurlijke achtergrondniveaus. Spectroscopische analyse onthult een synergistisch afvangmechanisme dat sterke halogeenbinding en elektrostatische interacties omvat, wat bevestigt dat deze materialen een zeer veelzijdig en effectief platform zijn voor de sanering van kernafval en waterzuivering.

In **hoofdstuk 3** presenteren we een eenvoudige post-synthetische omzetting van 2 imine-gekoppelde covalente organische roosters (COF's) naar hun thiazool-gekoppelde analogen, waardoor zeer efficiënte adsorbentia voor goudterugwinning worden gecreëerd. Deze modificatie

biedt meerdere voordelen: het verbetert de chemische stabiliteit en recycleerbaarheid, introduceert zwavelbindingsplaatsen om de adsorptiecapaciteit te verhogen, behoudt een hoge selectiviteit en verbetert de fotofysische eigenschappen van het materiaal aanzienlijk. Onder donkere omstandigheden behaalde het thiazool-gekoppelde TTT-TAPB-S COF een uitzonderlijke goudadsorptiecapaciteit van 3533 mg g^{-1}. Bovendien toonden we, door gebruik te maken van de verbeterde fotofysische eigenschappen van de materialen, een significante, door licht geïnduceerde verbetering van de goudopname aan. Het thiazool-gekoppelde Tfpy-PDA-S COF bereikte een recordhoge capaciteit van 7980 mg g^{-1} onder bestraling. Zowel de imine- als de thiazool-COF's vertoonden een hoge selectiviteit en praktische doeltreffendheid, waarbij ze tot 98% van het goud uit een complex CPU-afvalwater verwijderden, wat hun potentieel voor duurzame grondstofterugwinning valideert.

Tot slot bespreken we in **hoofdstuk 4** de algemene conclusies van dit werk samen met een vooruitzicht op de toekomst binnen dit onderzoeksveld.

1 Introduction

Porous materials have historically been pivotal in materials science, valued for their extensive surface areas and adaptable pore structures. These characteristics make them highly suitable for numerous applications, with adsorption being a particularly prominent one. The use of porous materials as adsorbents is not a recent development; activated carbon, for instance, sourced naturally, was employed in ancient times for the purification of water and air. Significant progress in adsorption technology was marked in the 20th century with the development of more sophisticated porous materials such as zeolites and silica gels.[1–5]

At its most basic, a pore is a void or cavity within a solid material. Nature itself showcases many examples of functional porosity, from stomata on plant leaves that facilitate gas exchange vital for photosynthesis and global elemental cycles, to the porous nature of bones that provides strength with minimal weight. Porosity in materials generally stems from structural aspects like inherent cavities in crystal lattices, voids created by the removal of certain components, or spaces formed due to the inefficient packing of particles or molecules. The innovation in and application of porous materials have resulted in considerable technological advancements. For example, the photoluminescence observed in porous silicon has driven progress in optoelectronics and sensor technology.[6]

Macroscopic porous materials are ubiquitous in everyday life, including natural substances like pumice and wood, and man-made products such as ceramic filters, sponges, insulating foams, and textiles. Beyond these macrostructures, the manipulation of materials possessing microscopic and nanoscopic pores has become a central theme in materials science.

The International Union of Pure and Applied Chemistry (IUPAC) provides a classification for pores based on their diameter (d), primarily determined through gas physisorption isotherm analysis **(Figure 1.1)**:

1. Macropores: $d > 50$ nm
2. Mesopores: $2 \text{ nm} < d < 50$ nm
3. Micropores: < 2 nm

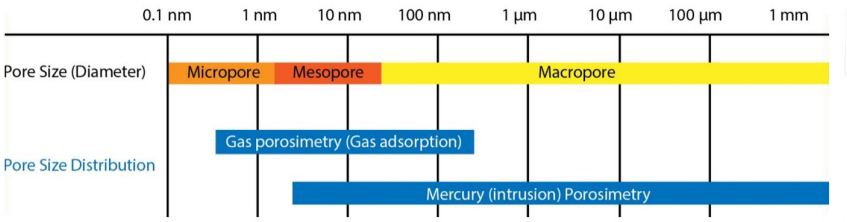

Figure 1.1. IUPAC Pore size classification.[7]

Pore connectivity (e.g., closed, blind/dead-end, or through-pores) and morphology (e.g., cylindrical, conical, ink-bottle, or slit-shaped) are further characteristics used to describe pores. It is also important to differentiate intrinsic porosity from surface roughness; surface irregularities are typically considered pores only if their depth is greater than their width.

Porous materials can be broadly classified by their method of formation:

- Inherent porosity from crystalline structures: Materials such as zeolites, Metal-Organic Frameworks (MOFs), and Covalent Organic Frameworks (COFs) have highly ordered, periodic networks that define pores with uniform size and shape at a molecular level.[8]
- Porosity via Selective Removal: Pores can be created by removing a sacrificial component or template from a precursor material, such as in dealloying metals to form nanoporous metals or etching

specific phases. Porosity can also arise from defects in crystalline materials, like MOFs with missing linkers or nodes.

- Hyper Cross-linked Polymers (HCPs): These are synthesized through extensive cross-linking reactions, often Friedel-Crafts alkylation, resulting in amorphous, robust networks with high surface areas and permanent microporosity. Examples include materials from cross-linked polystyrene or benzene networks, such as Knitting Aromatic Polymers (KAPs). Their stability and often cost-effective synthesis make them appealing for gas storage and separation.[9]

- Polymers of Intrinsic Microporosity (PIMs): Typically amorphous, the porosity in PIMs originates from inefficient chain packing due to rigid and contorted monomer structures, often containing spirocenters as seen in PIM-1. They achieve microporosity due to restricted bond rotation and shape persistence, rather than a designed framework structure. Many PIMs are soluble, which allows them to be processed into films for membrane applications.[10]

- Conjugated Microporous Polymers (CMPs): CMPs are amorphous networks characterized by extended π-conjugation throughout their covalently linked structure, combined with permanent porosity. Synthesized via reactions like Sonogashira or Suzuki coupling between aromatic units, their distinct combination of electronic properties and porosity suits them for applications in photocatalysis, light harvesting, sensing, and energy storage. Their insolubility and amorphous nature can, however, complicate detailed structural analysis.[11]

- Porous Aromatic Frameworks (PAFs): PAFs are generally amorphous, highly robust frameworks often built using strong, irreversible C-C bond-forming reactions like Yamamoto coupling. They feature a high density of aromatic rings. The archetypal PAF-1, constructed from tetrahedral tetrakis(4-bromophenyl)methane,

displayed a very high surface area of 5600 m^2g^{-1}. While offering exceptional stability and tunable building blocks, their amorphous nature precludes structure determination by diffraction methods.[12]

1.1 Covalent Organic Frameworks (COFs)

Since their discovery in 2005, Covalent Organic Frameworks (COFs) have rapidly gained recognition as a versatile and promising class of crystalline, porous polymers. A dramatic increase in scientific literature highlights the intense research activity in this field; a search indicates that well over 18000 articles on COFs had been published by early 2025 (**Figure A.1**). In 2024 alone, the annual publication rate surpassed 3000 papers on the subject. This considerable interest is predominantly fueled by the exceptional degree of structural designability that COF chemistry provides. The versatility of COFs arises from controllable variations at multiple levels, which will be discussed in the subsequent subsections.

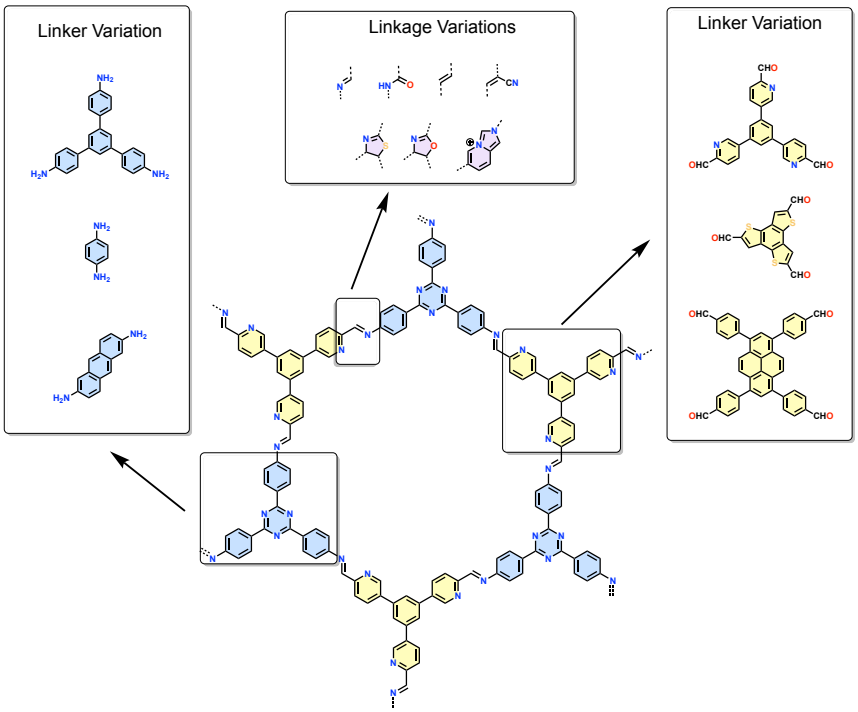

Figure 1.2. A selection of the possible variations of linkers and linkages in COF synthesis.

1.1.1 Linkers: Structure and Function

The fundamental modularity of Covalent Organic Frameworks (COFs) is derived from the wide array of organic monomers, or linkers, that function as their constituent building blocks. These molecular units determine the final structure, porosity, and chemical environment within the resulting framework (**Figure 1.2**). Linkers can differ considerably in size, shape, rigidity, and chemical functionality, presenting vast opportunities for material design.[13]

To successfully form a crystalline COF, a linker must meet certain criteria. Primarily, it needs to have at least two reactive functional groups

(e.g., amine, aldehyde, boronic acid, nitrile) capable of forming the chosen covalent linkage under the reaction conditions. Secondly, the linker must possess a suitable symmetry and geometry that is compatible with forming an extended, ordered, and periodic network when combined with complementary linkers. This geometric prerequisite is essential for achieving the long-range order characteristic of crystalline materials. Deviations from ideal geometries or symmetries frequently result in defects or amorphous products.[14]

Beyond these basic requirements, the chemical diversity of potential linkers is immense, limited mainly by the capacity of synthetic organic chemistry to produce the desired molecular structures. While **Figure 1.3** illustrates a small selection of reported linker architectures, including those utilized in this thesis, the library of known COF linkers is continually growing as researchers design and synthesize new building blocks. Linkers are commonly categorized based on their topicity, which indicates the number of reactive groups available for network polymerization. Common examples include:

- Ditopic linkers: Possessing two reactive groups, they act as linear extenders or spacers (e.g., terephthalaldehyde, 1,4-phenylenediamine).[15]
- With three reactive groups, often displaying C_{3v} or D_{3h} symmetry, they serve as trigonal nodes (e.g., 1,3,5-tris(4-aminophenyl)benzene (TAPB), 1,3,5-triformylbenzene (TFB)).[16]
- Bearing four reactive groups, typically with C_2, C_4, D_{2h}, D_{4h}, or T_d symmetry, they act as square, rectangular, or tetrahedral nodes (e.g., pyrene-based tetramines or tetraaldehydes, porphyrins, tetrakis(4-aminophenyl)methane (TAPM), N,N,N,N-tetrakis(4-aminophenyl)-1,4-phenyldiamine (TAPD)).[17]
- With six reactive groups, often possessing D_{3h} symmetry (e.g., hexahydroxytriphenylene).

Although pentatopic linkers have been reported, they are rare.[18] The combination of linkers with specific topicities dictates the overall network connectivity and the resulting topology of the framework; for example, combining tritopic and ditopic linkers typically yields hexagonal 2D nets.[19]

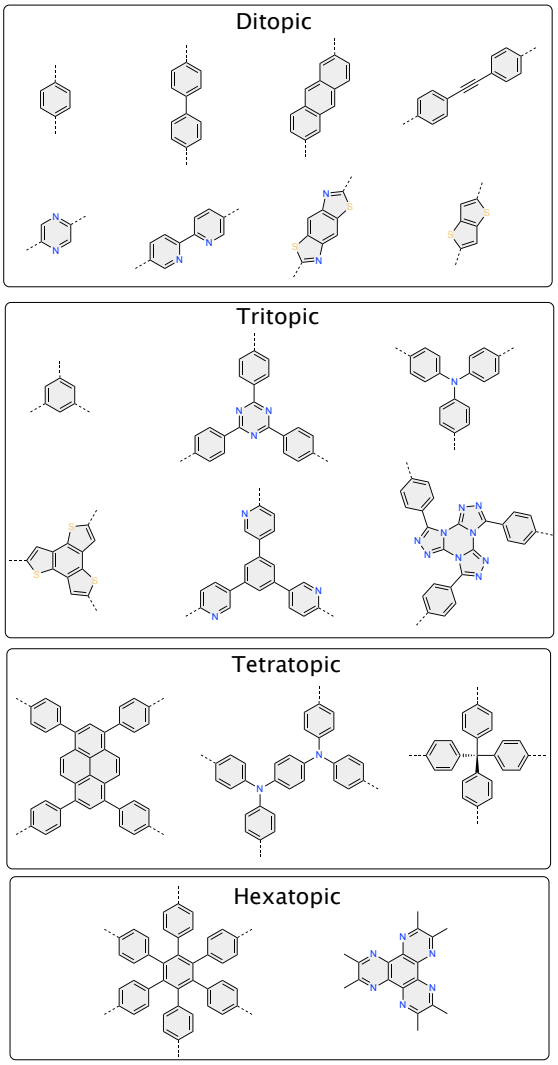

Figure 1.3. Overview of different linkers commonly used in COF synthesis sorted by topicity.

A dominant characteristic of most successful COF linkers is their structural rigidity and planarity, qualities often conferred by aromatic systems such as benzene rings, naphthalene, triphenylene, pyrene. Rigidity helps to enforce specific bond angles and spatial arrangements, thereby minimizing conformational disorder and promoting the formation of crystalline structures. Planarity is especially conducive to the formation of two-dimensional (2D) COFs through layer-by-layer stacking.[20] Consequently, the vast majority of reported COFs are 2D materials constructed from planar aromatic linkers. However, research has also investigated linkers that incorporate flexible units (e.g., alkyl chains, ether linkages) or even non-aromatic cores (e.g., cyclohexane derivatives), which can result in frameworks with dynamic properties or present unique challenges in achieving crystallinity.[21, 22] Furthermore, the use of inherently non-planar, three-dimensional (3D) linkers, such as those based on tetrahedral cores (e.g., adamantane, methane derivatives like tetrakis(4-aminophenyl)methane (TAPM)), is crucial for constructing 3D COF networks.[23, 24]

Crucially, the linker serves as the primary means for encoding desired chemical functionality into the COF material. By introducing specific substituents or incorporating heteroatoms into the linker's structure, the properties of the resulting framework can be precisely adjusted. Functional groups such as hydroxyls (-OH), halogens (-F, -Cl, -Br), amines ($-NH_2$), carboxylic acids (-COOH), sulfonic acids ($-SO_3H$), or alkyl chains can be appended to modify polarity, surface interactions, or potential for post-synthetic modification. Heteroatoms like nitrogen, sulfur, or oxygen can be incorporated within aromatic rings (e.g., using pyridine, thiophene, or furan-based linkers) to change electronic properties, introduce basic/acidic sites, or enhance affinity for specific adsorbates like CO_2.[14] More complex functionalities, including metal-chelating ligands (e.g., bipyridine, terpyridine, porphyrin), catalytically active units (e.g., transition metal complexes, organocatalytic moieties), or photo-/electroactive groups, can also be integrated via linker design, paving the way for

COFs tailored for catalysis, sensing, light harvesting, and energy storage applications.[8]

1.1.2 Linkages: Balancing Reversibility and Stability

While the diversity of linkers offers the primary way to customize the chemical environment and pore dimensions within a COF, the covalent linkage connecting these building blocks is equally vital. The choice of linkage chemistry not only dictates the connectivity pattern but also profoundly affects the framework's chemical stability, the conditions needed for its synthesis, and ultimately, its potential for achieving crystallinity. Compared to the extensive library of potential linkers, the range of linkage chemistries successfully used for crystalline COF synthesis is considerably more limited.

The formation of a well-defined, crystalline COF network places strict demands on the linkage-forming reaction, rooted in the principles of dynamic covalent chemistry (DCC). Firstly, the reaction must form a covalent bond that is thermodynamically favorable, supplying the driving force for polymerization and the formation of an extended structure. Secondly, and critically for achieving crystallinity, the linkage formation must exhibit a degree of reversibility. During the initial stages of polymerization, linkers connect, often forming kinetically favored but structurally disordered oligomers or amorphous networks. Reversibility allows these "errors", connections that deviate from the lowest energy, periodic structure, to be corrected. Bonds can break and reform, enabling the system to explore different configurations and anneal defects, eventually settling into the thermodynamically most stable state: the desired crystalline COF. This balance between bond formation and bond breaking determines whether the synthesis operates under thermodynamic control (favoring the most stable crystalline product through reversible reactions) or kinetic control (trapping potentially less stable, often amorphous structures due to irreversible reactions). Efficient error correction, necessary

for high crystallinity, typically requires significant reversibility, meaning the activation energies for both bond formation and bond cleavage must be accessible under the reaction conditions.

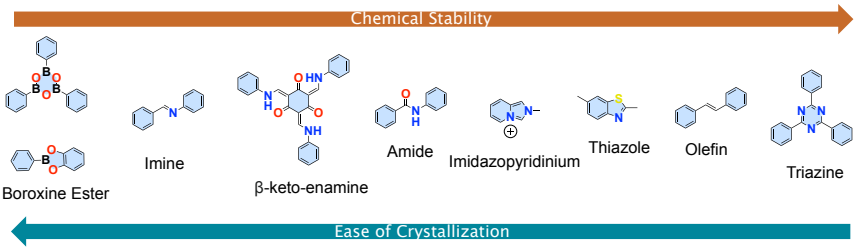

Figure 1.4. Overview of the most common linkages in COFs sorted by crystallinity and stability.

This leads to a central dilemma in COF synthesis: balancing linkage stability with the dynamicity required for crystallization.[20] Highly reversible linkages (often corresponding to lower bond stability), such as boroxine (-B-O-B-) or boronate ester linkages, facilitate efficient error correction under mild conditions, often yielding highly crystalline materials.[25] However, the lower intrinsic stability of these bonds can make the resulting COFs susceptible to degradation (e.g., hydrolysis), limiting their utility in many practical applications. Conversely, highly stable linkages, such as triazine or olefin bonds, impart exceptional chemical robustness to the framework, making them resistant to harsh chemical environments.[26] However, the high stability of these bonds implies poor reversibility (high activation energy for cleavage). Achieving crystallinity with such linkages often requires forcing conditions (e.g., high temperatures, strong catalysts) to provide sufficient energy for some error correction or structural reorganization to occur. These harsh conditions can, in turn, limit the scope of compatible linkers, as sensitive functional groups might degrade or undergo side reactions. Consequently, considerable research effort is directed towards identifying novel linkage chemistries that achieve an optimal balance, offering sufficient stability for desired applications while retaining enough dynamicity for effective crystallization under

reasonably mild conditions. Concurrently, strategies are explored to facilitate the crystallization of robust COFs, such as optimizing solvent systems, employing specific catalysts, or utilizing post-synthetic modification techniques.[27] **Figure 1.4** gives a conceptual overview of several common linkage types in COF synthesis, often arranged to reflect their relative chemical stability and associated chemical reversibility. The specific linkage chemistries relevant to the work in this thesis, namely, imine, imidazopyridinium, and thiazole linkages, are highlighted and will be discussed in detail in the following sections.

Imine

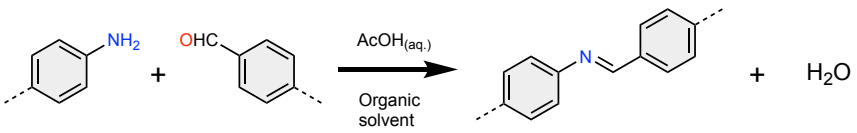

Figure 1.5. Imine synthesis scheme for imine-linked COFs.

Among the various covalent linkages used in COF synthesis, the imine linkage (-C=N-) holds a position of particular prominence. The first COF incorporating this linkage was reported in 2009 by Uribe-Romo et al. from Omar Yaghi's group.[28] Chemically, the imine bond is typically formed via a straightforward condensation reaction between a primary amine ($-NH_2$) group and an aldehyde (-CHO) group, resulting in the elimination of a water molecule (H_2O). While ketones can, in principle, also react with amines to form imines (specifically, ketimines), their use in COF synthesis is far less common compared to aldehydes.[29] Imine-linked COFs constitute the largest and most extensively studied class of COFs reported to date. Several factors contribute to their prevalence:

- **Balanced Reversibility and Stability:** The imine linkage strikes a practical balance between the thermodynamic stability required for a robust material and the kinetic lability (reversibility) necessary for effective error correction during crystallization. This allows for

the formation of relatively well-ordered crystalline materials under accessible conditions.

- **Accessible Precursors:** Aldehyde and amine functional groups are common motifs in organic chemistry, making a vast array of corresponding linkers either commercially available or synthetically accessible through established organic methodologies.

The most widely adopted method for synthesizing imine COFs is conventional solvothermal synthesis. In a typical procedure, the amine and aldehyde linkers are dissolved or suspended in a suitable organic solvent mixture **(Figure 1.5)**. An aqueous solution of an acid catalyst, most commonly acetic acid (CH_3COOH), is added. The reaction vessel is sealed and heated, often to 120 °C, for an extended period, typically 72 hours, under an inert atmosphere. The key components play specific roles: water facilitates the reversible hydrolysis of the imine bond, enhancing the rate of the reverse reaction and thus promoting dynamic error correction crucial for annealing defects and achieving crystallinity. Acetic Acid acts as a Brønsted acid catalyst, accelerating both the forward imine formation and the reverse hydrolysis reaction, thereby speeding up the overall process of reaching the thermodynamically favored crystalline state. These standard conditions generally yield imine COFs with moderate to high crystallinity, the quality of which can depend significantly on the specific linkers chosen.

Conventional solvothermal synthesis of imine-linked COFs is often impeded by operational complexities, particularly the requirement for rigorous degassing via freeze-pump-thaw cycles to ensure an inert atmosphere. Furthermore, the lack of a universal solvent system necessitates a trial-and-error approach to solvent selection, utilizing mixtures that are frequently hazardous or toxic. Addressing these limitations, Laemont et al. developed a mild, green, and general method for the scalable solvothermal synthesis of imine COFs.[30] This optimized method involves reacting the amine and aldehyde linkers in n-butanol containing

10% H_2O and 4M acetic acid at a lower temperature of 70°C for a significantly reduced time of 16 hours, typically under aerobic conditions in simple cap-closed vials. This approach uses n-butanol, a less hazardous and potentially bio-derived solvent, and avoids the need for rigorous degassing or specialized pressurized vessels. A key finding was that alcohols with longer, apolar alkyl chains, like n-butanol, promote more efficient stitching and ordered stacking of COF nanosheets, leading to larger, more robust particles that are less prone to pore collapse during activation. This improved robustness can simplify the activation process, sometimes allowing the use of milder solvents like diethyl ether instead of supercritical CO_2. The method proved to be general, successfully applied to a variety of COFs with different topologies, and notably scalable, with over 10 grams of an imine COF synthesized in a single batch.

Regarding chemical stability, typical imine COFs demonstrate good resistance to many organic solvents and neutral water.[31] However, they are generally susceptible to hydrolysis under strongly acidic or alkaline conditions, which can lead to framework degradation. The stability can be modulated to some extent through judicious linker design, for instance, by incorporating electron-withdrawing or sterically hindering groups near the imine bond. Nonetheless, their relative stability under a range of conditions is sufficient for them to be explored in a diverse range of applications, including gas storage, catalysis, sensing, and separation.

Post-Synthetic Modification of the Imine Linkage

While the direct synthesis of imine-linked COFs provides a versatile route to crystalline porous materials, the inherent properties of the imine bond, namely its moderate chemical stability and susceptibility to hydrolysis under certain conditions, can limit applications requiring extreme robustness. Furthermore, achieving crystallinity directly with highly stable linkages often necessitates harsh conditions incompatible with many

functional groups. To address these challenges and expand the functional scope of COFs, Post-Synthetic Modification (PSM) has emerged as a powerful strategy.[32] PSM involves performing chemical reactions directly on a pre-synthesized, intact framework material. In the context of imine COFs, PSM offers several advantages:

- **Leveraging Crystallinity:** It allows researchers to utilize the relative ease of forming well-defined, crystalline imine COFs as templates. Subsequent chemical transformations can then be performed while potentially preserving the long-range order established during the initial synthesis.
- **Enhancing Stability:** Imine linkages can be converted into significantly more robust chemical bonds (e.g., amides, thiazoles, oxazoles, secondary amines) that might be difficult or impossible to form directly into a crystalline framework due to poor reaction reversibility. This addresses the stability-crystallinity dilemma discussed previously.
- **Introducing New Functionality:** PSM can introduce functional groups or structural motifs that were either incompatible with the initial COF-forming conditions or are more easily installed after framework assembly. This includes modifying the linkage itself or targeting reactive sites on the linkers.

Common PSM strategies targeting the imine linkage in COFs include:

- **Reduction:** Converting the C=N double bond to a C-N single bond, forming secondary amine linkages, typically using reducing strategies such as the Leuckart-Wallach reaction with formic acid and ammonium formate.[33]
- **Oxidation:** The imine linkage in COFs can be oxidized to form amides or nitrones. This process typically involves oxidizing agents such as $KHSO_5$ or 3-chloroperbenzoic acid (mCPBA).[34, 35]

- **Cyclization/Condensation Reactions:** Reacting the imine bond with other reagents or suitably positioned functional groups on adjacent linkers to form new heterocyclic rings, such as thiazoles, oxazoles, benzimidazoles, or charged systems like imidazopyridiniums.[36, 37]

Successful PSM requires careful selection of reaction conditions to ensure high conversion efficiency and selectivity, minimizing side reactions or damage to the framework structure. Ideally, the modification should proceed without significant loss of the material's crystallinity or porosity. The development of effective PSM protocols significantly broadens the chemical space accessible within crystalline COF materials, enabling the creation of frameworks with enhanced stability and tailored functionalities beyond those achievable through direct synthesis alone.

Imidazopyridinium

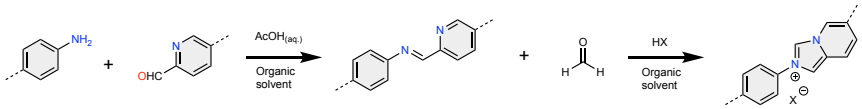

Figure 1.6. Imidazopyridinium synthesis scheme from picolinaldehyde-based imine COFs.

The conversion of neutral imine linkages into positively charged heterocyclic systems embedded within the COF backbone is a particularly attractive strategy for modulating material properties. Specifically, Li et al. introduced the transformation of imine linkages into imidazopyridinium moieties has emerged as a valuable PSM route.[37] This modification typically involves a multi-step reaction sequence performed directly on the solid COF material. This process generally proceeds via the reaction of the imine nitrogen and the adjacent aromatic ring, often derived from a picolinaldehyde (pyridine-2-carbaldehyde) based linker, under specific reaction conditions (e.g., presence of an acid catalyst and/or oxidant,

specific solvent, temperature)(**Figure 1.6**). The initial step often involves the formation of an aminal intermediate or direct nucleophilic attack, followed by an intramolecular cyclization. Subsequent aromatization, which may occur spontaneously or require heating, leads to the formation of the thermodynamically stable, planar, and permanently cationic imidazopyridinium ring system integrated into the linkage points of the framework.

The successful incorporation of these charged units fundamentally alters the nature of the COF. Key consequences include:

- **Introduction of permanent positive charges:** This transforms the neutral framework into a cationic porous material, enabling applications in anion exchange, selective anion capture, etc..
- **Enhanced chemical stability:** The aromatic imidazopyridinium linkage often exhibits greater hydrolytic and chemical stability compared to the original imine bond, potentially broadening the range of conditions under which the COF can be used.
- **Altered electronic and photophysical properties:** The extended π-conjugation and positive charge of the imidazopyridinium unit can significantly modify the electronic band structure, conductivity, and photoluminescence behavior of the material.

Thiazole

Alongside the formation of charged heterocycles, another important PSM strategy targeting imine linkages involves their conversion into robust, neutral heterocyclic systems such as thiazoles. The thiazole linkage represents a particularly robust covalent bond within framework materials due to its fused, extensively conjugated heterocyclic structure, which exhibits significant resistance to chemical cleavage. While the formation of thiazole linkages could theoretically be done directly via a condensation

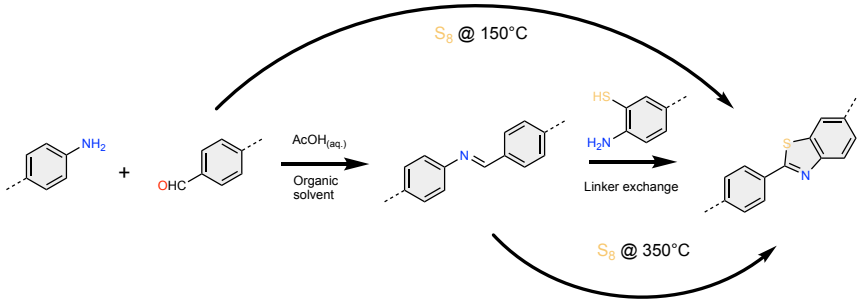

Figure 1.7. Thiazole-linked COF synthesis scheme via different methods.

reaction between an aldehyde and an aromatic amine bearing an ortho-thiol group, the practical synthesis of crystalline COFs through this route is challenging. The limited reversibility inherent in the thiazole formation reaction impedes the dynamic error correction processes necessary for achieving long-range structural order, typically resulting in amorphous or poorly crystalline materials.

To overcome this limitation, PSM has emerged as an effective strategy for accessing highly crystalline thiazole-linked COFs. This involves starting from a pre-formed crystalline imine COF, which serves as a template for the conversion of imine linkages into the more stable thiazole moieties (**Figure 1.7**). Although the imine-to-thiazole transformation itself is generally irreversible, the pre-existing crystallinity established during the reversible imine COF formation is largely preserved throughout the modification process. Consequently, PSM enables the generation of materials that synergistically combine high structural order with the enhanced chemical stability afforded by the thiazole linkage.

To date, three different methodologies have been reported for the post-synthetic conversion of imine COFs to their thiazole counterparts:

1. **Linker exchange followed by cyclization and oxidation:** Pioneered by Waller et al., this method involves treating a pre-synthesized imine COF (e.g., based on a 1,4-phenylenediamine linker) with a

thiol-functionalized diamine, such as 2,5-diaminobenzene-1,4-dithiol dihydrochloride.[38] This reagent undergoes linker exchange, introducing thiol groups in the ortho-position relative to the imine nitrogen. Subsequent intramolecular cyclization yields thiazoline intermediates, which are then oxidized, typically under an oxygen atmosphere, to form the final thiazole linkages. A parallel strategy using 2,5-diaminohydroquinone dihydrochloride allows access to benzoxazole linkages. While proceeding under mild conditions, this route's applicability is contingent upon the availability of appropriate thiol-functionalized (or hydroxyl-functionalized for oxazoles) monomers capable of efficient linker exchange. Furthermore, the reported procedure required a fourfold excess of the exchanging monomer to achieve sufficient conversion, and its generalizability was demonstrated for only a single imine COF system.

2. **Direct thionation with elemental sulfur:** Haase et al. introduced a significantly harsher, yet potentially more broadly applicable, conversion method in 2018.[39] This protocol involves treating the imine COF with molten elemental sulfur at elevated temperatures (initially 150°C, followed by 350°C) under an inert atmosphere. It is proposed that sulfur reacts with the imine bond to form a thioamide intermediate, which subsequently undergoes intramolecular cyclization to yield the thiazole ring. Key advantages of this method include the use of inexpensive and readily available elemental sulfur and comparatively short reaction times. Its efficacy was demonstrated on at least two different imine COF structures, and subsequent studies have further validated its wider applicability. However, the high reaction temperatures impose limitations on the substrate scope, precluding the use of imine COFs bearing thermally sensitive or readily oxidizable functional groups, which may undergo undesired side reactions or degradation under the stringent conversion conditions.

3. **One-pot imine formation and thiazole conversion:** Building upon the sulfur-mediated conversion, Wang et al. reported a one-pot multicomponent approach in 2020.[40] In this procedure, the imine COF synthesis (condensation of aldehyde and amine monomers) is performed directly in the presence of elemental sulfur at 150°C, utilizing a small quantity of DMSO as an oxidant to facilitate the thiazole formation. This strategy streamlines the process, reducing reaction time and reagent consumption. However, elemental analysis indicated that the imine-to-thiazole conversion was often incomplete, typically achieving efficiencies between 80% and 90%, contingent on the specific linker combination. More significantly, the demonstrated applicability of this one-pot method was restricted to COFs constructed from electron-rich amine linkers, specifically derivatives of anthracene-2,6-diamine or naphthalene-2,6-diamine. The original report explicitly mentioned that identical reaction conditions were unsuccessful for COFs derived from less electron-rich amines, such as aniline derivatives, thereby substantially limiting the structural diversity achievable via this route.

Consistent with the inherent stability of the linkage, thiazole-linked COFs demonstrate significant chemical resilience. For instance, they have been reported to largely maintain their crystallinity following treatment with strong acids (e.g., 14 M HCl), strong bases (e.g., 14 M NaOH), reductants (e.g., 1 M $NaBH_4$), and nucleophiles (e.g., 1 M N_2H_4). This highlights the effectiveness of PSM routes in accessing COFs, combining structural order with exceptional robustness.

1.1.3 Network Topology

Beyond the specific chemical identity of the molecular building blocks (linkers) and the nature of the covalent bonds connecting them (as discussed in **subsection 1.1.1** and **subsection 1.1.2**), the overall architecture

and resultant properties of a COF are also influenced by its network topology and dimensionality (**Figure 1.8**). The network topology is dependent on the geometry of a number of functional groups on the linkers used to synthesize the COF. This results in a specific network topology that can be represented as a graph (e.g., hexagonal, square). Dimensionality, on the other hand, refers to whether the covalent network extends infinitely (in theory) in two (2D) or three (3D) dimensions. These fundamental structural characteristics are predetermined by the symmetry, valency (number of connection points), and spatial orientation of the reactive sites on the linkers, embodying the core principles of reticular chemistry for predictable framework construction.

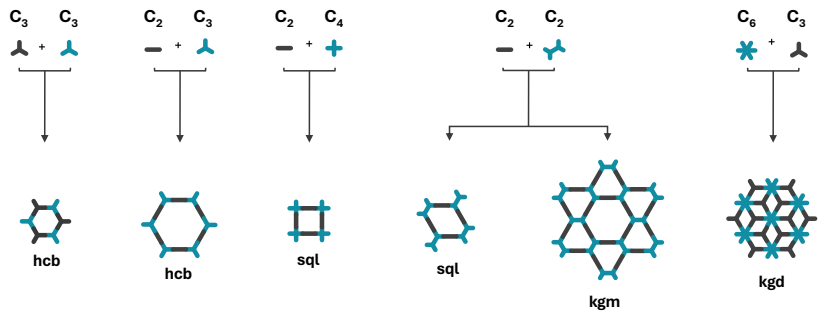

Figure 1.8. Overview of common topologies encountered for 2D COFs.

The dimensionality of the COF is primarily dictated by the geometry of the linkers used. Typically, planar monomers possessing reactive sites distributed within a single plane such as linear (D_{2h}, C_{2v}), trigonal planar (D_{3h}, C_{3v}), or square planar (D_{4h}) symmetries polymerize through covalent linkages to form extended 2D sheets. These individual 2D layers then stack via non-covalent interactions (e.g., van der Waals forces, π-π interactions) to assemble into a 3D crystalline solid. The precise stacking mode, commonly either eclipsed (AA) or various staggered arrangements (AB, ABC, etc.), significantly impacts the alignment of the pores running perpendicular to the sheets, influencing effective pore aperture and guest accessibility.

In contrast, the incorporation of monomers with non-planar geometries, where reactive sites are directed out of a single plane, facilitates the formation of intrinsically 3D COF networks. Tetrahedral monomers (T_d symmetry) are the most common building blocks used to achieve 3D connectivity, acting as nodes that extend the covalent framework isotropically or anisotropically, depending on the linker geometry. The use of such 3D nodes prevents layer formation and instead results in monolithic, covalently bonded networks spanning three dimensions.

The specific topology of the network, whether in 2D sheets or 3D frameworks, is determined by the combination of monomer symmetries and valencies.[41] For example, in 2D COFs:

- Combining trigonal (3-connecting) and linear (2-connecting) monomers typically results in a hexagonal (hcb) topology.
- Linking tetragonal (4-connecting) and linear (2-connecting) monomers often yields a square (sql) topology.
- Self-condensation of tetragonal monomers can also lead to the sql topology. In some instances, the same set of linkers can crystallize into different topologies depending on the synthetic conditions, for example, a ditopic C_2 linker and a tetratopic C_2 linker can form either a rhombic (sql) or a dual-pore Kagome (kgm) lattice.

Similarly, for 3D COFs, various topologies can be targeted based on the geometry of the 3D node and the connecting linkers. Common examples include diamondoid (dia), platinum sulfide (pts), or boracite (bor) topologies.[42–44] It has also been demonstrated that it is sometimes possible to form either a 2D or 3D COF from the same set of linkers by altering reaction conditions such as temperature. A notable feature often encountered in 3D COFs, particularly those designed with large intrinsic voids, is network interpenetration. This phenomenon, where two or more identical, independent networks coexist within the same crystal

volume, reduces the accessible pore size but can contribute to enhanced framework stability and modified sorption behavior.

Therefore, the rational selection of monomer geometry and connectivity serves as a critical design parameter, allowing for a priori control over the resulting COF's dimensionality and network topology. These structural features, in turn, dictate fundamental material properties such as pore size and shape, specific surface area, framework density, mechanical characteristics, and potential electronic band structure, ultimately governing the COF's suitability for targeted applications in areas like separation, storage, catalysis, and electronics. Mastering the interplay between molecular precursors and framework architecture is thus central to the continued development of functional COF materials. For example, Tang et al. demonstrated how structural topology impacts photocatalysis by developing two COFs, TBD-COF and TBC-COF, from the same building blocks but with aldehyde groups in different positions.[45] This variation created two distinct topologies (cpt and hcb). Comparing the two for photocatalytic H_2O_2 production, they found that controlling the topology allowed them to regulate key properties like unit cell dipole moments, photoinduced electron-hole separation, $O_2^{\bullet-}$ generation, and water affinity. These adjustments directly enhanced the photosynthetic activity for H_2O_2.

1.2 Adsorption Applications

Since the initial report by Yaghi et al. in 2005, the field of COFs has witnessed accelerated development. This growth is driven by the ability to precisely tailor their pore environments, their high surface areas, and, in many cases, exceptional stability.[46] These attributes make COFs exceptionally suited for a variety of applications, including catalysis, energy storage, and sensing. However, it is in adsorption where COFs exhibit particularly outstanding potential, rapidly establishing this as one of their most promising applications for real-world impact.[47, 48]

The inherent characteristics of COFs, namely their permanent porosity, low density, and extensive surface areas make them ideal candidates for diverse adsorption-based processes. These processes range from gas storage and separation to environmental remediation. The tunability of their building blocks enables the rational design of frameworks with specific pore sizes and chemical functionalities, allowing for the selective adsorption of target molecules.

While the focus of this work lies on specific environmental remediation and resource recovery challenges, it is vital to contextualize these efforts within the broader landscape of COF-based adsorption. Since their inception, the high surface area and permanent porosity of COFs have driven intense research into their use as advanced adsorbents. Currently, the field is dominated by gas storage and separation applications. The most extensively studied areas include:

- **Gas storage:** COFs have been widely investigated for the storage of energy-relevant gases such as hydrogen (H_2) and methane (CH_4). Their low density and high surface area allow for significant gravimetric uptake, although volumetric capacity remains a challenge compared to traditional materials.
- **Carbon Capture:** The separation of CO_2 from flue gas (CO_2/N_2) or natural gas (CO_2/CH_4) is perhaps the most prolific area of research. COFs offering specific pore sizes or functionalized with amine groups have shown remarkable selectivity and capacity.
- **Water Harvesting:** Leveraging the hydrolytic stability of certain linkages, researchers are increasingly exploring COFs for atmospheric water harvesting, where the material captures moisture from air at low humidity and releases it upon mild heating.
- **Liquid-Phase Pollutant Removal:** Beyond gases, COFs are used to adsorb organic pollutants such as dyes, pharmaceuticals, and pesticides from water.

Despite the dominance of gas-phase studies, liquid-phase separations targeting high-value or high-risk elements such as the gold and radioactive iodine addressed in this thesis are rapidly gaining traction. These applications require not just porosity, but precise chemical recognition and stability in harsh environments (e.g., acidic leachates or nuclear off-gases). By transitioning from general physisorption to specific chemisorption (as seen in iodine capture) or reductive adsorption (as seen in gold recovery), COFs can outperform traditional adsorbents like activated carbon, which often suffer from poor selectivity in complex mixtures.

Several factors underscore the intense research focus on COFs for adsorption applications. In a recent survey among researchers working in the field of reticular chemistry, adsorption ranked first among the areas of focus.[49] In terms of fields likely to achieve a breakthrough in the next 10 years, adsorption ranked third, just below gas separation and energy storage materials. Additionally, computational studies have explored vast libraries of hypothetical COF structures, with tens of thousands specifically screened for applications like carbon capture.[50, 51] This highlights the perceived potential and the effort to harness COFs for critical separation tasks. Furthermore, the recent establishment of the first company dedicated to COF commercialization, YOCOF MATERIAL CO. LTD in 2023, which specializes in the production of COF sorbents, provides tangible evidence of the industrial relevance and promise of COFs in adsorption technologies.[30] This transition from academic research to commercial endeavor signals strong confidence in the practical utility of COFs as advanced adsorbents. As such, the investigation into novel COF structures and their adsorption capabilities continues to be a vibrant and crucial area of materials science, paving the way for innovative solutions to pressing global challenges.

1.2.1 Iodine Capturing

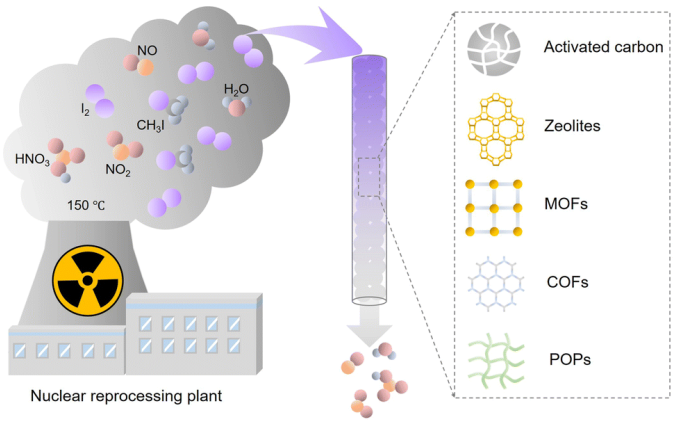

Figure 1.9. Iodine adsorption from nuclear reactors.[52]

The global pursuit of sustainable, secure, and low-carbon energy sources has positioned nuclear energy as a significant contributor to the world's electricity generation portfolio.[53, 54] Derived from the controlled fission of heavy atomic nuclei, typically uranium or plutonium, nuclear power offers several distinct advantages in the contemporary energy landscape. Chief among these is its exceptionally high energy density, allowing substantial power generation from a relatively small amount of fuel compared to conventional fossil fuels.[55] Critically, during operation, nuclear power plants produce virtually no direct greenhouse gas emissions, rendering them a vital tool in strategies aimed at mitigating anthropogenic climate change, a pressing global concern underscored by international agreements and scientific consensus. Furthermore, nuclear power provides a reliable and dispatchable baseload electricity supply, complementing intermittent renewable sources like solar and wind, and thereby contributing to grid stability and energy security for many nations. Indeed, in light of evolving geopolitical landscapes and the urgent need to transition away from carbon-intensive energy systems, as acutely

felt in the mid-2020s, there is a renewed interest and, in some regions, an expansion of nuclear capacity.[56]

However, the undeniable benefits of nuclear energy are intrinsically linked with significant challenges that require careful management and technological innovation. While operational safety standards are exceedingly high and continuously improving, the primary long-term concern associated with nuclear power is the generation of radioactive waste.[57] This waste, encompassing spent nuclear fuel and byproducts from fuel reprocessing, contains a spectrum of radionuclides with varying half-lives and radiotoxicities. The effective and safe management of these radioactive materials, from their initial generation through to their ultimate disposal, is paramount to ensuring the environmental sustainability and public acceptance of nuclear technology. It is within this context that specific waste components demand highly specialized solutions. The management of radioactive waste streams generated by the nuclear energy sector thus represents a significant scientific and societal challenge, and among the various radionuclides produced, certain volatile species present unique difficulties.[58]

Sources of Radioactive Iodine

Among these challenging radionuclides produced during nuclear fission and subsequent fuel reprocessing, radioactive isotopes of iodine, particularly iodine-129 (^{129}I) and iodine-131 (^{131}I), pose specific and considerable environmental and health risks. Understanding the sources, properties, and behavior of these isotopes is crucial for developing effective remediation and waste management strategies. Radioactive iodine isotopes are prominent fission products generated within nuclear reactors. They are primarily released during the reprocessing of spent nuclear fuel (SNF), where the fuel rods are dissolved (e.g., using the PUREX process) to recover uranium and plutonium (**Figure 1.10**).[59] During this dissolution, volatile iodine species, primarily molecular iodine (I_2) and

organic iodides (e.g., methyl iodide, ethyl iodide), are released into the off-gas streams. Accidental releases, such as those observed during the Chernobyl (1986) and Fukushima (2011) nuclear power plant accidents, can also introduce significant quantities of radioactive iodine into the environment.[60, 61] Minor sources include medical applications involving ^{131}I for diagnostics and therapy, although the quantities and half-lives involved present a different scale of management challenge compared to the nuclear fuel cycle.[62]

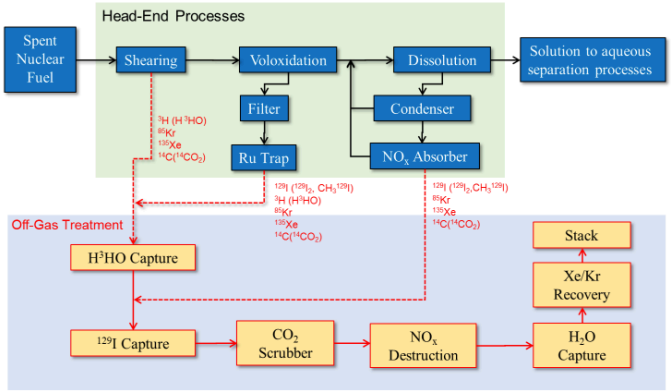

Figure 1.10. Head-end processes of spent nuclear fuel reprocessing and off-gas treatment systems. Adapted from Nan et al.[63]

Isotopes of Concern and their Properties

Two iodine isotopes are of primary concern in nuclear waste management, originating from the fission reactions of uranium-235 and plutonium-239:

- **Iodine-131 (^{131}I)**: This isotope has a relatively short half-life of approximately 8.02 days. It decays via beta emission, posing a significant short-term health risk immediately following a release due to its high specific activity and rapid biological uptake. Its shorter half-life means it decays relatively quickly, reducing its long-term environmental persistence.

- **Iodine-129 (^{129}I)**: This isotope presents a major long-term challenge due to its extremely long half-life of 15.7 million years. It also decays via beta emission. Its persistence ensures that, once released, it remains in the environment essentially indefinitely on human timescales, contributing to the long-term radiological dose. This poses a need for permanent disposal solutions.

Environmental and Health Risks

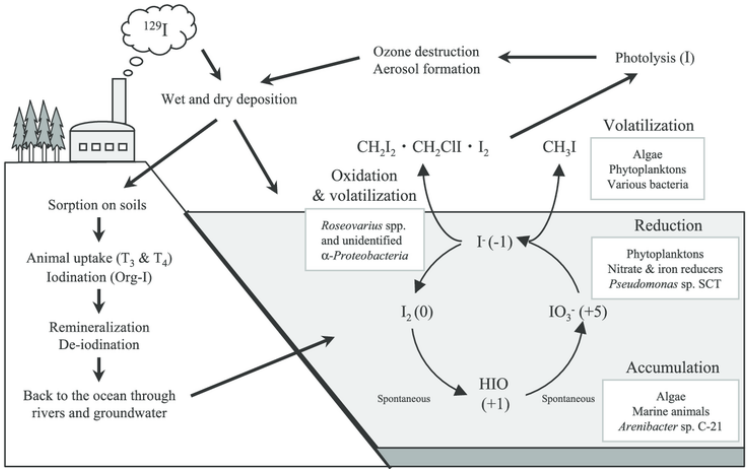

Figure 1.11. The biogeochemical cycle of iodine. Oxidation states of iodine are shown in parentheses. Adapted from Amachi et al.[64]

Iodine, in its various chemical forms (e.g., I_2, I^-, IO_3^-, organic iodides), exhibits significant volatility and mobility in the environment. As shown in **Figure 1.11**, it can readily disperse through biogeochemical cycles in air and water systems. Crucially, iodine is biologically essential, and the human body, particularly the thyroid gland, actively accumulates iodine to synthesize thyroid hormones (thyroxine and triiodothyronine). The thyroid gland does not distinguish between stable iodine (^{127}I) and its radioactive isotopes. Consequently, inhaled or ingested radioactive iodine selectively concentrates in the thyroid, where its radioactive decay can damage tissues and significantly increase the risk of thyroid cancer,

especially in children.[65] The combination of its environmental mobility, biological necessity, and long half-life (for ^{129}I) makes effective capture and immobilization obligatory.

Iodine Adsorbents and Separation Techniques

Given the risks, stringent regulations govern the release of radioactive iodine from nuclear facilities. Off-gas treatment systems in reprocessing plants aim to capture volatile iodine species with extremely high efficiency before atmospheric release. Furthermore, stable and durable waste forms are required for the long-term geological disposal of captured ^{129}I.[52, 66, 67] This necessitates the development of adsorbent materials that not only exhibit high capture capacity and selectivity under relevant industrial conditions (e.g., presence of water vapour, NO_x, CO_2) but also allow for the secure immobilization of the captured iodide.

Several classes of materials have been investigated and employed to meet these demanding criteria, each with inherent strengths and weaknesses. These can be broadly categorized into liquid scrubbing systems and solid adsorbents. Furthermore, in **Table 1.1** a summary of different state-of-the-art iodine-capturing adsorbents is shown.

- **Liquid Scrubbing Systems:** Wet scrubbing technologies using caustic solutions, nitric acid, or Mercurex have been considered for capturing iodine. While these systems can be effective for high-concentration streams, their efficiency diminishes significantly for the dilute streams (0.1–0.5 ppm) typical of off-gas waste. Furthermore, these processes often involve highly corrosive liquids, necessitating acid- or alkali-resistant infrastructure and complex procedures for secondary waste disposal.[67]

- **Silver-Impregnated Materials:** Materials functionalized with silver have long been the benchmark for radioactive iodine capture due to the strong chemical affinity between silver and iodine, leading

to the formation of silver iodide (AgI), a thermodynamically stable and poorly soluble compound.[68, 69] Reactions include $2Ag + I_2 \rightarrow 2\,AgI$ and $Ag + CH_3I \rightarrow AgI + CH_3\cdot$ (followed by other reactions). Examples include silver-exchanged zeolites (Ag-mordenite, Ag-ZSM-5), silver nitrate-impregnated silica gel ($AgNO_3/SiO_2$), silver-functionalized aerogels, and silver-doped activated carbons (Ag-AC). The advantage is high affinity and selectivity for various iodine species (I_2, CH_3I), leading to effective chemisorption and high decontamination factors, even in the presence of humidity. The resulting AgI is a relatively stable waste form. The primary drawback of these materials are the high costs and limited availability of silver. The process generates a significant volume of secondary radioactive waste containing silver, complicating final disposal. Furthermore, performance can be negatively impacted by sulfur compounds or high concentrations of NO_x in the off-gas waste stream.

- **Activated Carbons (AC):** Activated carbons are widely available, low-cost porous materials with high surface areas, traditionally used in various adsorption applications.[70] The mechanism behind iodine adsorption on pristine AC is primarily driven by physisorption (van der Waals forces) within the micropores. The capacity is strongly linked to surface area and pore volume but is often significantly reduced under humid conditions due to competitive adsorption of water molecules. Chemical functionalization (e.g., with nitrogen or sulfur groups, or impregnation with agents like triethylenediamine (TEDA)) can enhance interactions and improve performance, particularly for organic iodides. The advantages are low cost, readily available, high initial surface areas. The disadvantage is primarily its nature as a physisorbent for I_2, leading to lower capacity and weaker binding compared to Ag-materials, especially at higher temperatures or humidity. Its performance is further degraded by the presence of NO and NO_2 in off-gas streams, and the potential reaction of carbon with NOx can form unstable,

explosive compounds. Additionally, AC has limited recyclability capabilities.

- **Metal-Organic Frameworks MOFs:** MOFs are crystalline porous materials constructed from metal nodes or clusters linked by organic ligands. Their ultra-high surface areas, tunable pore sizes, and chemically versatile structures have made them attractive candidates for gas storage and separation, including iodine capture.[71] The adsorption mechanism in MOFs can involve both physisorption (driven by high surface area and pore confinement) and chemisorption. Chemisorption can occur via interactions with open metal sites (acting as Lewis acids), specific functional groups on the organic linkers (e.g., N-heterocycles, amine groups), or charge-transfer interactions with the framework. Some MOFs facilitate the formation of polyiodide species (I_3^-, I_5^-) within their pores. The advantages are exceptionally high surface areas, leading to potentially very high gravimetric uptake capacities. Tunability allows for targeted design of pore environments and binding sites. Some MOFs have shown relatively high iodine capacities (1 - 4 g/g) in laboratory settings. The disadvantages for many MOFs are their often insufficient chemical stability, particularly towards hydrolysis (humidity, acidic conditions common in off-gas) and radiolysis. Synthesis can be costly, and scalability remains a challenge for industrial deployment. Long-term stability under operational conditions is often uncertain.

Table 1.1. An overview of different types of iodine adsorption materials under dynamic conditions.

Name	Type	Adsorption Capacity (g/g)	Operating Temp. (°C)	Vapor Conc. (ppmv)	Reference
Ag-Mor	Zeolite	0.17	150	50	[72]
ZSM-5	Zeolite	0.52	75	400	[73]
23Ag/Y	Zeolite	0.22	100	1250	[74]
HKUST-1	MOF	0.38	25	400	[75]
ZIF-8	MOF	0.03	25	400	[75]
TGDM	COF	0.30	150	150	[76]
COF-TAPT	COF	1.25	25	150	[77]
COF-TAPB	COF	1.12	25	150	[77]

Limitations of Current Technologies

While Ag-materials remain the industrial standard due to their effectiveness, their cost and secondary waste issues are significant drivers for alternatives. Carbon-based materials suffer from performance limitations, particularly under process conditions. MOFs offer high capacity but often lack the required stability. This gap highlights the urgent need for robust, cost-effective, and highly efficient adsorbents, potentially offering tunable properties and improved stability – characteristics potentially addressable by Covalent Organic Frameworks.

Rationale for Using COFs for Iodine Capture

COFs possess several intrinsic features that make them highly promising candidates:

- **Permanent porosity and High Surface Area:** Like MOFs, COFs exhibit well-defined pores and high specific surface area (often 500-2500 m^2/g), maximizing the available sites for iodine interaction and accommodation.
- **Structural Pre-designability and Tunability:** The building blocks (monomers) and covalent linkages can be precisely chosen using the principles of reticular chemistry. This allows for fine-tuning of pore size, pore shape, and the chemical environment within the pores to optimize interactions with iodine species.
- **High Stability:** Depending on the covalent linkage chemistry (e.g., boronate esters, imines, triazines, B-O bonds), COFs can exhibit significant thermal and chemical stability, potentially surpassing many MOFs, especially under acidic or humid conditions. Stability under radiation is an area of ongoing investigation, but potentially favourable due to the organic nature.
- **Low Framework Density:** Composed of light elements, COFs have low skeletal densities, leading to high gravimetric adsorption capacities.
- **Metal-free:** COFs offer the possibility of highly efficient metal-free adsorbents, circumventing the cost and secondary waste issues associated with silver for example.

In general, when compared to conventional iodine adsorbents, COFs offer a compelling number of advantages. Their exceptional gravimetric capacities frequently outperform traditional materials.[78, 79] The chemical versatility inherent in COF synthesis allows for tunable affinity, enabling the optimization of specific interactions, including strong

and directional halogen bonds between iodine and the framework, or between iodine and captured anions. This tunability can also lead to high selectivity towards iodine over other gases like N_2 or CO_2, although selectivity against water vapor requires systematic investigation; N- and S-rich sites involved in halogen bonding are generally less hydrophilic than the open metal sites found in many MOFs. Furthermore, the robust covalent linkages in well-designed COFs have significant chemical and thermal stability, which is crucial for demanding operational conditions. Many COFs have demonstrated good regenerability through solvent washing or mild heating, and their entirely organic, metal-free design avoids reliance on expensive and problematic silver.

Mechanisms of Iodine Adsorption in COFs

Iodine (I_2) adsorption in COFs is a multifaceted process, often involving a synergistic interplay of several types of interactions. Physisorption, driven by Van Der Waals forces between iodine molecules and the extensive surface of the COF, contributes significantly, particularly at lower partial pressures or temperatures. This effect is amplified in appropriately sized micropores (< 2 nm) due to enhanced potential field overlap, a phenomenon known as the confinement effect.[80–82] Larger mesopores (2-50 nm) can accommodate greater quantities of iodine through multilayer adsorption.

Beyond physisorption, strong directional interactions, notably halogen bonding (XB), play a pivotal role in enhancing iodine capture specificity and strength.[83–86] Molecular iodine (I_2) is a potent halogen bond donor, possessing electrophilic regions (often termed σ-holes) located on its terminal atoms along the axis of the I-I bond. These electrophilic regions can engage in attractive, non-covalent interactions with Lewis basic sites within the COF framework, which act as halogen bond acceptors. Consequently, deliberately incorporated nitrogen-rich functionalities, such as N-heterocycles (e.g., pyridine, pyrimidine units within linkers)

and even the imine linkages (-C=N-) themselves, readily participate in N···I halogen bonds. Similarly, sulfur-containing functionalities like thioether or thiophene groups form robust S···I halogen bonds. The lone pairs on heteroatoms can transfer to the σ^* antibonding orbital of iodine to form charge-transfer complexes. The partial negative charge on the iodine atoms due to this electron transfer facilitates the formation of polyiodide ions, which are then fixed in place.[78] Oxygen-containing groups, if sufficiently Lewis basic (e.g., in ethers or carbonyls within some linkers), can also act as weaker XB acceptors. Extended π-conjugated systems within the COF structure (e.g., naphthalene, anthracene, carbazole units) can also serve as halogen bond acceptors, leading to π···I interactions, generally weaker than those involving heteroatom lone pairs but significant due to their prevalence in conjugated frameworks.

The scope of halogen bonding extends to interactions with anionic species, which can be particularly strong halogen bond acceptors. If halide counteranions (X^-, such as Cl^-, Br^-, or I^-) are present within the COF pores (e.g., in cationic COFs or due to co-adsorbed species), they can interact with molecular iodine (I_2) to form polyhalide or mixed polyhalide anions ($[I_2X]^-$).[87–89] Specifically, the iodide anion (I^-) is a potent halogen bond acceptor for I_2, leading to the well-known formation of the triiodide ion (I_3^-) via an $I_2 \cdots I^-$ interaction. This process, along with subsequent reactions to form higher polyiodides like I_5^- ($2\ I_2 + I^- \leftrightarrow I_5^-$), can significantly enhance the total iodine uptake capacity. Similar interactions can occur with Br^- to form $[I_2Br]^-$ or with Cl^- to form $[I_2Cl]^-$, with the stability and prevalence of these species depending on the specific conditions and anion availability. The formation of these polyhalide species, initiated by such anion-iodine halogen bonds, is crucial for achieving very high iodine loadings and fast adsorption kinetics. These polyhalides are often strongly bound and stabilized within the COF pores, particularly in frameworks designed with cationic charges that provide electrostatic attraction for the resultant anions.

A qualitative comparison of halogen bond strengths relevant to iodine capture in COFs can be interpreted as follows. Generally, halogen bonds formed between I_2 (as the XB donor) and anionic acceptors (X^-) are significantly stronger than those formed with neutral Lewis basic sites within the COF framework, owing to the enhanced electrostatic contribution in the former. Among the halide anions acting as XB acceptors for I_2, the strength typically follows the order of their Lewis basicity and polarizability: $I^- > Br^- > Cl^-$. Thus, the $I_2 \ldots I^-$ interaction leading to I_3^- is generally the most robust among these simple halide-iodine adducts. For neutral XB acceptors within the COF structure, sulfur-containing sites (e.g., thioethers) tend to form stronger halogen bonds with I_2 compared to nitrogen-containing sites (e.g., pyridines, imines). This is often attributed to better orbital energy matching and the higher polarizability of sulfur (a softer Lewis base, interacting favorably with the soft Lewis acid I_2). Oxygen-containing Lewis basic sites typically form weaker halogen bonds than nitrogen or sulfur sites. π-systems, while capable of acting as XB acceptors, generally result in weaker interactions compared to heteroatoms with distinct lone pairs. These relative strengths guide the design of COF functionalities for targeted iodine affinity.

Design Strategies for Enhancing Iodine Capture

The inherent tunability of COFs allows researchers to employ a variety of sophisticated design strategies to maximize iodine adsorption performance. A primary approach involves pore engineering, where pore sizes are tailored to match the dimensions of iodine species (kinetic diameter of I_2 is ~0.5 nm) to enhance confinement effects and optimize packing density. The creation of hierarchical pore structures, combining micropores for strong binding and mesopores for rapid diffusion, is also a promising avenue.

The most extensively explored strategy is the incorporation of iodinephilic functional groups, which often serve as potent halogen bond ac-

ceptors for molecular iodine, leveraging the strength hierarchy discussed previously. This involves synthesizing COFs from monomers containing moieties known for their strong iodine affinity. Given their efficacy, sulfur-containing groups (e.g., thioether linkages or thiophene-based monomers) are highly sought after for their ability to form strong S···I halogen bonds.[90] Nitrogen heterocycles are also frequently used, leading to materials like imine COFs functionalized with pyridine or bipyridine units, designed to maximize N···I halogen bonding.[91, 92] COFs built from highly electron-rich π-systems with components like tetrathiafulvalene (TTF), leverage their capacity to act as π-electron halogen bond acceptors or engage in broader charge-transfer interactions with iodine.[93] The density and accessibility of these purposefully introduced sites are crucial for achieving high performance.

Another effective design involves creating charged frameworks. COFs synthesized to possess permanent positive charges, typically by incorporating quaternary ammonium groups, provide strong electrostatic binding sites for various polyhalide anions ($[I_2X]^-$, including I_3^-, I_5^-) themselves often formed via initial halogen bonding between I_2 and precursor halide anions, resulting in exceptionally high capacities.[76]

Furthermore, beyond the direct functionalization of building blocks, the choice of linkage chemistry employed to construct the COF backbone is a pivotal design parameter with profound implications for iodine capture. The nature of the covalent bonds (e.g., imine, triazine, β-ketoenamine, amide, or post-synthetically modified linkages like thiazole) not only dictates the overall chemical and thermal stability of the framework, a critical factor for deployment in harsh environments, but also intrinsically shapes the pore's electronic environment. For instance, imine (-C=N-) linkages can themselves act as modest halogen bond acceptors due to the lone pair on nitrogen, contributing to the overall iodine affinity, although their reversibility can sometimes compromise stability under certain conditions. Conversely, highly robust linkages like those forming triazine rings or thiazole units (often obtained via post-synthetic modifi-

cation) might offer exceptional stability, potentially at the cost of direct participation in binding, thereby shifting the focus of iodine interaction entirely to the functional groups on the building blocks. The inherent polarity and electron-donating/withdrawing character of the linkage can also modulate the Lewis basicity of adjacent functional groups and influence the framework's overall polarizability, thereby tuning the strength of halogen bonding and charge-transfer interactions with iodine. Thus, a judicious selection of linkage chemistry is essential for balancing framework robustness and synthetic accessibility with the creation of optimal host-guest interactions for effective iodine sequestration.

Performance Under Application-Relevant Conditions

Numerous studies have demonstrated the potential of COFs for gas-phase iodine capture, initially often highlighted by remarkable static (equilibrium) uptake capacities. Nitrogen-rich COFs, including various triazine-based structures (e.g., CTF-1) and imine-linked COFs functionalized with pyridine or bipyridine moieties, have consistently shown high static iodine uptakes, frequently reported in the range of 50-500 wt% (gram I_2 per gram COF). These capacities are largely attributed to the effective N···I halogen bonds facilitated by the accessible nitrogen sites.[94, 95] Similarly, sulfur-containing COFs, constructed with thioether linkages or thiophene-based monomers, have exhibited even more significant iodine affinity in static tests, with some materials achieving capacities exceeding 600 wt%, underscoring the strength of S···I halogen bonding. Electron-rich COFs, such as those based on tetrathiafulvalene (TTF), also owe their capacity due to charge-transfer interactions and as π-electron halogen bond acceptors to achieve high static uptake levels.[93, 96]

However, for practical application in off-gas treatment, performance under dynamic flow conditions and in the presence of humidity is of paramount importance. Consequently, an increasing number of studies

are evaluating COFs using breakthrough experiments, where a continuous stream of iodine gas is passed through a packed bed of the adsorbent. These tests provide crucial data on dynamic binding capacity (DBC), which is the amount of iodine captured before it is detected in the effluent, and the sharpness of the breakthrough curve, indicative of adsorption kinetics and mass transfer efficiency. For instance, select N-rich or S-rich COFs have demonstrated good dynamic performance, maintaining a significant fraction of their static capacity under flow, with sharp breakthrough fronts suggesting efficient iodine removal. Some COFs have also been subjected to multiple adsorption-desorption cycles in dynamic setups, showing good retention of capacity and structural integrity, which is vital for regenerable systems.[77, 97, 98]

The influence of humidity on gas-phase iodine uptake is another critical factor, as industrial off-gas streams invariably contain moisture. Water molecules can competitively adsorb on material surfaces or block pores, potentially reducing iodine capture efficiency. Research has shown that the hydrophobicity of the COF framework plays a significant role.[77] COFs designed with hydrophobic backbones or pore surfaces tend to exhibit better resistance to humidity, maintaining high iodine uptake even at elevated relative humidity (RH) levels (e.g., >70-90% RH). In contrast, more hydrophilic COFs, or those with easily hydrolyzable linkages, might show a more pronounced decrease in performance in moist air. Nevertheless, COFs with exceptionally strong and specific iodine binding sites (e.g., potent halogen bond donors/ acceptors) can sometimes overcome the competitive effects of water, retaining good iodine affinity even if the framework itself is not overtly hydrophobic. At high temperatures, the competition effect with water is less pronounced; it was previously reported that high temperatures suppress the competitive adsorption of water.[99] The development of COFs that demonstrate robust iodine capture across a wide range of humidity levels remains a key objective.

Regarding organic iodides, which are also volatile components of nuclear off-gases, research continues to explore COF capabilities. While

the majority of studies focus on elemental I_2, some COFs, particularly those with quaternized amine sites or specific pore architectures, are being investigated for the capture of methyl iodide (CH_3I) from the gas phase, though capacities and dynamic performance for organic iodides generally lag behind those for I_2 and require further dedicated material design.[52, 97, 100]

In addition to gas-phase capture, COFs have also demonstrated significant potential for sequestering iodine species from aqueous environments, which is crucial for remediating contaminated water or treating certain industrial liquid effluents. In these scenarios, iodine may be present as dissolved molecular iodine (I_2), iodide (I^-), or triiodide (I_3^-) and other polyiodides (e.g., in I_2/KI solutions). Cationic COFs, featuring permanent positive charges within their frameworks (e.g., from quaternary ammonium or imidazolium groups), have shown exceptional efficacy in capturing anionic iodine species like I^- and particularly I_3^- from water.[79] This occurs through strong electrostatic interactions and ion exchange mechanisms, leading to reported capacities that can be extremely high, sometimes exceeding several grams of iodine per gram of COF, along with rapid uptake kinetics and good selectivity against common competing anions like Cl^- or SO_4^{2-}. Neutral COFs functionalized with potent halogen bond acceptor sites (e.g., N- or S-moieties) have also been investigated for extracting dissolved I_2 from aqueous solutions or interacting with I_3^- species. While the direct capture of I_2 from pure water is limited by its low solubility, these COFs show promise in solutions where I_2 or I_3^- concentrations are higher. The ability to regenerate these COFs after aqueous capture (e.g., by solvent washing or displacement) and their long-term stability in aqueous media, including varying pH conditions, are key areas of ongoing research for practical water remediation applications. The mechanisms often involve a combination of physisorption, halogen bonding between I_2 and the COF, and for cationic COFs, the strong electrostatic binding of I_3^- or other polyiodide anions formed through the halogen bonding of I_2 with I^- or other available halide anions.

1.2.2 Gold Adsorption

Gold Recovery from Electronic Waste

Gold (Au) remains a cornerstone of modern technology and global economies due to its unique physical and chemical properties, including exceptional conductivity, resistance to corrosion, and catalytic activity. While traditional mining addresses a portion of the global demand, the declining grades of primary ores, coupled with the significant environmental and social impacts of conventional mining, have intensified the search for sustainable secondary gold resources. Among these, end-of-life electronic components, particularly Central Processing Units (CPUs) from discarded computers, servers, and consumer electronics, represent a highly concentrated and rapidly growing "urban mine". Efficiently recovering gold from this complex e-waste stream is not only economically attractive but also crucial for resource conservation and mitigating the environmental burden of hazardous waste disposal.[101–103]

CPUs contain gold in various forms, including bonding wires, plated contacts, and layers within the intricate circuitry. The sheer volume of e-waste generated globally, tens of millions of tonnes annually, with CPUs being a key valuable fraction, translates to a substantial untapped reservoir of gold. However, CPUs are complex assemblies of metals (Cu, Pd, Pt, Ni, Pb, Al, Fe), ceramics, and plastics. Recovering gold necessitates sophisticated processes that can selectively extract it from this heterogeneous matrix. Improper disposal or rudimentary recycling methods for e-waste, especially in informal sectors, lead to the loss of valuable resources and the release of hazardous substances (heavy metals, flame retardants) into the environment, posing severe health and ecological risks. Therefore, developing advanced, selective, and environmentally sound methods for gold recovery from CPUs is a pressing technological and societal need.[104]

Limitations of Conventional Methods

Adapting conventional hydrometallurgical techniques for gold recovery from CPU waste presents specific challenges. Pyrometallurgical methods (smelting) can recover gold but are energy-intensive, may generate toxic emissions if not properly controlled, and often require large, centralized facilities.[105] Hydrometallurgical routes, involving leaching followed by recovery from solution, are generally preferred due to their selectivity and lower energy requirements during processing.[106, 107] However, the leaching process itself often uses aggressive and hazardous chemicals. For instance, while cyanidation is effective for gold, its application to e-waste is complicated by the presence of other metals that consume cyanide (like copper) and the extreme toxicity of cyanide, necessitating stringent environmental controls and detoxification steps, which are often costly and complex for diverse e-waste streams.[108] Chloride-based leaching using agents like aqua regia or solutions containing $HCl/FeCl_3$ can effectively dissolve gold from CPUs as $[AuCl_4]^-$, but these lixiviants are highly corrosive and generate acidic leachates containing a complex mixture of dissolved metals, making selective gold recovery difficult.[109]

Once gold is in solution, conventional recovery methods such as activated carbon adsorption, ion exchange, and solvent extraction face limitations when applied to CPU waste leachates. These include poor selectivity in the presence of high concentrations of competing metals (especially copper), susceptibility to fouling from residual organics or particulates from dissolved PCBs, the high cost of some selective reagents, and the generation of secondary waste streams that require further treatment. This context underscores the urgent need for advanced adsorbent materials that can offer high capacity, exceptional selectivity for gold from complex multi-elemental CPU leachates, operational stability in aggressive media, and sustainable regeneration pathways. The shortcomings of established techniques underscore the urgent need for advanced adsorbent materials that possess a combination of high capacity, exceptional selectivity (especially in complex matrices such as e-waste leachates), rapid kinetics,

and good stability under harsh leaching conditions, including low pH or high salinity. A summary of different adsorbent materials and their adsorption properties for gold is represented in **Table 1.2**. Furthermore, facile and sustainable regeneration, alongside overall cost-effectiveness, are critical attributes for the next generation of gold recovery agents capable of handling diverse leachates, including those from emerging, milder leaching processes.[110–112]

Table 1.2. An overview of the best-performing gold adsorption materials.

Name	**Type**	**Capacity** (mg/g)	**Rate coeff.** (k_2) (g/mg/min)	**Regeneration Cycles**	**Reference**
Coconut CIP	Carbon	37	/	0	[113]
Amberjet	IX resin	97	0.095	2	[112]
NH_2-MCM-41	Silica	275	/	4	[114]
UiO-66-$(OH)_2$	MOF	1570	7.3×10^{-3}	5	[115]
M-Cu-BDC-NH2	MOF	1194	4×10^{-3}	30	[116]
JNU-1	COF	1124	1.04	4	[117]
N^+-PYTA-PATA	COF	1834	4.73×10^{-4}	10	[118]
$TpTG_{Cl}$	COF	1895	9.69×10^{-5}	3	[119]

Gold in CPU Waste Leachates

The chemical form of dissolved gold from CPUs depends heavily on the leaching process:

- **Chloride Leaching:** This is a common approach for e-waste. When using aqua regia or other strong chloride-based oxidizing systems (e.g., HCl–H_2O_2, HCl–NaOCl), gold is typically oxidized to Au(III) and stabilized as the tetrachloroaurate(III) anion, $[AuCl_4]^-$.[120] These leachates are highly acidic and will contain high concentrations of other dissolved metals from the CPU, such as copper

(as Cu^{2+} or chloro-complexes), nickel (Ni^{2+}), iron ($Fe^{2+/3+}$), aluminum (Al^{3+}), tin ($Sn^{2+/4+}$), lead (Pb^{2+}), and other precious metals like silver (Ag^{+}) and palladium (Pd^{2+} as $[PdCl_4]^{2-}$), all presenting a significant challenge for selective gold recovery.

- **Cyanide Leaching:** If cyanide is used, gold will form the dicyanoaurate(I) complex, $[Au(CN)_2]^-$. The presence of abundant copper in CPUs would lead to high cyanide consumption and the formation of various copper-cyanide complexes, complicating gold recovery.[108]

- **Alternative Systems:** To address environmental concerns and potentially improve selectivity, various "greener" or milder lixiviants are being researched for e-waste. Thiosulfate leaching ($S_2O_3^{2-}$), for instance, forms anionic gold(I) thiosulfate complexes ($[Au(S_2O_3)_2]^{3-}$), while thiourea ($CS(NH_2)_2$) in acidic media forms cationic gold(I) thiourea complexes ($[Au(CS(NH_2)_2)_2]^+$).[121, 122] Another innovative approach gaining attention for e-waste, including CPUs, involves the use of N-Bromosuccinimide (NBS) as an oxidant in conjunction with pyridine.[123] This system operates under relatively mild conditions compared to aqua regia and avoids the use of free cyanide. Pyridine acts as both a base and a complexing agent for gold, which is typically solubilized as a gold-pyridine complex, potentially as a cationic species like $[Au(py)_2]^+$ or a neutral/anionic bromo-pyridine mixed-ligand complex depending on the exact stoichiometry and conditions. The resulting gold species from these alternative systems present different chemical targets for subsequent recovery steps compared to the common chloro- or cyano-complexes, and their stability and co-leached impurities are subjects of active investigation.

Gold Extraction Methods

- **Activated Carbon (AC) Adsorption:** While activated carbon is a workhorse in primary gold mining for adsorbing $[Au(CN)_2]^-$, its application to CPU waste leachates faces considerable hurdles. The primary mechanism, often involving ion-pair adsorption or weak physisorption, offers poor selectivity for gold when numerous other metal complexes are present in high concentrations, as is typical for e-waste leachates.[124] Copper, in particular, if present as a cyanide complex, strongly competes with gold for adsorption sites on AC. Furthermore, organic compounds leached from the plastic components of CPUs or reagents used in pre-treatment can foul the AC pores, reducing its efficiency. While elution and thermal regeneration are established processes, the energy cost and the non-selective nature of AC make it less appealing as a primary recovery agent for gold from complex CPU leachates without extensive pre-purification.

- **Ion Exchange (IX) resins:** Ion exchange resins, particularly strong base anion (SBA) exchangers with quaternary ammonium groups or weak base anion (WBA) exchangers with amine functionalities (protonated at lower pH), can theoretically adsorb anionic gold complexes like $[AuCl_4]^-$ or $[Au(CN)_2]^-$. They can offer higher capacities and faster kinetics than AC. However, the key challenge in the context of CPU waste is achieving high selectivity for gold over the myriad of other anionic chloro- or cyano-complexes of base metals (e.g., $[FeCl_4]^-$, $[CuCl_3]^-$) or other anions present in the leachate. Many commodity IX resins exhibit poor selectivity, leading to rapid saturation with impurities and low gold purity in the eluate. Specialized, gold-selective resins have been developed, but they are often more expensive. Fouling of resins by organic matter or precipitated solids from the complex leachate, and the need for efficient elution and regeneration using specific chemical agents

(e.g., zinc cyanide), also add to the operational complexity and cost when processing CPU-derived solutions.[125]

- **Solvent Extraction (SX):** Solvent extraction can achieve high selectivity and purity in gold recovery and is used in some gold refining operations. For CPU waste leachates, extractants like certain amines (e.g., Alamine 336 for $[AuCl_4]^-$) or organophosphorus compounds (e.g., TBP, Cyanex 923 for $[AuCl_4]^-$) dissolved in an organic diluent can be used.[126] The process typically involves extraction, scrubbing (to remove co-extracted impurities like iron), and stripping stages to obtain a concentrated, purified gold solution. However, SX is capital-intensive and involves the handling of large volumes of organic solvents, which raises environmental concerns regarding solvent losses (volatilization, entrainment, degradation) and worker exposure. The presence of surfactants or fine particulates in CPU leachates can also lead to stable emulsions, complicating phase separation and reducing efficiency.[111]

- **Other Adsorbent Materials:** Research continues into alternative adsorbents for gold recovery from e-waste. Biomass-derived materials (e.g., treated algae, chitosan, agricultural residues) offer a low-cost, potentially sustainable option, utilizing functional groups like amines, carboxyls, and thiols for gold binding, sometimes via bioreduction.[127–129] However, they often suffer from low capacities, recyclability issues, and limited chemical stability. Functionalized silica materials, with gold-specific ligands (e.g., mercaptopropyl groups) grafted onto silica supports, provide better-defined binding sites and higher surface areas.[130] While offering good potential, the cost of functionalization and the stability of these organic ligands under aggressive leaching conditions typical for CPU waste can be limiting. Metal-Organic Frameworks (MOFs) have also been explored, showcasing high surface areas and tunable functionalities for gold capture, sometimes including reductive precipitation of Au(0). However, as with iodine capture, the chemical stability

of many MOFs in the highly acidic or complexing environments of CPU leachates remains a significant barrier to their practical application.[131, 132]

COFs for Gold Recovery from E-waste Leachates

The inherent limitations of these conventional methods when applied to the unique challenges of CPU waste, particularly the need for extreme selectivity in highly concentrated multi-metal acidic leachates, robustness, and cost-effective, environmentally sound operation, drive the urgent search for novel adsorbent platforms. Covalent Organic Frameworks, with their potential for precisely engineered selectivity and stability, are emerging as promising candidates to fill this technological gap.

The application of COFs to gold recovery from CPU waste is compelling due to several key attributes. Their tailor-made binding sites allow for the strategic incorporation of chemical functionalities with high affinity and selectivity specifically for gold species (predominantly $[AuCl_4]^-$ in many CPU leachates) over common interfering ions like Cu(II), Fe(III), Ni(II), and Al(III).[133] The inherent high surface area and accessible, ordered pores of COFs maximize the contact between the leachate and these active sites, promoting rapid adsorption kinetics and potentially high gold loading capacities, even from dilute solutions. Furthermore, carefully chosen robust covalent linkages can impart COFs with significant chemical stability, enabling them to withstand the highly acidic and oxidative conditions often employed in the leaching of CPUs. The crystalline and well-defined structure of COFs facilitates a deeper understanding of adsorption mechanisms, guiding the rational design of next-generation materials with enhanced performance for this specific application. The potential for COFs to act as reductive frameworks, converting captured Au(III) ions directly into easily recoverable metallic gold Au(0), also offers an attractive simplification to the overall recovery process.[134]

Advantages of COFs for Gold Recovery

- **Exceptional Selectivity Potential:** The ability to molecularly design binding sites specific for gold ($[AuCl_4]^-$ or other species) over abundant base metals in CPU leachates.
- **High Adsorption Capacity:** Their porous nature and high density of functional sites can lead to very high gold loadings per unit mass of adsorbent.
- **Chemical Stability in Harsh Media**: Appropriately chosen linkages can render COFs stable in the highly acidic and oxidative conditions characteristic of CPU leachates, where many other porous materials degrade.
- **Rapid Adsorption Kinetics:** Ordered porosity facilitates efficient mass transport of gold species to the active binding sites.
- **Tunable Reductive Capabilities:** COFs can be designed to not only adsorb gold ions but also reduce them to metallic gold, simplifying downstream processing.
- **Well-Defined Structures for Mechanistic Studies:** The crystallinity of COFs allows for a clearer understanding of host-guest interactions, enabling more rational design improvements.

Mechanisms of Gold Adsorption/Reduction by COFs

When interacting with CPU waste leachates, which typically contain gold as $[AuCl_4]^-$ in acidic, multi-elemental solutions, COFs can engage gold via several mechanisms:

- **Chelation/Coordination:** This is a primary strategy. COFs functionalized with strong Lewis basic ligands, particularly those containing soft donor atoms like sulfur (e.g., thiols, thioethers, thioureas) or specific nitrogen functionalities (e.g., certain amines,

pyridines, imines), can directly coordinate to the Au(III) center in $[AuCl_4]^-$.[135–137] Gold(III) is a soft acid and preferentially binds to soft bases. These interactions can lead to the displacement of one or more chloride ligands, forming strong coordinate bonds with the COF framework. The selectivity arises from the higher affinity of these carefully chosen ligands for gold compared to other base metals present in CPU leachates.

- **Ion Exchange:** While less common for targeting $[AuCl_4]^-$ with standard cationic COFs unless specifically designed with very high charge density or unique binding pockets, if gold were present as other anionic complexes (e.g., from alternative lixiviants or if $[AuCl_4]^-$ forms outer-sphere ion pairs), COFs with positively charged frameworks (e.g., containing quaternary ammonium groups) could bind them electrostatically. However, selectivity would be a major challenge in highly saline CPU leachates.[138]

- **Reductive Adsorption:** This mechanism is highly attractive as it directly yields pure, metallic gold (Au(0)). The process is a spontaneous redox reaction governed by the standard reduction potential (E^0). For a COF to reduce the gold complex ($[AuCl_4]^-$, with $E^0 = +1.002\,V$), its own functional groups must have a lower reduction potential, which creates the thermodynamic driving force for electron transfer. This reduction occurs via two main pathways: direct chemical reduction. Electron-rich COFs, especially those with sulfur or nitrogen moieties, have the intrinsic ability to donate electrons directly to the gold ions. A second pathway is photocatalytic reduction; photo-active COFs use light energy to generate excited electrons that reduce the gold. This process is often made more efficient by adding a sacrificial electron donor. In both cases, the resulting Au(0) precipitates as nanoparticles within the COF, which also acts as a stabilizing matrix. [139–141]

Design Strategies of COFs for Gold Recovery

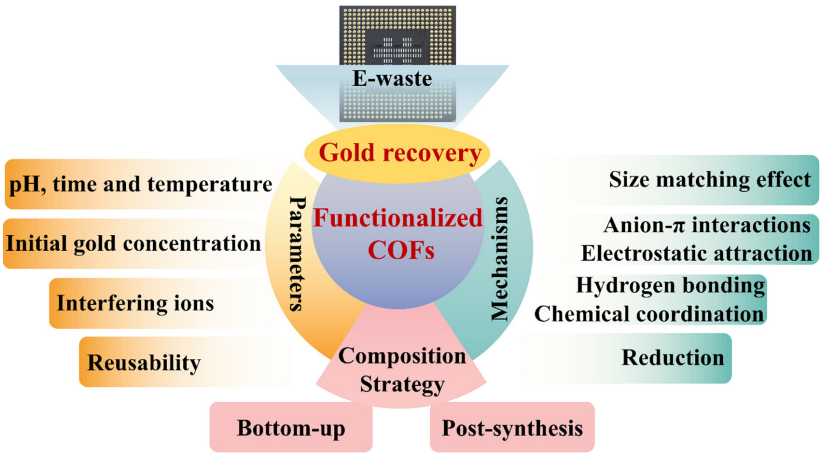

Figure 1.12. An overview of the strategies and parameters that are important in the development of COFs for gold recovery from electronic waste.[134]

The development of Covalent Organic Frameworks for the challenging task of gold recovery from CPU waste leachates is guided by rational design principles aimed at maximizing both efficacy and selectivity. These strategies inherently leverage and realize the key advantages that COFs offer over conventional materials.

A paramount strategy is the functionalization with specific ligands to achieve a high selectivity for gold. By incorporating monomers bearing moieties with high affinity for gold species (such as $[AuCl_4]^-$ or other complexes derived from CPU leaching) over the plethora of interfering ions (Cu, Ni, Fe, Al, Sn, Pb, Ag, Pd), COFs can be endowed with a remarkable selectivity potential. Sulfur-containing ligands, including thiols (-SH), thioethers (-SR), dithiocarbamates, and thioureas, are highly favored due to the formation of strong Au-S coordinate bonds, reflecting gold's soft acid character.[136, 142] Similarly, nitrogen-based ligands, particularly those offering specific chelating geometries like polyamines or appropriately configured N-heterocyclic groups (e.g., imidazole, pyridine), are explored for their strong coordination to gold.[143] The precise molecu-

lar engineering of these binding sites within the COF's ordered structure not only enhances selectivity but also contributes to high adsorption capacities, as these sites can be incorporated at high density throughout the porous material.

The ability to create redox-active frameworks is another significant design approach that translates into a distinct advantage. By selecting electron-rich building blocks (e.g., based on hydroxyls or amines) or designing specific redox-active linkages, COFs can be engineered to selectively reduce Au(III) from solution to Au(0).[139, 144] This tunable reductive capability is highly advantageous as it can lead to the direct precipitation of metallic gold nanoparticles within the COF pores, potentially simplifying downstream recovery and yielding a high-purity product. This in-situ reduction can also enhance selectivity if the COF's redox potential is carefully matched to that of gold relative to other co-existing metals.

The choice of linkage chemistry is fundamental to the practical utility of COFs in aggressive CPU waste leachates. Selecting robust covalent bonds such as thiazoles, β-ketoenamines, triazines, or certain amides/imides is critical for ensuring the COF's chemical stability in harsh media. This intrinsic stability allows COFs to maintain their structural integrity and adsorption performance in acidic, oxidative, or complexing environments where many other porous materials, including some MOFs and functionalized silicas, might degrade. This robustness is key for sustained operation and potential reusability. Moreover, the linkage chemistry also influences the electronic properties and geometry of the pores, further tuning the COF's interaction with gold species.

Control over the pore environment, including pore size, polarity (hydrophilicity/hydrophobicity or organophilicity for non-aqueous leachates like N-bromosuccinimide (NBS)/pyridine systems), and the development of hierarchical porosity (combining micropores and mesopores), directly impacts performance. Well-defined, accessible pores contribute to rapid adsorption kinetics by facilitating efficient mass transport of the gold complexes to the active binding sites within the framework.

Micropores can enhance binding strength and selectivity through confinement effects, while mesopores can improve diffusion rates, especially for bulkier gold complexes or in viscous media. This careful engineering of porosity complements the chemical functionalization to maximize both the rate and extent of gold uptake.

Furthermore, the design of charged frameworks offers another avenue for targeted gold recovery. Depending on the speciation of gold, anionic complexes like $[AuCl_4]^-$ or potentially cationic complexes like $[Au(py)_2]^+$ from NBS/pyridine leaching, COFs can be synthesized with either cationic or anionic backbones, respectively. For instance, cationic COFs featuring quaternary ammonium groups can effectively sequester $[AuCl_4]^-$ via ion exchange, while theoretically, anionic COFs could target cationic gold species, although this is less explored for gold.[119, 145] This targeted electrostatic interaction contributes to both capacity and selectivity.

Collectively, these design strategies are underpinned by the well-defined, crystalline structures of COFs, which allow for detailed characterization and a fundamental understanding of structure-property relationships and host-guest interactions. This facilitates rational design and iterative improvement of materials. Finally, as solid adsorbents, COFs offer the practical advantage of facile solid-liquid separation from the treated leachate, simplifying the overall recovery process compared to techniques like solvent extraction (**Table 1.3**). These combined attributes underscore the significant potential of COFs as advanced materials for selective and efficient gold recovery from challenging CPU waste streams.

Name	Au(III) conc. (ppm)	Leaching agent	Removal (%)	Reference
CF-COF	8.92	Aqua regia	90.3	[119]
Ionic-COF-Cl	18.92	Aqua regia	99.0	[145]
Tp-BTD-AA	3.67	NBS/pyridine	97.8	[146]
Ty-Hz COF	81.80	Aqua regia	89.1	[147]

Table 1.3. Comparison of gold removal from real and simulated electronic waste leachates with COFs.

Case Studies and Examples

Research into COFs for gold recovery has increasingly focused on demonstrating efficacy in contexts relevant to e-waste, particularly CPU leachates. Many studies utilize simulated leachates containing Au(III) (as $[AuCl_4]^-$) alongside high concentrations of typical interfering ions such as Cu(II), Ni(II), Fe(III), and Al(III). Sulfur-rich COFs have emerged as standout candidates. For example, COFs constructed with thioether-functionalized linkers or by incorporating thiophene units have demonstrated exceptionally high adsorption capacities for gold (often >1000 mg/g in optimal conditions) from acidic chloride media, coupled with remarkable selectivity.[139, 142] The strong covalent-like Au-S interaction allows these COFs to preferentially bind gold even when competing base metals are present in vast excess. The adsorbed gold can often be eluted using acidic thiourea, allowing for COF regeneration. Nitrogen-functionalized COFs, especially those incorporating chelating polyamine chains or strategically placed N-heterocyclic groups capable of coordination, have also shown promise for selective gold capture from acidic solutions, though their selectivity against copper can sometimes be a challenge if the nitrogen sites are not optimally configured for gold.[143, 144, 148]

COFs designed for reductive adsorption have successfully demonstrated the precipitation of Au(0) nanoparticles from $[AuCl_4]^-$ solutions (**Figure 1.13**). For instance, COFs based on electron-donating units like tetrathiafulvalene (TTF) or thiadiazole have shown the ability to reduce Au(III) to Au(0) either directly or under photoirradiation, with the gold nanoparticles forming within the COF pores.[140, 146] This approach is attractive as it yields metallic gold directly, but controlling nanoparticle size and preventing pore blockage are important considerations. Selectivity in the reduction step is also critical.

Performance evaluation in these studies emphasizes not only the maximum adsorption capacity (q_m) and adsorption kinetics but, critically for e-waste, the selectivity in multi-metal systems. This is often quantified using distribution coefficients (K_d) and selectivity coefficients. Furthermore, the stability of the COF in highly acidic media (e.g., pH < 1) and its reusability over multiple adsorption-elution cycles are key metrics. While many promising results have been obtained in batch studies with simulated solutions, a growing number of investigations are focusing on performance in actual e-waste leachates and under continuous flow conditions to better assess practical viability.

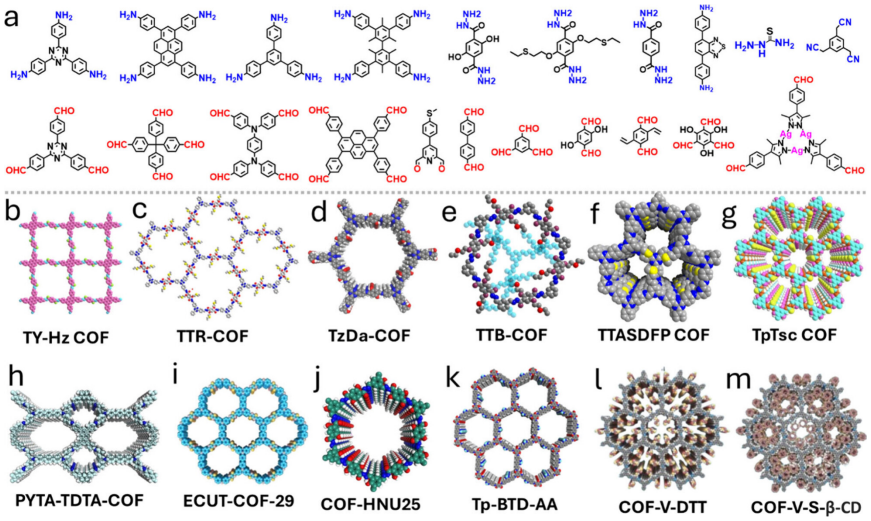

Figure 1.13. An overview of a) linkers and b-m) COFs used for gold recovery.[149]

1.2.3 Thesis Outline

In **chapter 1**, we lay the groundwork by discussing the origins of porous materials and the fundamental concept of porosity. Subsequently, the focus shifts to Covalent Organic Frameworks (COFs), highlighting the synthetic challenges, particularly for imine-linked systems. The chapter then explores post-synthetic modification strategies, detailing how imine linkages can be transformed into imidazopyridinium or thiazole structures to achieve enhanced material properties compared to their precursors. Concluding this section, the critical role of advanced adsorbents, such as COFs, is emphasized, particularly for addressing pressing needs in iodine sequestration from nuclear waste streams and gold recovery from electronic waste.

In **chapter 2**, we address the challenges of iodine management, specifically its capture from nuclear waste streams under demanding industrial conditions and its removal from water post-disinfection. Recognizing the limitations of conventional adsorbents, this work develops and evaluates

a novel imidazopyridinium-based COF from a picolinaldehyde imine COF as a precursor.

In **chapter 3**, we address the urge for materials that could selectively capture gold from electronic waste leachates, which is a critical step towards sustainable resource management. Addressing the significant limitations of conventional gold extraction methods, we explore a tailored COF-based approach. We synthesize pyrene-based and triazolo-based imine COFs and leverage their extended π-conjugated systems, followed by their post-synthetic modification (PSM) into more robust and functional thiazole-linked COFs. The incorporation of thiazole linkages is strategically designed to introduce sulfur atoms as additional binding sites for Au(III). Next to these additional binding sites, thiazole linkages should improve the robustness and photophysical properties of the COFs.

References

1. Das, S., Heasman, P., Ben, T. & Qiu, S. *Porous Organic Materials: Strategic Design and Structure-Function Correlation* Feb. 2017.
2. Day, G. S., Drake, H. F., Zhou, H. C. & Ryder, M. R. *Evolution of porous materials from ancient remedies to modern frameworks* Dec. 2021.
3. Wang, A., Ma, Y. & Zhao, D. *Pore engineering of Porous Materials: Effects and Applications* Aug. 2024.
4. Khan, I., Altaf, A., Sadiq, S., *et al. Towards sustainable solutions: Comprehensive review of advanced porous materials for CO capture, hydrogen generation, pollutant degradation, and energy application* Mar. 2025.
5. Hutt, J. T. & Aron, Z. D. Efficient, Single-Step Access to Imidazo[1,5-a]pyridine N-Heterocyclic Carbene Precursors. *Organic Letters* **13,** 5256–5259 (Oct. 2011).
6. Fauchet, P. M. Photoluminescence and electroluminescence from porous silicon. *Journal of Luminescence* **70,** 294–309 (1996).
7. White, R. J., Budarin, V., Luque, R., Clark, J. H. & Macquarrie, D. J. Tuneable porous carbonaceous materials from renewable resources. *Chemical Society Reviews* **38,** 3401–3418 (2009).
8. Geng, K., He, T., Liu, R., *et al.* Covalent organic frameworks: design, synthesis, and functions. *Chemical reviews* **120,** 8814–8933 (2020).
9. Tan, L. & Tan, B. *Hypercrosslinked porous polymer materials: Design, synthesis, and applications* June 2017.
10. McKeown, N. B. Polymers of Intrinsic Microporosity (PIMs). *Polymer* **202** (Aug. 2020).
11. Lee, J. S. M. & Cooper, A. I. Advances in Conjugated Microporous Polymers. *Chemical Reviews* **120,** 2171–2214 (Feb. 2020).
12. Tian, Y. & Zhu, G. Porous Aromatic Frameworks (PAFs). *Chemical Reviews* **120,** 8934–8986 (Aug. 2020).

13. Jiang, D., Tan, V. G. W., Gong, Y., *et al.* Semiconducting Covalent Organic Frameworks. *Chemical Reviews* (May 2025).

14. Ge, S., Wei, K., Peng, W., *et al.* A comprehensive review of covalent organic frameworks (COFs) and their derivatives in environmental pollution control. *Chemical Society Reviews* **53,** 11259–11302 (2024).

15. Kuo, C.-T., Lu, Y., Arab, P., *et al.* 18.1% single palladium atom catalysts on mesoporous covalent organic framework for gas phase hydrogenation of ethylene. *Cell Reports Physical Science* **2,** 100495 (2021).

16. Kang, C., Yang, K., Zhang, Z., *et al.* Growing single crystals of two-dimensional covalent organic frameworks enabled by intermediate tracing study. *Nature Communications* **13,** 1370 (2022).

17. Krishnaraj, C., Sekhar Jena, H., Bourda, L., *et al.* Strongly Reducing (Diarylamino)benzene-Based Covalent Organic Framework for Metal-Free Visible Light Photocatalytic H2O2 Generation. *Journal of the American Chemical Society* **142,** 20107–20116 (Nov. 2020).

18. Wang, X., Han, X., Cheng, C., *et al.* 2D Covalent Organic Frameworks with cem Topology. *Journal of the American Chemical Society* **144,** 7366–7373 (Apr. 2022).

19. Zhang, Z., Bi, S., Meng, F., *et al.* Hexatopic Vertex-Directed Approach to Vinylene-Linked Covalent Organic Frameworks with Heteroporous Topologies. *Journal of the American Chemical Society* **145,** 16704–16710 (Aug. 2023).

20. Haase, F. & Lotsch, B. V. Solving the COF trilemma: towards crystalline, stable and functional covalent organic frameworks. *Chemical Society Reviews* **49,** 8469–8500 (2020).

21. Zou, L., Yang, X., Yuan, S. & Zhou, H.-C. Flexible monomer-based covalent organic frameworks: design, structure and functions. *CrystEngComm* **19,** 4868–4871 (2017).

22. Xu, T., Wang, Z., Zhang, W., *et al.* Constructing Photocatalytic Covalent Organic Frameworks with Aliphatic Linkers. *Journal of the American Chemical Society* (2024).

23. Uribe-Romo, F. J., Hunt, J. R., Furukawa, H., *et al.* A Crystalline Imine-Linked 3-D Porous Covalent Organic Framework. *Journal of the American Chemical Society* **131,** 4570–4571 (Apr. 2009).

24. Trandafir, M. M., Pop, L., Hădade, N. D., *et al.* An adamantane-based COF: stability, adsorption capability, and behaviour as a catalyst and support for Pd and Au for the hydrogenation of nitrostyrene. *Catalysis Science & Technology* **6,** 8344–8354 (2016).

25. Côté, A. P., Benin, A. I., Ockwig, N. W., *et al.* Porous, Crystalline, Covalent Organic Frameworks. *Science* **310,** 1166–1170 (Nov. 2005).

26. Liu, M., Guo, L., Jin, S. & Tan, B. Covalent triazine frameworks: synthesis and applications. *Journal of Materials Chemistry A* **7,** 5153–5172 (2019).

27. Xiao, J., Chen, J., Liu, J., Ihara, H. & Qiu, H. Synthesis strategies of covalent organic frameworks: An overview from nonconventional heating methods and reaction media. *Green Energy & Environment* **8,** 1596–1618 (2023).

28. Uribe-Romo, F. J., Hunt, J. R., Furukawa, H., *et al.* A crystalline imine-linked 3-D porous covalent organic framework. *Journal of the American Chemical Society* **131,** 4570–4571 (2009).

29. Chen, H., Liu, W., Laemont, A., *et al.* A visible-light-harvesting covalent organic framework bearing single nickel sites as a highly efficient sulfur–carbon cross-coupling dual catalyst. *Angewandte Chemie* **133,** 10915–10922 (2021).

30. Laemont, A., Matthys, G., Lavendomme, R. & Van Der Voort, P. Mild and Scalable Conditions for the Solvothermal Synthesis of Imine-Linked Covalent Organic Frameworks. *published on ChemRXiv - under review at Angewandte Chemie* (2024).

31. Li, X., Cai, S., Sun, B., *et al.* Chemically Robust Covalent Organic Frameworks: Progress and Perspective. *Matter* **3,** 1507–1540 (2020).

32. Segura, J. L., Royuela, S. & Mar Ramos, M. Post-synthetic modification of covalent organic frameworks. *Chemical Society Reviews* **48,** 3903–3945 (2019).

33. Grunenberg, L., Savasci, G., Terban, M. W., *et al.* Amine-Linked Covalent Organic Frameworks as a Platform for Postsynthetic Structure Interconversion and Pore-Wall Modification. *Journal of the American Chemical Society* **143,** 3430–3438 (Mar. 2021).

34. Zhou, Z.-B., Han, X.-H., Qi, Q.-Y., *et al.* A Facile, Efficient, and General Synthetic Method to Amide-Linked Covalent Organic Frameworks. *Journal of the American Chemical Society* **144,** 1138–1143 (Jan. 2022).

35. Grunenberg, L., Savasci, G., Emmerling, S. T., *et al.* Postsynthetic Transformation of Imine- into Nitrone-Linked Covalent Organic Frameworks for Atmospheric Water Harvesting at Decreased Humidity. *Journal of the American Chemical Society* **145,** 13241–13248 (June 2023).

36. Hou, Y., Zhou, P., Liu, F., *et al.* Rigid covalent organic frameworks with thiazole linkage to boost oxygen activation for photocatalytic water purification. *Nature Communications* **15,** 7350 (2024).

37. Li, X., Zhang, K., Wang, G., *et al.* Constructing ambivalent imidazopyridinium-linked covalent organic frameworks. *Nature Synthesis* **1,** 382–392 (May 2022).

38. Waller, P. J., AlFaraj, Y. S., Diercks, C. S., Jarenwattananon, N. N. & Yaghi, O. M. Conversion of Imine to Oxazole and Thiazole Linkages in Covalent Organic Frameworks. *Journal of the American Chemical Society* **140,** 9099–9103 (July 2018).

39. Haase, F., Troschke, E., Savasci, G., *et al.* Topochemical conversion of an imine- into a thiazole-linked covalent organic framework

enabling real structure analysis. *Nature Communications* **9,** 2600 (2018).

40. Wang, K., Jia, Z., Bai, Y., *et al.* Synthesis of stable thiazole-linked covalent organic frameworks via a multicomponent reaction. *Journal of the American Chemical Society* **142,** 11131–11138 (2020).

41. Gui, B., Lin, G., Ding, H., *et al.* Three-Dimensional Covalent Organic Frameworks: From Topology Design to Applications. *Accounts of Chemical Research* **53,** 2225–2234 (Oct. 2020).

42. Liu, M., Kong, H.-Y., Bi, S., *et al.* Non-Interpenetrated 3D Covalent Organic Framework with Dia Topology for Au Ions Capture. *Advanced Functional Materials* **33,** 2302637 (Aug. 2023).

43. Zeng, L., Chen, Y., Huang, H., *et al.* Cyclometalated ruthenium (II) anthraquinone complexes exhibit strong anticancer activity in hypoxic tumor cells. *Chemistry–A European Journal* **21,** 15308–15319 (2015).

44. Li, Z., Hsueh, C., Tang, Z., *et al.* Rational design of imine-linked three-dimensional mesoporous covalent organic frameworks with bor topology. *SusMat* **2,** 197–205 (Apr. 2022).

45. Yue, J.-Y., Luo, J.-X., Pan, Z.-X., *et al.* Regulating the Topology of Covalent Organic Frameworks for Boosting Overall H2O2 Photogeneration. *Angewandte Chemie International Edition* **63,** e202405763 (June 2024).

46. Lohse, M. S. & Bein, T. Covalent Organic Frameworks: Structures, Synthesis, and Applications. *Advanced Functional Materials* **28,** 1705553 (Aug. 2018).

47. Aslam, A. A., Irshad, A., Nazir, M. S. & Atif, M. A review on covalent organic frameworks as adsorbents for organic pollutants. *Journal of Cleaner Production* **400,** 136737 (2023).

48. Yin, Y., Zhang, Y., Zhou, X., *et al.* Ultrahigh–surface area covalent organic frameworks for methane adsorption. *Science* **386,** 693–696 (Nov. 2024).

49. Desai, A. V., Canossa, S., Chernova, E. A., *et al.* Retrospective Review on Reticular Materials: Facts and Figures Over the Last 30 Years. *Advanced Materials* **n/a,** 2414736 (May 2025).

50. Nugent, P., Belmabkhout, Y., Burd, S. D., *et al.* Porous materials with optimal adsorption thermodynamics and kinetics for CO2 separation. *Nature* **495,** 80–84 (2013).

51. Mashhadimoslem, H., Abdol, M. A., Karimi, P., *et al.* Computational and Machine Learning Methods for CO2 Capture Using Metal–Organic Frameworks. *ACS Nano* **18,** 23842–23875 (Sept. 2024).

52. Pan, T., Yang, K., Dong, X. & Han, Y. Adsorption-based capture of iodine and organic iodides: status and challenges. *Journal of Materials Chemistry A* **11,** 5460–5475 (2023).

53. Yolcan, O. O. World energy outlook and state of renewable energy: 10-Year evaluation. *Innovation and Green Development* **2,** 100070 (2023).

54. Alharbi, S. S., Al Mamun, M., Boubaker, S. & Rizvi, S. K. A. Green finance and renewable energy: A worldwide evidence. *Energy Economics* **118,** 106499 (2023).

55. Wang, Q., Li, R. & He, G. Research status of nuclear power: A review. *Renewable and Sustainable Energy Reviews* **90,** 90–96 (2018).

56. Barragan-Contreras, S. J., Paterson, M., Jackson, J., *et al.* Capturing the disruptive nature of green energy transitions: A political economy approach. *Energy Research & Social Science* **123,** 104039 (2025).

57. Deng, D., Zhang, L., Dong, M., *et al.* Radioactive waste: A review. *Water Environment Research* **92,** 1818–1825 (Oct. 2020).

58. Khelurkar, N., Shah, S. & Jeswani, H. *A review of radioactive waste management* in *2015 International Conference on Technologies for Sustainable Development (ICTSD)* (2015), 1–6.

59. Taylor, R. *Reprocessing and recycling of spent nuclear fuel* (Elsevier, 2015).

60. Hirose, K. 2011 Fukushima Dai-ichi nuclear power plant accident: summary of regional radioactive deposition monitoring results. *Journal of Environmental Radioactivity* **111,** 13–17 (2012).

61. Hatch, M., Ron, E., Bouville, A., Zablotska, L. & Howe, G. The Chernobyl disaster: cancer following the accident at the Chernobyl nuclear power plant. *Epidemiologic reviews* **27,** 56–66 (2005).

62. Lee, S. L. Radioactive iodine therapy. *Current Opinion in Endocrinology, Diabetes and Obesity* **19,** 420–428 (2012).

63. Nan, Y. *Adsorption of Iodine and Water on Silver-Exchanged Mordenite* tech. rep. (2017).

64. Amachi, S. *Microbial contribution to global iodine cycling: Volatilization, accumulation, reduction, oxidation, and sorption of iodine* 2008.

65. Daniels, G. H. & Ross, D. S. Radioactive Iodine: A Living History. *Thyroid®* **33,** 666–673 (June 2023).

66. Rong, Q., Hao, M., Zhongshan, C., *et al.* Advancing porous materials for radioiodine capture. *Nanotechnology* (2025).

67. Asmussen, R. M., Turner, J., Chong, S. & Riley, B. J. *Review of recent developments in iodine wasteform production* Dec. 2022.

68. Chapman, K. W., Chupas, P. J. & Nenoff, T. M. Radioactive iodine capture in silver-containing mordenites through nanoscale silver iodide formation. *Journal of the American Chemical Society* **132,** 8897–8899 (2010).

69. Tyupina, E. A. & Pryadko, A. V. Use of silver-containing sorbents in anionic species of radioactive iodine management in nuclear industry and the methods of obtaining them. *Journal of Radioanalytical and Nuclear Chemistry* **333,** 599–613 (2024).

70. Huve, J., Ryzhikov, A., Nouali, H., *et al. Porous sorbents for the capture of radioactive iodine compounds: A review* 2018.

71. Yang, X., Li, Z. & Yang, M. Crystalline Porous Materials for Gaseous Iodine Capture: A Comprehensive Review. *ChemPlusChem,* 2500087 (2025).

72. Shen, Z., Wiechert, A. I., Ladshaw, A. P., *et al.* Adsorption of molecular iodine and alkyl iodides from spent-nuclear-fuel-reprocessing off-gas using reduced silver mordenite. *Chemical Engineering Journal* **482,** 149083 (2024).

73. Li, Q. F., Yu, R. L., Li, Z. L. & Xia, L. Z. Iodine capture by ZSM-5 with different Si/Al ratios: An experimental and molecular simulation investigation. *Microporous and Mesoporous Materials* **354,** 112536 (Apr. 2023).

74. Azambre, B., Chebbi, M., Leroy, O. & Cantrel, L. Effects of Zeolitic Parameters and Irradiation on the Retention Properties of Silver Zeolites Exposed to Molecular Iodine. *Industrial & Engineering Chemistry Research* **57,** 1468–1479 (Feb. 2018).

75. Pham, T. C. T., Docao, S., Hwang, I. C., *et al.* Capture of iodine and organic iodides using silica zeolites and the semiconductor behaviour of iodine in a silica zeolite. *Energy & Environmental Science* **9,** 1050–1062 (2016).

76. Zhang, Z., Dong, X., Yin, J., *et al.* Chemically stable guanidinium covalent organic framework for the efficient capture of low-concentration iodine at high temperatures. *Journal of the American Chemical Society* **144,** 6821–6829 (2022).

77. Xie, Y., Pan, T., Lei, Q., *et al.* Efficient and simultaneous capture of iodine and methyl iodide achieved by a covalent organic framework. *Nature Communications* **13,** 2878 (2022).

78. Fu, J., Kang, J.-Y., Gao, W., *et al.* Covalent organic frameworks for radioactive iodine capture: structure and functionality. *Chemical Communications* **61,** 2235–2256 (2025).

79. Zheng, Z., Lin, Q., Gao, Y., *et al.* Recent advances in iodine adsorption from water. *Coordination Chemistry Reviews* **511,** 215860 (2024).

80. Kim, J. Y., Oh, H. & Moon, H. R. Hydrogen Isotope Separation in Confined Nanospaces: Carbons, Zeolites, Metal–Organic Frameworks, and Covalent Organic Frameworks. *Advanced Materials* **31,** 1805293 (May 2019).

81. Chang, S., Li, J., Li, Y., *et al.* Study on the microstructure and adsorption mechanism of different silver-based iodine adsorbents. *Inorganica Chimica Acta* **569,** 122135 (2024).

82. Liu, M., Chen, Q., Cao, X., *et al.* Physicochemical Confinement Effect Enables High-Performing Zinc–Iodine Batteries. *Journal of the American Chemical Society* **144,** 21683–21691 (Nov. 2022).

83. Terraneo, G., Resnati, G. & Metrangolo, P. Iodine and halogen bonding. *Iodine Chemistry and Applications,* 159–194 (2014).

84. Xie, Y., Huang, P., Gao, Q., *et al.* Halogen-bond induced unusual polyhalogen anions formation in hydrogen-bonded frameworks to secure iodine sequestration. *Nano Research* **17,** 6766–6772 (2024).

85. Yan, C. & Mu, T. Investigation of ionic liquids for efficient removal and reliable storage of radioactive iodine: a halogen-bonding case. *Physical Chemistry Chemical Physics* **16,** 5071–5075 (2014).

86. Junthod, K., Todee, B., Khamphaijun, K., *et al.* Halogen-Bonding Interaction-Mediated Efficient Iodine Capture of Highly Nitrogen-Functionalized Hyper-Crosslinked Polymers. *ACS Applied Polymer Materials* **6,** 7124–7136 (June 2024).

87. Redeker, F. A., Kropman, A., Müller, C., *et al.* Theoretical investigation of the structures, stabilities and vibrational properties of triatomic interhalide ions and their alkali ion pairs. *Journal of Fluorine Chemistry* **216,** 81–88 (2018).

88. Gutsev, G. L. Electronic structure of XYZtrihalide anions (X, Y, Z = Cl, Br, I). *Journal of Structural Chemistry* **30,** 733–737 (1989).

89. Dominikowska, J. Halide Anions as Halogen Bond Acceptors. *Crystal Growth & Design* **25,** 3906–3914 (June 2025).

90. Ran, Y., Wang, Y., Yang, M., *et al.* Constructing covalent organic frameworks with dense thiophene S sites for effective iodine capture. *RSC Advances* **14,** 32451–32459 (Oct. 2024).

91. Song, J., Huang, X., Chen, S., *et al.* Bearing exceptionally high content pyridine-N into covalent organic frameworks to facilitate the adsorption of iodine and methyl iodide simultaneously. *Journal of Environmental Chemical Engineering* **13,** 117894 (Oct. 2025).

92. Pourebrahimi, S. & Pirooz, M. Reversible iodine vapor capture using bipyridine-based covalent triazine framework: Experimental and computational investigations. *Chemical Engineering Journal Advances* **8,** 100150 (Nov. 2021).

93. Chang, J., Li, H., Zhao, J., *et al.* Tetrathiafulvalene-based covalent organic frameworks for ultrahigh iodine capture. *Chemical Science* **12,** 8452–8457 (2021).

94. He, W., Wang, S., Hu, H., *et al.* Exploration of iodine adsorption performance of pyrene-based two-dimensional covalent organic frameworks. *RSC Advances* **14,** 25695–25702 (2024).

95. He, X., Zhang, S. Y., Tang, X., *et al.* Exploration of 1D channels in stable and high-surface-area covalent triazine polymers for effective iodine removal. *Chemical Engineering Journal* **371,** 314–318 (Sept. 2019).

96. Zeng, W., Liu, M., Cai, X., *et al.* A carbazole–porphyrin-based COF: synthesis, characterization, and fluorescence and iodine adsorption properties. *New Journal of Chemistry* **49,** 8782–8792 (2025).

97. He, L., Chen, L., Dong, X., *et al.* A nitrogen-rich covalent organic framework for simultaneous dynamic capture of iodine and methyl iodide. *Chem* **7,** 699–714 (2021).

98. Yugang, Z., Linwei, H., Tingting, P., *et al.* Superior Iodine Uptake Capacity Enabled by an Open Metal-Sulfide Framework Composed of Three Types of Active Sites. *CCS Chemistry* **5,** 1540–1548 (July 2022).

99. Li, B., Dong, X., Wang, H., *et al.* Capture of organic iodides from nuclear waste by metal-organic framework-based molecular traps. *Nature communications* **8,** 485 (2017).

100. Tang, Y., He, Z., Xue, W., Huang, H. & Zhang, G. Dynamic polyiodide anions formation in cationic covalent organic framework for efficient iodine capture. *Chemical Engineering Journal* **470** (Aug. 2023).

101. He, Y., Hosseinzadeh-Bandbafha, H., Kiehbadroudinezhad, M., *et al.* Environmental footprint analysis of gold recycling from electronic waste: A comparative life cycle analysis. *Journal of Cleaner Production* **432,** 139675 (Dec. 2023).

102. Rao, M. D., Singh, K. K., Morrison, C. A. & Love, J. B. Challenges and opportunities in the recovery of gold from electronic waste. *RSC Advances* **10,** 4300–4309 (2020).

103. Fritz, B., Aichele, C. & Schmidt, M. Environmental impact of high-value gold scrap recycling. *The International Journal of Life Cycle Assessment* **25,** 1930–1941 (2020).

104. Duan, H. & Zhu, X.-N. Recent advances in recovering technology for recycling gold from waste printed circuit boards: a review. *Energy Sources, Part A: Recovery, Utilization, and Environmental Effects* **44,** 1640–1659 (Mar. 2022).

105. Park, H. S., Han, Y. S. & Park, J. H. Massive Recycling of Waste Mobile Phones: Pyrolysis, Physical Treatment, and Pyrometallurgical Processing of Insoluble Residue. *ACS Sustainable Chemistry & Engineering* **7,** 14119–14125 (Aug. 2019).

106. Sethurajan, M., van Hullebusch, E. D., Fontana, D., *et al.* Recent advances on hydrometallurgical recovery of critical and precious elements from end of life electronic wastes - a review. *Critical Reviews in Environmental Science and Technology* **49,** 212–275 (Feb. 2019).

107. Kim, E. Y., Kim, M. S., Lee, J. C. & Pandey, B. D. Selective recovery of gold from waste mobile phone PCBs by hydrometallurgical process. *Journal of Hazardous Materials* **198,** 206–215 (Dec. 2011).

108. Gökelma, M., Birich, A., Stopic, S. & Friedrich, B. A review on alternative gold recovery re-agents to cyanide. *Journal of Materials Science and Chemical Engineering* **4,** 8–17 (2016).

109. Wang, R., Zhang, C., Zhao, Y., *et al.* Recycling gold from printed circuit boards gold-plated layer of waste mobile phones in "mild aqua regia" system. *Journal of Cleaner Production* **278,** 123597 (2021).

110. Zhang, H., Ritchie, I. M. & La Brooy, S. R. The adsorption of gold thiourea complex onto activated carbon. *Hydrometallurgy* **72,** 291–301 (Mar. 2004).

111. Rao, M. D., Singh, K. K., Morrison, C. A. & Love, J. B. Recycling copper and gold from e-waste by a two-stage leaching and solvent extraction process. *Separation and Purification Technology* **263,** 118400 (May 2021).

112. Choi, J. W., Song, M. H., Bediako, J. K. & Yun, Y. S. Sequential recovery of gold and copper from bioleached wastewater using ion exchange resins. *Environmental Pollution* **266,** 115167 (Nov. 2020).

113. Yalcin, M. & Arol, A. I. Gold cyanide adsorption characteristics of activated carbon of non-coconut shell origin. *Hydrometallurgy* **63,** 201–206 (2002).

114. Lam, K. F., Yeung, K. L. & McKay, G. An Investigation of Gold Adsorption from a Binary Mixture with Selective Mesoporous Silica

Adsorbents. *The Journal of Physical Chemistry B* **110,** 2187–2194 (Feb. 2006).

115. Yao, W., Chen, Y. & Guo, X. Rapid and selective adsorption of gold ions with hydroxyl-functionalized UiO-66-type metal–organic frameworks. *New Journal of Chemistry* **49,** 9663–9668 (2025).

116. Xiang, Y., Cheng, C.-Y., Liu, M.-H., *et al.* Efficient recovery of gold using Macroporous Metal-Organic framework prepared by the 'MOF in MOF' method. *Separation and Purification Technology* **335,** 126131 (2024).

117. Qian, H.-L., Meng, F.-L., Yang, C.-X. & Yan, X.-P. Irreversible Amide-Linked Covalent Organic Framework for Selective and Ultrafast Gold Recovery. *Angewandte Chemie International Edition* **59,** 17607–17613 (Sept. 2020).

118. Liu, M., Jiang, D., Fu, Y., *et al.* Modulating Skeletons of Covalent Organic Framework for High-Efficiency Gold Recovery. *Angewandte Chemie International Edition* **63,** e202317015 (Jan. 2024).

119. Xu, Q., Du, X.-H., Luo, D., *et al.* Gold recovery from E-waste using freestanding nanopapers of cellulose and ionic covalent organic frameworks. *Chemical Engineering Journal* **458,** 141498 (2023).

120. Oestreicher, V., García, C. S., Soler-Illia, G. J. A. A. & Angelomé, P. C. Gold Recycling at Laboratory Scale: From Nanowaste to Nanospheres. *ChemSusChem* **12,** 4882–4888 (Nov. 2019).

121. Ray, D. A., Baniasadi, M., Graves, J. E., Greenwood, A. & Farnaud, S. Thiourea leaching: an update on a sustainable approach for gold recovery from E-waste. *Journal of Sustainable Metallurgy* **8,** 597–612 (2022).

122. Xu, B., Kong, W., Li, Q., *et al.* A review of thiosulfate leaching of gold: Focus on thiosulfate consumption and gold recovery from pregnant solution. *Metals* **7,** 222 (2017).

123. Yue, C., Sun, H., Liu, W.-J., *et al.* Environmentally benign, rapid, and selective extraction of gold from ores and waste electronic materials. *Angewandte Chemie* **129,** 9459–9463 (2017).

124. Xia, J., Marthi, R., Twinney, J. & Ghahreman, A. A review on adsorption mechanism of gold cyanide complex onto activation carbon. *Journal of Industrial and Engineering Chemistry* **111,** 35–42 (July 2022).

125. Gomes, C. P., Almeida, M. F. & Loureiro, J. M. Gold recovery with ion exchange used resins. *Separation and Purification Technology* **24,** 35–57 (2001).

126. Nguyen, T. N. H., Song, S. J. & Lee, M. S. Solvent extraction separation of Au(III) from Pd(II), Cu(II), Ni(II) in HCl solution using cationic, neutral and basic extractants. *Journal of Chemical Technology & Biotechnology* **99,** 396–404 (Feb. 2024).

127. Biswas, F. B., Rahman, I. M., Nakakubo, K., *et al.* Highly selective and straightforward recovery of gold and platinum from acidic waste effluents using cellulose-based bio-adsorbent. *Journal of Hazardous Materials* **410,** 124569 (May 2021).

128. Bui, T. H., Jeon, S. & Lee, Y. Facile recovery of gold from e-waste by integrating chlorate leaching and selective adsorption using chitosan-based bioadsorbent. *Journal of Environmental Chemical Engineering* **9,** 104661 (Feb. 2021).

129. Peydayesh, M., Boschi, E., Donat, F. & Mezzenga, R. Gold recovery from E-waste by food-waste amyloid aerogels. *Advanced Materials* **36,** 2310642 (2024).

130. Chen, S., Zi, F., Hu, X., *et al.* Interfacial properties of mercaptopropyl-functionalised silica gel and its adsorption performance in the recovery of gold(I) thiosulfate complex. *Chemical Engineering Journal* **393,** 124547 (Aug. 2020).

131. Sun, D. T., Gasilova, N., Yang, S., Oveisi, E. & Queen, W. L. Rapid, selective extraction of trace amounts of gold from complex water mixtures with a metal–organic framework (MOF)/polymer composite. *Journal of the American Chemical Society* **140,** 16697–16703 (2018).

132. Xue, T., He, T., Peng, L., *et al.* A customized MOF-polymer composite for rapid gold extraction from water matrices. *Science Advances* **9,** eadg4923 (2023).

133. Guo, W., Liu, J., Tao, H., *et al.* Covalent Organic Framework Nanoarchitectonics: Recent Advances for Precious Metal Recovery. *Advanced Materials* **36,** 2405399 (Aug. 2024).

134. Mei, D. & Yan, B. Functionalized covalent organic frameworks for gold recovery. *Coordination Chemistry Reviews* **539,** 216769 (Sept. 2025).

135. Li, Z., Zhao, W., Li, C., *et al.* Electronegative Strategic Positions in Covalent Organic Frameworks: Unlocking High-Efficiency Gold Recovery. *Angewandte Chemie International Edition* **64,** e202502199 (May 2025).

136. Abubakar, S., Das, G., Prakasam, T., *et al.* Enhanced Removal of Ultratrace Levels of Gold from Wastewater Using Sulfur-Rich Covalent Organic Frameworks. *ACS Applied Materials & Interfaces* **17,** 17794–17803 (Mar. 2025).

137. Liu, F., Wang, S., Hu, Z. & Hu, B. Post-synthetically functionalized covalent organic frameworks for highly efficient recovery of gold from leaching liquor of electronic waste. *Separation and Purification Technology* **329,** 125218 (Jan. 2024).

138. Liu, M., Xu, Q. & Zeng, G. Ionic Covalent Organic Frameworks in Adsorption and Catalysis. *Angewandte Chemie International Edition* **63,** e202404886 (May 2024).

139. Zhong, S., Wang, Y., Bo, T., *et al.* Efficient and selective gold recovery from e-waste by simple and easily synthesized covalent organic framework. *Chemical Engineering Journal* **455,** 140523 (Jan. 2023).

140. Zadehnazari, A., Auras, F., Altaf, A. A., *et al.* Recycling e-waste into gold-loaded covalent organic framework catalysts for terminal alkyne carboxylation. *Nature Communications* **15,** 10846 (2024).

141. Zhou, M. Y., Wang, X., Zeng, S. H., *et al.* Synergistic electrostatic, coordination, and redox mechanisms in cationic covalent organic frameworks for ultrafast and selective gold recovery. *Chemical Engineering Journal* **519,** 165295 (Sept. 2025).

142. Wu, Y., Zeng, S.-H., Xu, W., *et al.* Thiophene-functionalized covalent triazine frameworks for photo-enhanced gold recovery. *Separation and Purification Technology* **345,** 127408 (2024).

143. Ge, B., Yao, L., Chen, Y., *et al.* Diverse Nitrogen Functional Sites Decorated Covalent Organic Framework Nanotrap Boosting Iodine Capture and Gold Recovery. *ACS Materials Letters* **6,** 4230–4239 (Sept. 2024).

144. Zhang, L., Zheng, Q. Q., Xiao, S. J., *et al.* Covalent organic frameworks constructed by flexible alkyl amines for efficient gold recovery from leaching solution of e-waste. *Chemical Engineering Journal* **426,** 131865 (Dec. 2021).

145. Zhao, J., Qiao, Z., He, Y., *et al.* Anion-Regulated Ionic Covalent Organic Frameworks for Highly Selective Recovery of Gold from E-Waste. *Angewandte Chemie International Edition* **64,** e202414366 (Jan. 2025).

146. Yang, S., Li, T., Cheng, Y., *et al.* Covalent Organic Framework Isomers for Photoenhanced Gold Recovery from E-Waste with High Efficiency and Selectivity. *ACS Sustainable Chemistry & Engineering* **10,** 9719–9731 (Aug. 2022).

147. Zhang, L., Fan, J.-Q., Zheng, Q.-Q., *et al.* A 2D mesoporous hydrazone covalent organic framework for selective detection and ultrafast recovery of Au(III) from electronic waste. *Chemical Engineering Journal* **454,** 140212 (2023).

148. Li, K., Mei, D., Liu, Y.-s. & Yan, B. Three-Dimensional Covalent Organic Frameworks Containing Diverse Nitrogen Sites for Gold Adsorption. *Chemistry of Materials* **37,** 2535–2545 (Apr. 2025).

149. Abubakar, S., Jrad, A., Das, G., *et al.* From Waste to Wealth: Covalent Organic Frameworks for Gold Detection and Recovery from Secondary Sources. *ACS Applied Materials & Interfaces* (Aug. 2025).

2

Imidazopyridinium Covalent Organic Frameworks as Efficient Iodine Capturing Materials

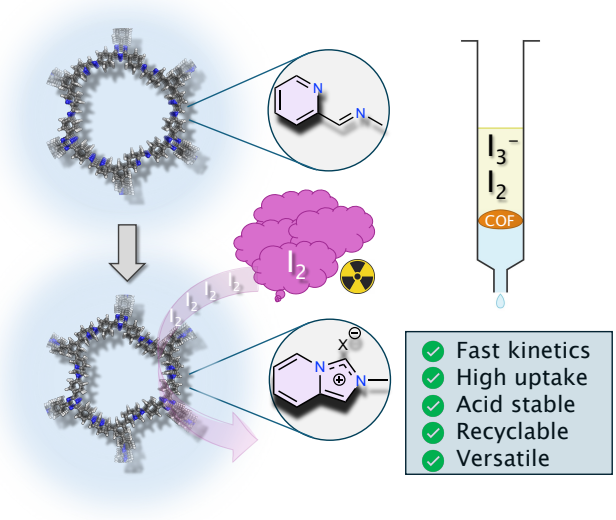

[1] ***Parts of this work have been published in:*** Matthys, G., Laemont, A., De Geyter, N., Morent, R., Lavendomme, R. & Van Der Voort, P. Robust Imidazopyridinium Covalent Organic Framework as Efficient Iodine Capturing Materials in Gaseous and Aqueous Environment. *accepted at Small* (2024) .

2.1 Introduction

As mentioned in **subsection 1.2.1**, which highlights a critical need for robust, cost-effective, and highly efficient adsorbents with tunable properties, covalent organic frameworks (COFs) have emerged as an exceptionally promising class of materials to address these limitations. Their construction from light elements via strong covalent bonds affords permanent porosity, high surface areas, and, crucially, the potential for exceptional chemical and thermal stability. Furthermore, the principles of reticular chemistry allow for the precise, molecular-level design of their pore environments, enabling the incorporation of specific functionalities to target desired guest molecules.

Despite their promising performance, many of the COFs reported to date for iodine capture have a significant weakness: they are based on the imine linkage (C=N). Although the formation of imines is one of the most robust and versatile reactions for the synthesis of COFs, the resulting bond is inherently susceptible to hydrolysis, especially in the acidic and humid conditions typical of nuclear off-gas streams.[1] Previous attempts to improve the performance of imine-COFs, for example, by attaching ionic groups to the side chains of the linkers, have indeed increased iodine uptake capacity and kinetics.[2, 3] However, these strategies leave the vulnerable imine bond in the backbone of the material intact, leaving the fundamental problem of structural instability unsolved.

This research proposes a fundamentally different and more robust approach. Instead of functionalizing the building blocks of the COF, the imine linkage itself is chemically converted via a post-synthetic modification (PSM). Specifically, the imine linkage, formed from a picolinaldehyde precursor, is converted into an inherently more stable, heterocyclic, and cationic imidazopyridinium linkage.

The central hypothesis of this dissertation is that this post-synthetic linkage conversion will lead to a class of materials, the imidazopyridinium-

COFs (impyr-COFs), with a unique combination of properties. It is hypothesized that these impyr-COFs will:

1. Exhibit significantly enhanced chemical and thermal stability compared to their parent imine analogue, making them suitable for use under harsh industrial conditions.

2. Demonstrate superior adsorption performance, particularly a drastic increase in adsorption kinetics, for iodine species (I_2, I_3^-) in both the gas and aqueous phases. This is expected through the introduction of new, powerful binding mechanisms, including strong electrostatic interactions between the cationic framework and anionic (poly)iodide species, and the possibility of halogen bonding with the incorporated counter-anions.

By following this strategy, this work aims not only to develop a new, high-performance material but also to provide fundamental insight into the relationship between the structure of the COF framework at the molecular level and its macroscopic adsorption properties.

2.2 Results and Discussion

2.2.1 Synthesis and Characterization of Imidazopyridinium COFs

The novel imidazopyridinium-based covalent organic frameworks (impyr-COFs) were synthesized via a two-step process that begins with the formation of a crystalline imine-linked precursor, followed by a post-synthetic conversion of the linkages.

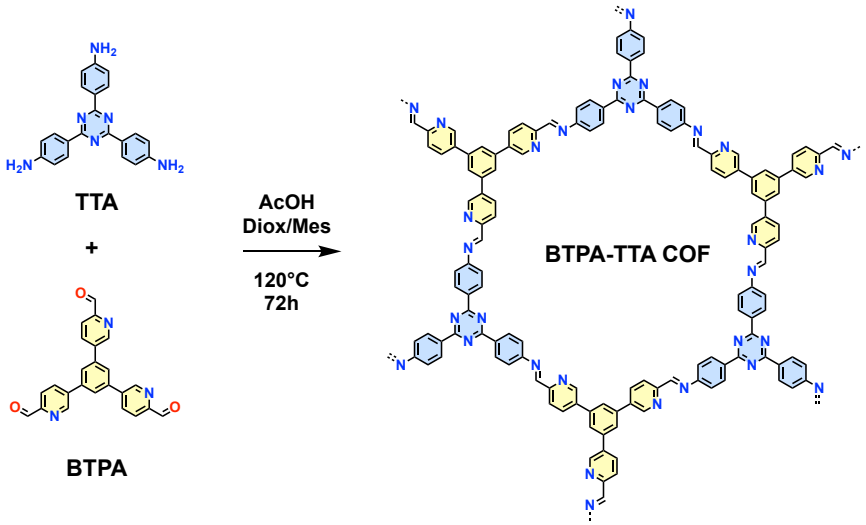

Figure 2.1. The synthesis and structure of BTPA-TTA COF.

The initial framework, BTPA-TTA COF, was produced through the solvothermal polycondensation of 4,4',4"-(1,3,5-triazine-2,4,6-triyl)trianiline (TTA) and 5,5',5"-(1,3,5-benzenetriyl)tris(2-pyridine carboxaldehyde) (BTPA). The reaction was conducted in a dioxane and mesitylene solvent mixture, using an aqueous acetic acid solution as a catalyst (**Figure 2.1**). In the subsequent post-modification step, the parent BTPA-TTA COF was treated with a mixture of mesitylene, 1-butanol, an aqueous formalin solution, and various acids (HX, where X = CF_3COO^-, Cl^-, or Br^-) to convert the imine linkages into robust imidazopyridinium linkages (**Figure 2.2**).

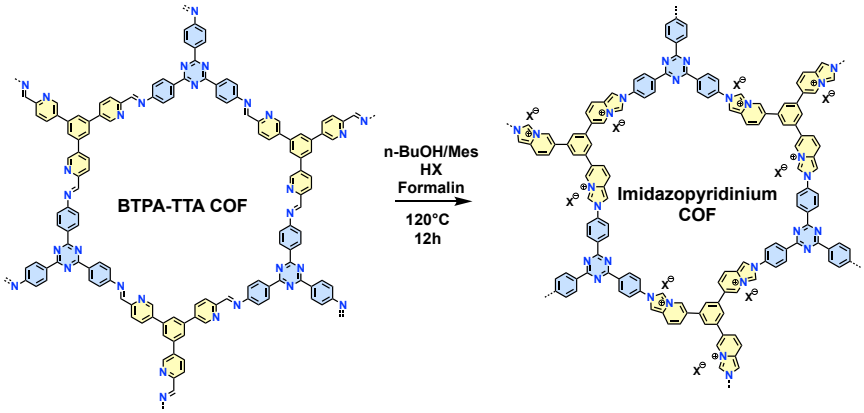

Figure 2.2. The synthesis (post-modification) of BTPA-TTA COF into imidazopyridinium COF.

The successful synthesis and high crystallinity of the materials were confirmed by Powder X-ray Diffraction (PXRD). The symmetry of both amine and aldehyde monomers is tritopic; this results in the formation of a hexagonal 2D layered structure (P3 space group). The parent BTPA-TTA COF displayed prominent reflection peaks at 3.96°, 6.87°, 8.05°, 10.63°, 14.54°, and 25.03°, corresponding to the (100), (110), (200), (210), (310), and (001) reflections, respectively. After post-synthetic modification to the different imidazopyridinium COFs, a slight loss in crystallinity was observed (peak broadening). The peaks shifted to higher angles; for impyr-HCl COF, the (100), (110), (200), (210), and (001) reflections shifted to 4.15°, 7.26°, 8.42°, 11.10°, and 26.20°. This shift is attributed to the formation of a smaller unit cell in the imidazopyridinium COFs (**Figure 2.3A**). The optimized unit cell parameters based on the experimental data were a = b = 26.599 Å and c = 3.908 Å, $\alpha = \beta = 90°$, and $\gamma = 120°$ (with residual factors $R_{wp} = 6.44\%$ and $R_p = 9.81\%$) for BTPA-TTA COF and a = b = 24.275 Å and c = 3.508 Å with residual factors ($R_{wp} = 5.69\%$ and $R_p = 5.14\%$) for impyr-HCl COF, showing good agreement with theoretical models.

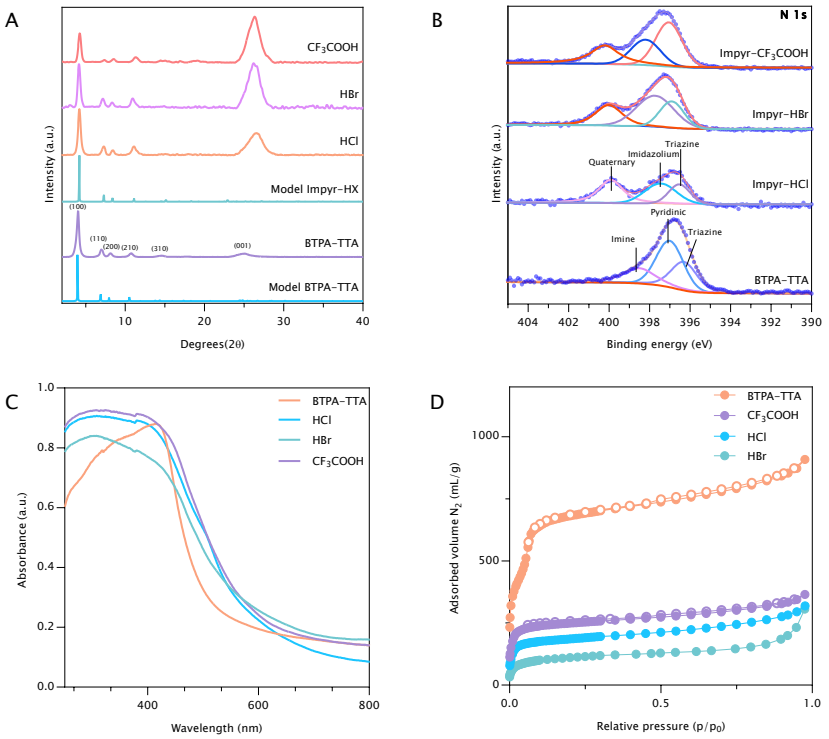

Figure 2.3. A) PXRD pattern of BTPA-TTA COF and impyr-HX (X = Cl^-, Br^-, CF_3COO^-) COFs with their corresponding simulated PXRD patterns; B) High-resolution N 1s region of the XPS spectra; C) Solid-State UV–vis absorption spectra; D) Nitrogen sorption isotherms.

The chemical transformation was further verified by spectroscopic analysis. Fourier Transform Infrared (FTIR) spectroscopy confirmed the formation of the imine linkage in BTPA-TTA COF through the disappearance of the aldehyde C=O (1730 cm^{-1}) and amine N-H (3100-3500 cm^{-1}) stretching bands, along with the appearance of a characteristic imine stretch at 1620 cm^{-1} (**Figure A.5**). After modification, this band shifted to higher wavenumbers, indicating the formation of the imidazopyridinium ring (**Figure A.6**). X-ray Photoelectron Spectroscopy (XPS) provided definitive evidence of the conversion, showing a significant shift of the imine nitrogen species to higher binding energy as it became a quaternary ni-

trogen species upon cyclization (**Figure 2.3B**). Additionally, a shift in the pyridinic nitrogen species of BTPA-TTA was observed towards higher binding energies (from 397.0 to 397.5 eV), resulting in a partial positive charge on the imidazole-type nitrogen. Solid-state UV-vis spectroscopy revealed a blueshift for the imidazopyridinium COFs compared to the parent material, which is attributed to the smaller unit cell and weakened π-π interactions between the COF sheets resulting from ionic repulsion **(Figure 2.3C)**.

Nitrogen sorption experiments at 77 K were performed to evaluate the porosity of the frameworks. The parent BTPA-TTA COF exhibited a Type-IV isotherm profile, characteristic of a mesoporous material, with a high Brunauer-Emmett-Teller (BET) surface area of 1868 m^2g^{-1} and a pore size of 2.2 nm. In contrast, the post-modified impyr-COFs displayed Type-I isotherms, indicative of microporous materials. Their BET surface areas were significantly lower: 970 m^2g^{-1} for impyr-CF_3COOH, 710 m^2g^{-1} for impyr-HCl, and 402 m^2g^{-1} for impyr-HBr **(Figure 2.3D)**. This decrease is attributed to a combination of factors, including the filling of pores by counter-anions, disorder in the layer stacking due to ionic repulsion, and an increase in framework weight from the incorporated anions. To calculate the pore size distributions, quenched-solid density functional theory (QS-DFT) was used. The pore sizes of BTPA-TTA COF, impyr-CF_3COOH, impyr-HCl, impyr-HBr were 2.2, 1.1, 1.1, and 1.2 nm, respectively (**Figure A.3**). SEM showed that the morphology of the frameworks was retained after the post-modification (**Figure A.9**).

2.2.2 Iodine Capture from the Gas Phase

The nitrogen-rich structure of the parent BTPA-TTA COF and the cationic nature of the impyr-COFs suggested a high affinity for molecular iodine (I_2).

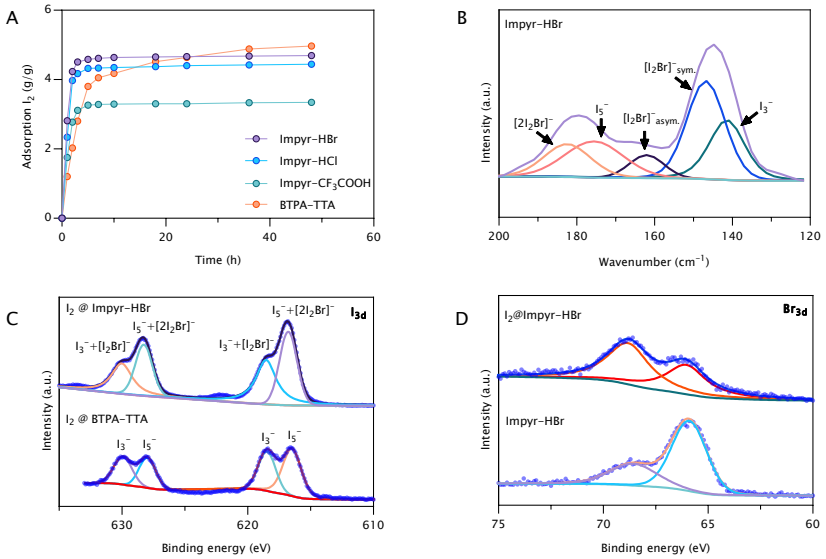

Figure 2.4. A) Static adsorption of iodine plots; B) Raman spectrum of Impyr-HBr COF; C) High-resolution iodine 3d XPS spectra of BTPA-TTA COF and impyr-HBr COF; D) High-resolution bromide 3d XPS spectra of iodine doped and undoped impyr-HBr COF.

Static Adsorption and Mechanistic Insight

Static iodine vapor adsorption experiments were conducted at 75°C. All COFs rapidly changed color from yellow to black upon exposure to iodine vapor. The imidazopyridinium COFs demonstrated dramatically faster adsorption kinetics than their imine precursor; for instance, the best-performing impyr-HBr reached saturation in approximately 5 hours (kinetics, K_{80}%: 2.62 g $g^{-1}h^{-1}$), whereas the BTPA-TTA COF required 24 hours (K_{80}%: 0.66 g $g^{-1}h^{-1}$). The total iodine capture capacities were exceptionally high, measured at 4.97 g g^{-1} for BTPA-TTA, 3.37 g g^{-1} for impyr-CF_3COOH, 4.40 g g^{-1} for impyr-HCl, and 4.66 g g^{-1} for impyr-HBr **(Figure 2.4A)**. These values are superior to most reported adsorbent materials, including commercially available activated carbons and silver-based zeolites.[4, 5] Despite their significantly lower surface areas, the

impyr-COFs maintained iodine capacities nearly as high as the parent imine COF, indicating a different and highly efficient binding mechanism. After the static adsorption tests, these imidazopyridinium COFs were left open to the air for 7 days and exhibited negligible weight loss (<5%), which indicates excellent retention capacity(**Figure A.21**). In nuclear gaseous waste streams, there is an additional presence of organic iodides; therefore, static adsorption tests were performed with methyl iodide (**Figure A.22**). BTPA-TTA COF showcased a higher uptake in methyliodide than the different imidazopyridinium COFs. This is in accordance with the findings of Xie et al. who reported that the presence of nucleophilic nitrogen sites, such as imines, are the preferred site for organic iodides, resulting in a loss of the material's structural integrity.[6] A low uptake of methyl iodide in the imidazopyridinium COFs in comparison with BTPA-TTA COF can be rationalized by the absence of these nucleophilic N-sites.

To elucidate the origins of these different performances, the interactions between the iodine guest and the respective COF frameworks were probed using a combination of spectroscopic and analytical techniques, revealing two distinct capture mechanisms.

Mechanism 1: The Parent Imine COF (BTPA-TTA)

For the parent imine framework, the adsorption process is primarily governed by Lewis acid-base and charge-transfer interactions. The framework is rich in electron-donating nitrogen sites, located in both the imine linkages and the pyridine rings. These sites function as Lewis bases, interacting with the electron-accepting iodine molecule (I_2). This interaction proceeds via the donation of electron density from the nitrogen lone-pair orbitals to the antibonding orbital (σ^*) of the iodine molecule, which forms a charge-transfer complex (e.g., N···I-I). This initial complexation polarizes the iodine and facilitates the attraction of additional I_2 molecules, leading to the in-situ formation of stable polyiodide anions, predominantly triiodide (I_3^-) and pentaiodide (I_5^-). This mechanism was corroborated by Raman spectroscopy of the iodine-loaded BTPA-TTA,

which showed a broad peak in the 100-190 cm^{-1} region corresponding to a combination of the symmetric stretch of I_3^-(110 cm^{-1}), the anti-symmetric stretch of I_3^- (145 cm^{-1}), and the stretching mode of I_5^- (170 cm^{-1})(**Figure A.15**). Further evidence was obtained from XPS analysis, where the I 3d spectrum displayed two distinct pairs of peaks assigned to I_3^- and I_5^- species (**Figure 2.4C**).

Mechanism 2: The Cationic Imidazopyridinium COFs (impyr-HX)

In contrast, the cationic imidazopyridinium frameworks employ a more complex, cooperative, and ultimately more efficient mechanism. This multi-stage process leverages the unique chemical features introduced via post-synthetic modification:

1. **Halogen Bonding Nucleation:** The adsorption is initiated by a potent halogen bonding interaction between an incoming gaseous I_2 molecule and the framework's halide counter-anion (X^-). Halogen bonding is a strong, highly directional noncovalent interaction between an electrophilic region on a halogen atom (in I_2) and a nucleophile (the X^- anion). This initial step rapidly forms (hetero)polyhalide anions such as $[I_2X]^-$.

2. **Electrostatic Anchoring:** The newly formed, negatively charged polyhalide complex is then immediately and powerfully stabilized by a strong electrostatic attraction to the permanent positive charge of the nearby imidazopyridinium center within the COF framework. This powerful coulombic interaction acts as a robust anchor, firmly trapping the iodine species.

3. **Hydrogen Bonding Stabilization:** The binding is further reinforced by hydrogen bonding interactions between the captured polyhalide anion and the acidic C-H protons of the imidazopyridinium ring.

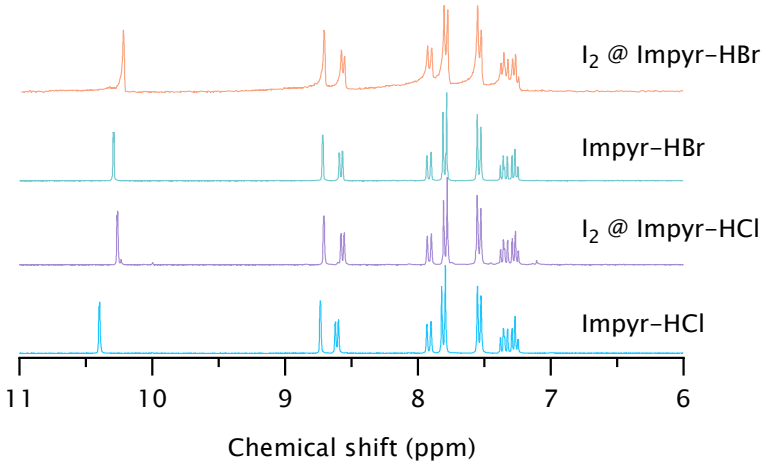

Figure 2.5. ^{1}H NMR spectra of Impyr-HCl/ Impyr-HBr model compounds and their corresponding samples with 3 eq. of I_2 added.

Several pieces of evidence support this proposed mechanism. Raman spectra of iodine-loaded impyr-HX COFs showed a broad peak centered around 170 cm^{-1}, indicative of a predominant presence of higher polyhalides like I_5^- and their hetero-halogen analogues, such as $[2I_2X]^-$**(Figure 2.4B)**. Furthermore, the high-resolution I 3d XPS spectrum corroborated these findings, showing distinct peaks assignable to hetero-polyhalide species like $[I_2X]^-$ and $[2I_2X]^-$ alongside the expected polyiodides (**Figure 2.4C**). Furthermore, XPS analysis provided proof of the counter-anion's active role. Upon iodine adsorption, a clear shift in the binding energy of the counter-anion itself was observed (e.g., in the Br 3d spectrum for impyr-HBr), confirming its direct electronic involvement in the binding process (**Figure 2.4D)**.

Other evidence for this mechanism came from experiments with synthesized small-molecule model compounds (**Figure 2.9)**. When iodine was added to a solution of an imidazopyridinium chloride model compound, ^{1}H NMR spectroscopy revealed a notable upfield chemical shift of $\Delta\delta$ = -0.24 ppm for the N-CH-N proton of the imidazopyridinium ring.

A similar shift of $\Delta\delta$ = -0.13 ppm was observed for the bromide model compound (**Figure 2.5**). An upfield shift indicates increased electron shielding around the proton. This is explained by the proposed mechanism: the formation of a large, diffuse, negatively charged polyhalide anion ($[I_xX]^-$) near the N-CH-N proton increases the local electron density, shielding it from the external magnetic field. This provides direct, solution-state evidence that the iodine is captured via the counter-anion and then anchored onto the cationic ring. This mechanistic elucidation reveals that the counter-anion is not a passive charge-balancer but an active and essential component in the adsorption machinery, acting as the nucleation site that initiates the capture process and enables the powerful electrostatic trap responsible for the dramatically enhanced kinetics.

A similar mechanism for both kinds of COFs can be elucidated from these observations. In the first stage, the iodine (I_2) physisorption takes place due to the porous nature of both COFs. In the second stage, strong interactions between the iodine and electron-rich nitrogen atoms are generated when they approach each other. In the final stage, electron transfer complexes (I_3^- and I_5^-) are generated, leading to chemisorption. Due to the post-modification of the pyridyl-imine motif, the electron-rich nitrogen content is decreased in the imidazopyridinium COFs, leading to a reduced potential for binding of homo-polyiodide via charge-transfer complexes. Nonetheless, the presence of halogen counter anions in the imidazopyridinium COF compensates for the lack of electron-rich nitrogen in the framework. These anions have the potential to form strong halogen bonds, leading to (hetero)polyhalide complexes $[I_2X]^-$ /$[2I_2X]^-$, which can then be bound by the imidazopyridinium framework via ionic interactions and hydrogen bonding.

Dynamic Adsorption under Industrial More Practical Conditions

To assess performance under more practical scenarios, dynamic breakthrough experiments were conducted using a lab-scale fixed-bed column breakthrough setup (**Figure 2.10**).

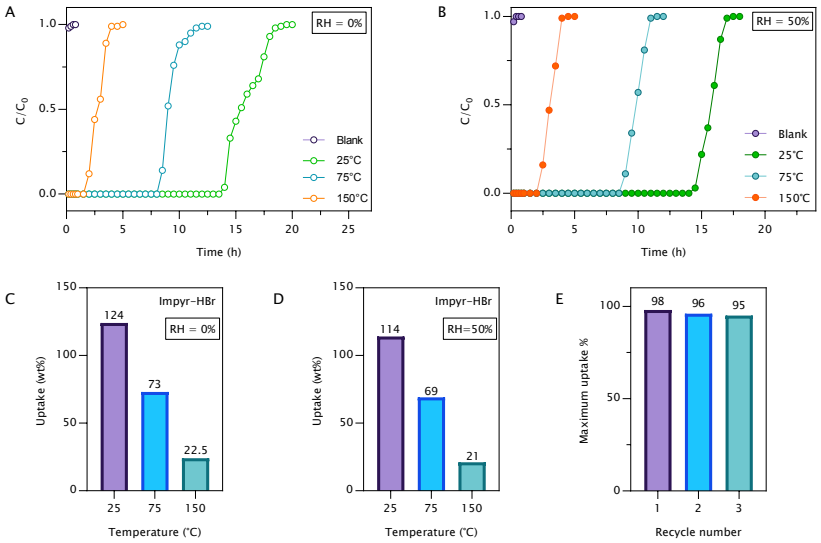

Figure 2.6. Iodine breakthrough curve at different temperatures (25, 75, 150 °C) using Impyr-HBr with a relative humidity (RH) of A) 0% and B) 50%. Gravimetric iodine uptake of impyr-HBr COF in dynamic adsorption conditions at different temperatures with RH of C) 0% and D) 50%. E) Retained iodine uptake of impyr-HBr at 150 °C at 0% RH compared with the first run.

- **Performance and Stability:** The breakthrough profiles revealed that there is a single breakthrough step after 14 h at 25 °C, 8.5 h at 75 °C, and 2 h at 150 °C (**Figure 2.6A,C**). The iodine adsorption capacity at these dynamic conditions was 124 wt.% at 25 °C, 73 wt.% at 75 °C, and 22.5 wt.% at 150 °C for impyr-HBr COF. The material showed excellent stability, retaining its crystallinity after immersion in a

concentrated acid solution for three days and thermal stability up to 200°C (**Figure A.4, Figure A.7**).

- **Performance under Humidity:** Since nuclear off-gas streams contain water vapor, the experiment was repeated at 150°C with a relative humidity of 50%(**Figure 2.6B**). Under these challenging conditions, impyr-HBr still exhibited a remarkable iodine uptake of 21 wt% (**Figure 2.6D**). This performance surpasses that of currently used industrial silver-based zeolite adsorbents, such as Ag@MOR, which has a reported uptake of 17 wt% under similar conditions. This demonstrates the high selectivity of the framework for iodine over water, especially at elevated temperatures. The breakthrough profiles are very similar to those under dry conditions: only a small reduction of the iodine adsorption capacity was observed. This illustrates that although the impyr-HBr COF is hydrophilic due to its ionic character, the uptake selectivity toward the iodine species is higher. At high temperatures, the competition effect with water is less pronounced for the adsorption of iodine species; it was previously reported that high temperatures suppress the competitive adsorption of water.[7]

- **Recyclability:** The material's potential for practical application was further confirmed by its recyclability. After iodine adsorption, the impyr-HBr COF could be regenerated by washing with an ethanol/-sodium bromide solution, retaining 95% of its original adsorption capacity after 3 cycles (**Figure 2.6E**). PXRD analysis confirmed that the crystalline structure was preserved after washing (**Figure A.20**).

2.2.3 Iodine Capture from Aqueous Environments

The excellent vapor-phase performance prompted an investigation into the materials' efficacy for iodine capture from aqueous solutions, a significant challenge as contaminated water can contain various polyiodide species.

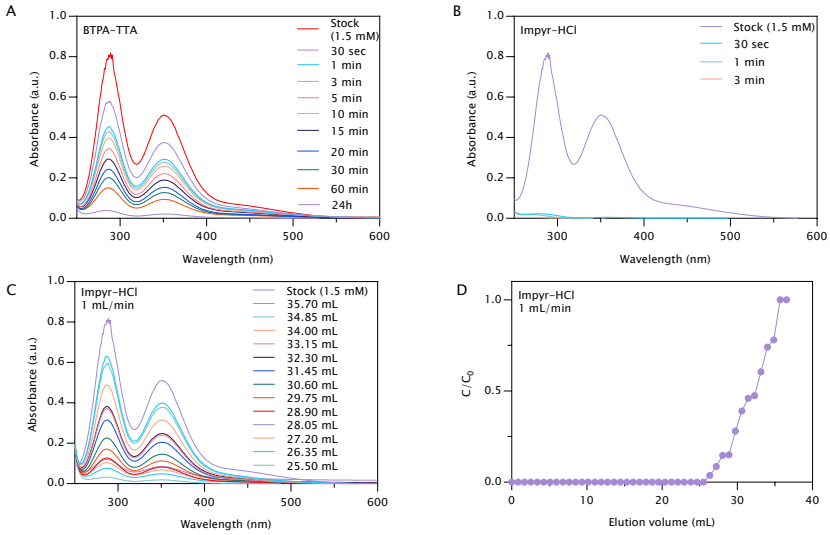

Figure 2.7. UV–vis absorption spectra monitoring the static adsorption of triiodide (I_3^-) by A) BTPA-TTA COF and B) impyr-HCl COF after several time intervals. C) UV–vis absorption spectra of the eluent after a dynamic flow-through adsorption experiment of 1.5 mmol L^{-1} I_3^- with impyr-HCl COF. D) Corresponding breakthrough profile of a 1.5 mmol L^{-1} I_3^- dynamic flow-through adsorption experiment with impyr-HCl.

Removal of Triiodide I_3^-

Static adsorption tests were performed using a 1.5 mmol L^{-1} solution of triiodide (I_3^-) ions, which show absorbance bands at 287 and 351 nm in UV–Vis spectroscopy. The impyr-COFs demonstrated extraordinary efficiency.

- **Kinetics and Capacity:** When 10 mg of impyr-HCl was added to a 15 mL solution of 1.5 mmol L^{-1} I_3^-, it removed 98% of the triiodide anions in just 1 minute (**Figure 2.9B**). Visually, the color of the triiodide solution turned from yellow-brownish to colorless. In contrast, the parent BTPA-TTA COF required 24 hours to achieve 96% removal (**Figure 2.6A**). All the adsorption experiments in aquatic me-

dia showed pseudo-second order kinetics, which suggests that the I_3^- ions are chemisorbed onto the COFs (**Figure A.28**). The faster kinetics of the impyr-COFs are attributed to the strong electrostatic interactions between the cationic imidazopyridinium sites and the anionic triiodide molecules, as well as their more hydrophilic nature, which facilitates dispersion in water. We noticed as well an influence of the anion inside the imidazopyridinium COFs regarding the uptake kinetics of triiodide (I_3^-). Faster I_3^- adsorption kinetics were observed when using imidazopyridinium COFs with smaller halide anions (Cl^-, Br^-) compared to the bulky CF_3COO^- anion. We infer that this trend is due to sterical hindrance: the bulkier trifluoroacetate anions are sterically shielding the imidazopyridinium unit from the I_3^- anions, thus slowing their approach to bind electrostatically. This leads to a sluggish approach of the I_3^- anion to the imidazopyridinium unit and subsequently slower adsorption kinetics. The total uptake capacities from I_3^- solutions were determined to be 3.79, 4.22, 4.03, and 3.17 g g^{-1} for BTPA-TTA, impyr-HCl, impyr-HBr, and impyr-CF_3COOH, respectively.

- **Selectivity and Stability:** The impyr-HCl COF maintained its high removal efficiency (>98%) across a broad pH range of 3 to 10 (**Figure A.25**). In contrast, the performance of the parent BTPA-TTA COF degraded significantly under acidic or basic conditions (**Figure A.24**). Furthermore, the presence of a high concentration (5 mM) of competing anions (NO_3^-, SO_4^{2-}, and Cl^-) did not affect the iodine removal efficiency of impyr-HCl, highlighting its excellent selectivity for the highly polarizable I_3^- anion.

- **Dynamic flow-through experiment:** The practical applicability of impyr-HCl was further confirmed in dynamic flow-through experiments, which simulate real-world water purification scenarios (**Figure 2.11**). When a 1.5 mmol L^{-1} triiodide solution was passed through a column packed with 10 mg of impyr-HCl at a flow rate of 1 mL min^{-1}, the material demonstrated a sharp breakthrough

profile. The breakthrough curve shows that the column completely removed all triiodide ions from the first 25 mL of the solution, reducing the concentration in the eluent to near-zero levels before saturation began (**Figure 2.9C, D)**. This high efficiency was maintained even when the flow rate was increased to 3 mL min^{-1}, a condition under which the parent BTPA-TTA COF showed a much earlier breakthrough due to its slower kinetics.

Performance in Real-World Conditions

To simulate a practical water purification scenario, a dynamic flow-through experiment was conducted using seawater spiked with 5 ppm of I_3^- ions, a concentration relevant to post-disinfection water systems.

- **Purification to ppb levels:** The effluent water was analyzed by ICP-MS. While the parent BTPA-TTA COF removed 81.1% of the iodine, leaving a residual concentration of 0.95 ppm, the impyr-HCl COF removed 99.9% of the I_3^-, reducing the concentration to just 61 ppb. This final concentration is around the natural level of iodine found in seawater, demonstrating the material's capability for highly effective water purification.
- **Aqueous Recyclability:** The impyr-HCl adsorbent could be successfully regenerated by washing with a saturated NaCl/EtOH mixture, retaining 93% of its maximum uptake capacity after three cycles while maintaining its structural integrity (**Figure A.29**).

2.2.4 Conclusion

In this chapter, the development of novel imidazopyridinium-based COFs for high-performance iodine capture was successfully demonstrated. Through a two-step, post-synthetic modification strategy, a parent imine-linked COF was converted into a series of robust, cationic frameworks

with varying counter-anions. These materials were shown to be exceptional adsorbents for iodine in both gaseous and aqueous phases, addressing key limitations of existing technologies.

The key findings of this work are:

- The imidazopyridinium COFs exhibit extremely rapid iodine adsorption kinetics (e.g., K_{80}% of 2.62 g $g^{-1}h^{-1}$ for impyr-HBr) and high gravimetric capacities of up to 4.66 g g^{-1}.
- Under industrially relevant dynamic conditions (150°C and 50% relative humidity), the impyr-HBr COF demonstrated an iodine uptake of 21 wt%, outperforming the current industrial benchmark, silver-based zeolites.
- In aqueous media, the impyr-HCl COF removed 98% of triiodide ions within one minute and effectively purified a real seawater sample from 5 ppm down to a residual concentration of 61 ppb.
- The materials demonstrated excellent stability in harsh acidic conditions, selectivity against competing ions, and robust recyclability in both gaseous and aqueous applications.

The enhanced performance is attributed to a synergistic mechanism involving strong halogen bonding between iodine and the framework's counter-anions, followed by powerful electrostatic and hydrogen bonding with the cationic imidazopyridinium centers. Overall, the imidazopyridinium COFs developed in this work represent a highly effective and versatile platform, demonstrating significant potential for practical application in critical areas of nuclear waste management and water purification.

2.3 Experimental Section

2.3.1 Monomer Synthesis

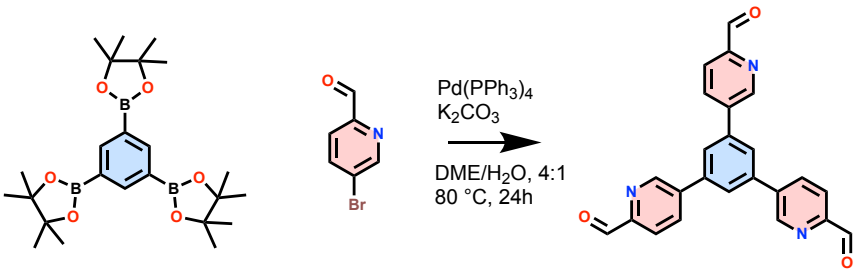

Figure 2.8. Synthesis of 5,5',5"-(1,3,5-benzenetriyl)tris(2-pyridine carboxaldehyde) (BTPA) linker.

The BTPA linker was synthesized via a Suzuki coupling reaction. To a solution of K_2CO_3 (2.08 g, 15.1 mmol) in 20 mL of water, 80 mL of 1,2-dimethoxyethane (DME) was added, and the mixture was degassed by bubbling with argon for 20 minutes. Following degassing, 5-bromopyridine-2-carbaldehyde (2.10 g, 11.3 mmol), 1,3,5-tris(4,4,5,5-tetramethyl-1,3,2-dioxaborolan-2-yl)benzene (1.14 g, 2.50 mmol), and tetrakis(triphenylphosphine)palladium(0) (173 mg, 0.150 mmol) were added. The mixture was stirred vigorously at 80°C for 24 hours under an argon atmosphere.

After cooling to room temperature, the solid product was reduced to a powder by sonication and allowed to settle for 3 hours. The white precipitate was collected by filtration and washed sequentially with methanol (10 mL), water (2 x 10 mL), methanol (2 x 10 mL), and diethyl ether (2 x 10 mL). The final product was dried under vacuum, yielding 727 mg of BTPA as a white powder (74% yield). The purity was confirmed by ^{1}H NMR spectroscopy in DMSO-d_6.

^{1}H NMR (300 MHz, DMSO-d_6, 298 K) δ (ppm) = 10.09 (s, 3H), 9.47 (d, J = 1.4 Hz, 3H), 8.68 (dd, J = 8.1, 1.8 Hz, 3H), 8.43 (s, 3H), 8.09 (d, J = 8.1 Hz, 3H).

2.3.2 COF Synthesis

BTPA-TTA COF

The parent imine-linked COF was synthesized via a solvothermal condensation reaction.

- **Small-Scale Synthesis** BTPA (39.5 mg, 100 μmol) and 4,4',4"-(1,3,5-triazine-2,4,6-triyl)trianiline (TTA) (35.4 mg, 100 μmol) were combined in a 20 mL vial with 2 mL of dioxane and 2 mL of mesitylene. The mixture was sonicated for 1 minute before adding 200 μL of 6 mol L^{-1} aqueous acetic acid. After an additional 5 minutes of sonication, the tightly sealed vial was heated in an oven at 120°C for 72 hours. The resulting yellow solid was collected by filtration, washed three times with acetone, and dried under vacuum at 120°C overnight, affording 54.6 mg (79% yield).
- **Large-Scale Synthesis:** The procedure was scaled up using BTPA (197 mg, 501 μmol) and TTA (177 mg, 499 μmol) in a solvent mixture of 9 mL of dioxane and 6 mL of mesitylene, with 1.0 mL of 6 mol L^{-1} aqueous acetic acid as the catalyst. This yielded 338 mg of the yellow solid (98% yield).

Post-Synthetic Modification: Imidazopyridinium (Impyr-HX) COFs

The imidazopyridinium COFs were prepared through a general post-synthetic modification procedure. In a 20 mL vial, 50 mg of the parent BTPA-TTA COF was suspended in a mixture of 2.5 mL of mesitylene

and 2.5 mL of n-butanol. A 37% aqueous formalin solution (200 µL, 2.68 mmol) was added, and the mixture was sonicated for 1 minute. Subsequently, 1 mL of a 6 mol L^{-1} aqueous solution of the desired acid (HX, where X = CF_3COO^-, Cl^-, or Br^-) was added. The sealed vial was sonicated again and then heated in an oven at 120°C for 16 hours. After cooling, the resulting red solid was collected by filtration and washed sequentially with water (3 x 10 mL), ethanol (3 x 10 mL), and acetone (3 x 10 mL). The final dark yellow solid was dried under vacuum at 120°C overnight.

Model compound + addition of I_2

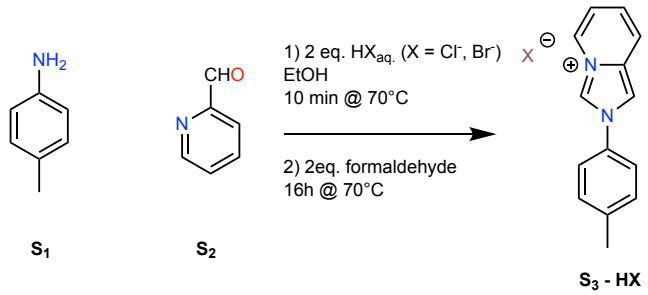

Figure 2.9. Synthesis of the imidazopyridinium model compound

107 mg (1 mmol) of p-toluidine (S_1), 95 µL (1 mmol) of picolinaldehyde (S_2) and 167 µL of HCl_{aq}.(12 mol L^{-1}, 2 mmol) or 224.7 µL of HBr (8.9 mol L^{-1}, 2 mmol) was added to 8 mL of absolute ethanol and heated to 70 °C, resulting in a yellow solution. After 10 minutes of stirring at 70 °C, 149 µL of 37% aqueous formaldehyde solution (13.4 mol L^{-1}, 2 mmol) was added, and the mixture was left stirring at 70°C for 16 h. The solution was left to cool to room temperature, and volatiles were evaporated with a rotavapor. The residue was recrystallized from water, collected, and dried under vacuum.

^{1}H NMR (300 MHz, 298K, DMSO-d_6) of S_3-HCl model compound δ 10.39 (d,J=1.2 Hz, 1H), 8.73 (s, 1H), 8.60 (dd, J= 7.1, 1.1Hz, 1H), 7.91 (d, J = 9.3

Hz, 1H), 7.80 (d, J = 8.5 Hz, 2H), 7.53 (d, J = 8.7 Hz, 2H), 7.34 (ddd, J = 9.3, 6.7, 1.0 Hz, 1H), 7.26 (td, J= 6.8, 1.3 Hz, 1H), 2.44 (s, 3H). 1H NMR (300 MHz, DMSO-d_6) of S_3-HBr model compound d 10.28 (s, 1H), 8.71 (s, 1H), 8.57 (d, J = 7.0Hz, 1H), 7.91 (d, J = 9.2 Hz, 1H), 7.79 (d, J = 8.5 Hz, 2H), 7.53 (d, J = 8.2 Hz, 2H), 7.35 (dd, J = 9.3, 6.5, 1H), 7.26 (t, J= 6.8, 1H), 2.44 (s, 3H).

a) 5 mg (0.020 mmol, 1 eq.) of S_3-HCl and 15.1 mg of I_2 (0.060 mmol, 3 eq.)
b) 5 mg (0.017 mmol, 1 eq.) of S_3-HBr and 12.9 mg of I_2 (0.051 mmol, 3 eq.)
was added together in an NMR tube containing DMSO-d6.

2.3.3 Materials Characterization

For spectroscopic and structural analysis, several methods were employed. Nuclear Magnetic Resonance (NMR) Spectroscopy was used to record ^{1}H NMR spectra on a Bruker Avance I spectrometer at 7.0 Tesla, with chemical shifts referenced to residual DMSO-d_6 (2.50 ppm) and $CDCl_3$ (7.26 ppm). Powder X-Ray Diffraction (PXRD) patterns were collected on a Bruker D8 Advance diffractometer using a Cu-Kα source (λ = 1.5405 Å). Fourier Transform Infrared (FTIR) Spectroscopy was performed on a Perkin Elmer FTIR SPECTRUM 1000 with an Attenuated Total Reflection (ATR) unit, scanning from 4000 to 600 cm^{-1}. Additionally, Raman Spectroscopy data were collected on an RXN1 Raman spectrometer with a 532 nm laser at 40 mW, and Ultraviolet/Visible (UV-Vis) Spectroscopy was conducted on a Shimadzu UV 2600 Scanning Spectrophotometer.The material's physical and chemical properties were further investigated. The morphology was examined with Scanning Electron Microscopy (SEM) using a JCM-7000 NeoScopeTM Benchtop SEM, where samples were fixed on carbon tape and sputter-coated twice with gold. The surface chemical composition was analyzed by X-Ray Photoelectron Spectroscopy (XPS) on a PHI 5000 VersaProbe II spectrometer with a monochromatic Al Kα

X-ray source (hν = 1486.6 eV). Thermogravimetric Analysis (TGA) was performed on a Perkin-Elmer STA6000 analyzer under an air atmosphere, with a heating rate of 10°C/min. Finally, iodine content was determined by Inductively Coupled Plasma Mass Spectrometry (ICP-MS) on a NexION 300 instrument, monitoring mass 127 with a ^{128}Te internal standard. Nitrogen Sorption isotherms were measured at 77 K using a Micromeritics TriStar II 3020 analyzer after samples were activated overnight under vacuum at 120°C. The range for calculation of the BET surface area was chosen so that the following criteria were met:

1. The term $V_{ads}(1 - \frac{p}{p_0})$ must continuously increase with $\frac{p}{p_0}$

2. C must be positive

3. The value for R^2 must be equal to or greater than 0.995

4. The $\frac{p}{p_0}$ value corresponding to V_m must lie within the selected BET range.

To complement the experimental data, computational studies were performed. Geometry optimization of the Covalent Organic Framework (COF) structures was carried out using the Forcite module of BIOVIA Materials Studio 2017 with the Universal Force Field (UFF). The Reflex module was used for the Pawley refinement of experimental PXRD patterns to determine unit cell parameters. For the porosity analysis, Brunauer-Emmett-Teller (BET) surface areas were calculated from the nitrogen sorption data, and pore size distributions (PSD) were modeled using the Quantachrome ASiQwin program with the "carbons (cylindrical/sphere pores QSDFT adsorption branch)" DFT method.

2.3.4 Iodine Sorption Methodology

Gas Phase Iodine Sorption

Static Vapor Adsorption: 10 mg of COF was placed in a 4 mL vial, which was then set inside a larger 40 mL vial containing solid iodine. The sealed system was heated in an oven at 75°C. The weight of the COF-containing vial was measured at defined time intervals to determine the iodine uptake until saturation was reached. The static iodine vapor capture capacity (q_t) was calculated using the formula:

$$q_t = \frac{(m_t - m_1) - (M_t - M_0)}{(m_1 - m_0)} \tag{2.1}$$

q_t: The static iodine vapor capture capacity at a certain time t in gg^{-1}.
m_t: The weight of the vial containing the COF at time t.
m_1: The weight of the vial containing the COF before the experiment.
m_0: The weight of the empty vial (containing the sample material).
M_t: The weight of the reference vial at time t.
M_0: The weight of the reference vial before the experiment.

The adsorption kinetics were determined at 80% ($K_{80\%}$) of the maximum iodine adsorption capacity expressed in $gg^{-1}h^{-1}$.

Dynamic Vapor Adsorption: Iodine capturing breakthrough experiments were conducted with a lab-scale fixed bed reactor at different temperatures (25 °C, 75 °C, and 150 °C). In a typical experiment, 50 mg of impyr-HX COF was vacuum activated at 120 °C overnight. The COF was subsequently packed into a borosilicate column (5 mm inside diameter, 2 mm thickness, and 200 mm length) with 100 mg of degreased cotton wool. Before the breakthrough experiments, a dry argon flow (at 10 mL/min) was used to purge the adsorbent at room temperature. Subsequently, a dry argon gas flow was passed through a glass bottle containing iodine, and the resulting mixture of Ar/I_2 gas mixture was passed through the adsorbent column. Finally, the effluent gas from the adsorbent column

was passed through hexane to scrub the iodine vapor. To control the humidity in the gas stream, a water bubbler was placed between the glass bottle containing iodine and the adsorbent column. The relative humidity of the gas stream was measured with a relative humidity sensor every 30 min and controlled with temperature. The iodine content was detected by UV-Vis spectroscopy (every 30 min) at a wavelength of 523 nm. The blank was determined by using a column containing only degreased cotton wool at the different working temperatures. The flow rate of iodine in an argon carrier gas was determined to be 4.31 mg h^{-1} via UV-Vis spectroscopy of the blank. The dynamic iodine adsorption capacity was determined gravimetrically.

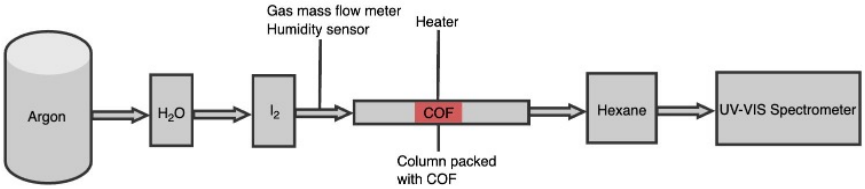

Figure 2.10. Dynamic gaseous Iodide adsorption setup

Aqueous Phase Iodine Sorption

Static Adsorption fo Triiodide (I_3^-): A 1.5 mM stock solution of I_3^- was prepared by dissolving NaI and I_2 in water. In a typical experiment, 10 mg of COF was added to 15 mL of the stirring I_3^- solution. Aliquots were taken at specific time intervals, filtered, and analyzed by UV-Vis spectroscopy at 286 nm to determine the removal efficiency. Adsorption kinetics were fitted using the pseudo-second-order.

Dynamic Adsorption of Triiodide (I_3^-): A Pasteur pipette was loaded with 10 mg of COF, fixed between two layers of degreased cotton wool. An aqueous solution of I_3^- (1.5 mmol L^{-1}) was passed through the column using a syringe pump at a controlled flow rate (1 mL/min or 3 mL/min). The eluent was collected and analyzed by UV-Vis spectroscopy to generate breakthrough curves. The same procedure was used for molecular

iodine (I_2) solutions and for real-world water samples (seawater) spiked with iodine.

Figure 2.11. Dynamic aqueous Iodide adsorption setup

References

1. Taylor, R. *Reprocessing and recycling of spent nuclear fuel* (Elsevier, 2015).
2. Xie, Y., Pan, T., Lei, Q., *et al.* Ionic Functionalization of Multivariate Covalent Organic Frameworks to Achieve an Exceptionally High Iodine-Capture Capacity. *Angewandte Chemie - International Edition* **60,** 22432–22440 (Oct. 2021).
3. Yang, J., Hu, S. J., Cai, L. X., Zhou, L. P. & Sun, Q. F. Counteranion-mediated efficient iodine capture in a hexacationic imidazolium organic cage enabled by multiple non-covalent interactions. *Nature Communications* **14** (Dec. 2023).
4. Nan, Y. *Adsorption of Iodine and Water on Silver-Exchanged Mordenite* tech. rep. (2017).

5. Juhola, A. J. Iodine adsorption and structure of activated carbons. *Carbon* **13,** 437–442 (1975).

6. Xie, Y., Pan, T., Lei, Q., *et al.* Efficient and simultaneous capture of iodine and methyl iodide achieved by a covalent organic framework. *Nature Communications* **13,** 2878 (2022).

7. Li, B., Dong, X., Wang, H., *et al.* Capture of organic iodides from nuclear waste by metal-organic framework-based molecular traps. *Nature communications* **8,** 485 (2017).

3

Thiazole-Linked Covalent Organic Frameworks for Enhanced (Photo)reductive Gold Recovery from E-waste

[1] ***This work has been submitted to:*** Matthys, G., Laemont, A., Bourda, L., Van Hamme, D., Wang, R., Mohamed, A. W., Leus, K., De Geyter, N., Morent, R., Lavendomme, R. & Van Der Voort, P. Thiazole-Linked Covalent Organic Frameworks for Enhanced Photoreductive Gold Recovery from E-Waste. *Submitted to Green Chemistry* (2025) .

3.1 Introduction

As discussed in **subsection 1.2.2**, the efficient recovery of gold from secondary sources, particularly the rapidly growing stream of electronic waste (e-waste), is a critical challenge for sustainable resource management. Conventional hydrometallurgical methods for gold extraction often rely on hazardous reagents like cyanide or highly corrosive acids, and subsequent recovery from complex, multi-metal leachates is hampered by issues of low selectivity, fouling, and the generation of secondary waste. This context underscores the urgent need for advanced adsorbent materials that offer high capacity, exceptional selectivity, and robust performance in the harsh chemical environments typical of e-waste processing.

Covalent Organic Frameworks (COFs) have emerged as a highly promising platform for this application due to their inherent porosity, high surface area, and, most importantly, their unparalleled chemical tunability. By carefully selecting molecular building blocks, it is possible to engineer COFs with specific binding sites tailored for gold species. However, a central challenge in COF synthesis is the trade-off between crystallinity and chemical stability; the reversible imine linkages that facilitate the formation of well-ordered frameworks are often susceptible to degradation under the acidic conditions required for e-waste leaching.

This chapter explores a linkage engineering strategy to overcome this limitation. We address the need for materials capable of selectively capturing gold from electronic waste leachates by leveraging a post-synthetic modification (PSM) approach. We begin with the synthesis of two distinct imine-linked COFs, one based on a light-harvesting pyrene core and another on a nitrogen-rich triazolo-triazine core, chosen for their extended π-conjugated systems. Subsequently, these frameworks are converted into more robust and functional thiazole-linked analogues. This transformation is strategically designed to introduce sulfur atoms, soft Lewis base sites known for their affinity for the soft Lewis acid Au(III), into the COF

backbone, thereby enhancing both chemical stability and gold adsorption performance in line with Hard-Soft Acid-Base (HSAB) theory. This study systematically investigates the impact of this imine-to-thiazole conversion on the materials' structural, chemical, and photophysical properties, and evaluates their performance in the (photo)reductive recovery of gold from both ideal solutions and complex, real-world CPU leachates.

3.2 Results and Discussion

3.2.1 Synthesis and characterization

Two distinct COF systems were synthesized to investigate the effect of post-synthetic linkage conversion. The first, a pyrene-based COF (Tfpy-PDA), was chosen for its excellent light-harvesting properties and extended π-surface.[1] The second system, based on a [1,2,4]-triazolo-[1,3,5]-triazine core (TTT-TAPB), was selected for its planar structure and high density of nitrogen sites, which are known to coordinate with gold(III). These imine-linked COFs were synthesized via polycondensation reactions (**Figure 3.1**) and subsequently converted to their thiazole-linked analogues (Tfpy-PDA-S and TTT-TAPB-S) through a post-synthetic modification (PSM) with elemental sulfur (**Figure 3.2**). This reaction transforms the imine bonds into more robust thiazole rings, simultaneously enhancing chemical stability and introducing sulfur atoms as additional gold-binding sites.

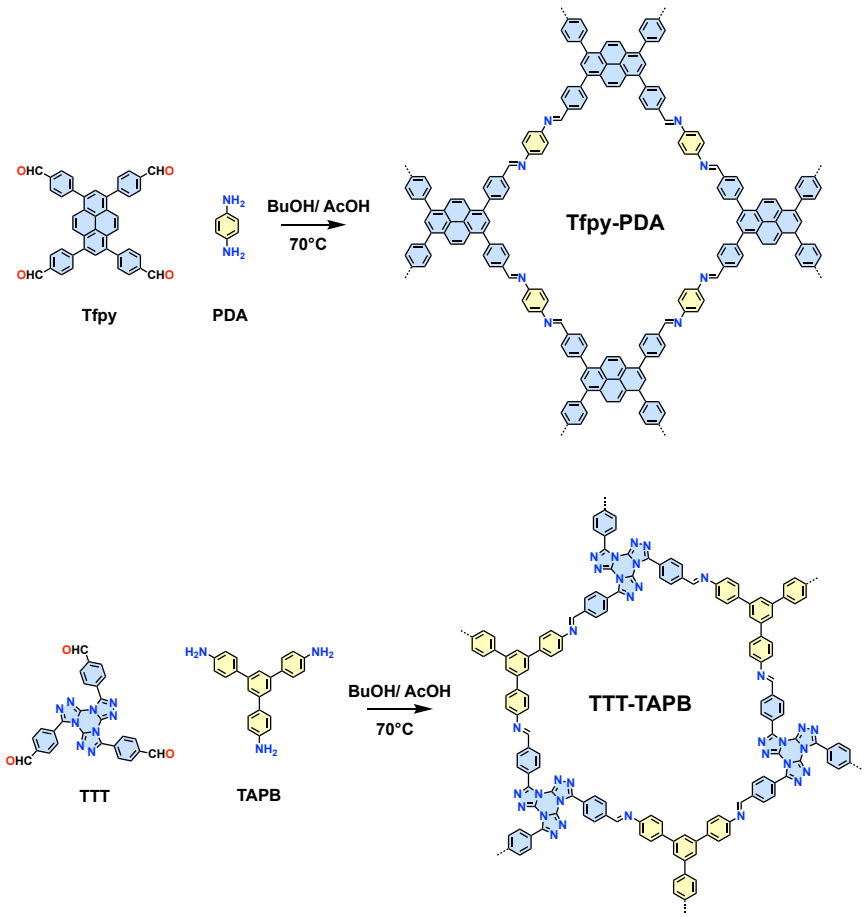

Figure 3.1. Synthesis of the imine COF Tfpy-PDA and TTT-TAPB.

- For the Tfpy-PDA system, the combination of a tetratopic Tfpy monomer and a ditopic PDA monomer resulted in a rhombic 2D layered structure with Cmm2 space group symmetry. The experimental pattern showed high crystallinity, with pronounced peaks at 3.71°, 5.38°, 7.47°, 8.45°, 11.24°, 12.1°, and 15.05° corresponding to the (110), (020), (220), (130), (330), (240), and (440) reflections, respectively. The optimized unit cell parameters based on the experimental data were a= 34.25 Å, b= 32.75 Å, c= 4.42 Å, and $\alpha = \beta = \gamma = 90°$, with residual factors R_{wp}= 7.78 % and R_p = 6.13 % (**Figure 3.3A**).

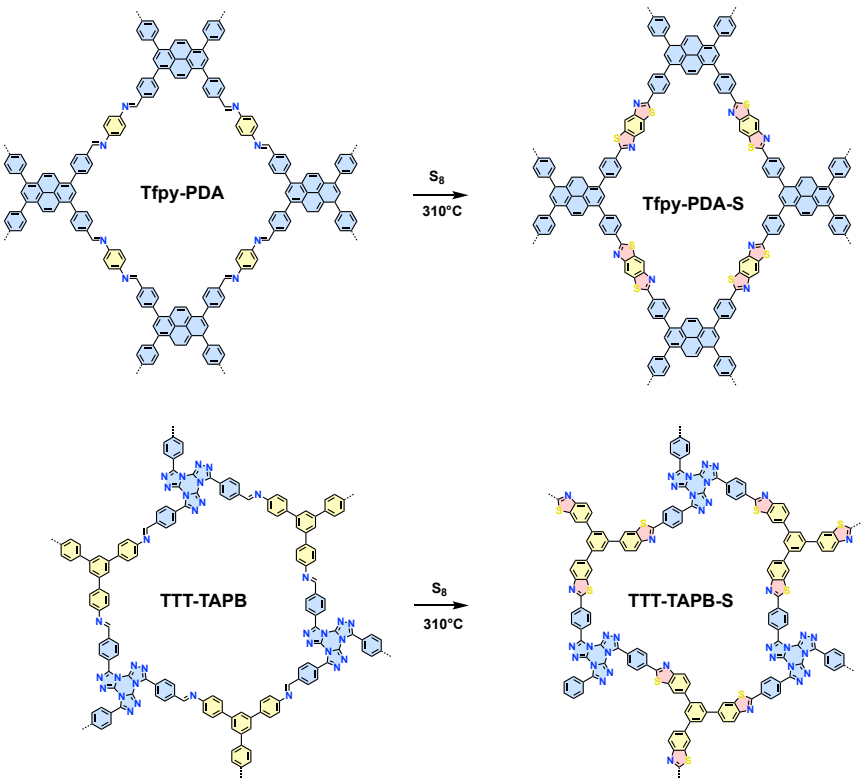

Figure 3.2. Conversion of the imine-linked COFs Tfpy-PDA and TTT-TAPB into thiazole-linked COFs Tfpy-PDA-S and TTT-TAPB-S.

After conversion to Tfpy-PDA-S, the material remained highly crystalline, but the main diffraction peaks shifted to higher angles, with the (110), (020), and (220) facets appearing at 3.90°, 5.55°, and 7.70°, respectively. This shift is indicative of a smaller unit cell (a = 32.60 Å, b = 33.62 Å, c = 3.68 Å) resulting from the contraction of the framework upon thiazole ring formation with residual factors R_{wp}= 6.10 % and R_p = 3.62 % (**Figure 3.3B**).

- The TTT-TAPB system, formed from two tritopic monomers, adopted a 2D layered structure with hexagonal pores and P-6 space group symmetry. Its experimental PXRD pattern showed characteristic peaks at 3.8°, 6.6°, 7.6°, and 10° corresponding to the (100),

(110), (200), and (120) reflections of an AA stacking model. The refined unit cell parameters were a = b = 26.88 Å, c = 3.29 Å, $\alpha = \beta =$ 90°, and γ = 120° with residual factors R_{wp}= 1.53% and R_p = 2.66% (**Figure 3.3C**). The post-modified TTT-TAPB-S showed a highly similar pattern, which agreed well with a simulated thiazole-linked COF with AA stacking. The (100) and (110) peaks shifted slightly to 3.9° and 6.7°, indicating a small contraction of the unit cell (a = b = 26.59 Å) upon linkage conversion (**Figure 3.3D**).

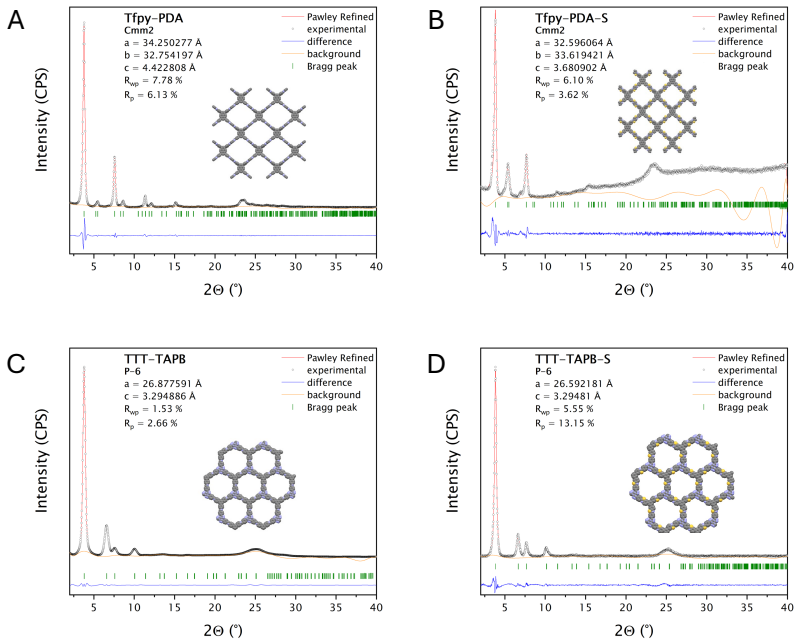

Figure 3.3. Powder XRD Pawley refinement of A) Tfpy-PDA, B) Tfpy-PDA-S, C) TTT-TAPB, D) TTT-TAPB-S.

The good correspondence between the experimental data and theoretical models for all materials confirmed the successful synthesis and structural transformation.

FTIR spectroscopy confirmed the successful formation of both Tfpy-PDA and TTT-TAPB COFs through the disappearance of characteristic vibrational bands of the aldehyde C=O stretch (around 1700 cm^{-1} for Tfpy and TTT) and the amine N-H stretch (between 3100 – 3500 cm^{-1} for PDA and TAPB). Subsequently, a new stretching vibration corresponding to the imine bond (N=CH) appeared at approximately 1625 cm^{-1} for both COFs (**Figure A.50**). Following the sulfur post-modification the imine stretch vibration disappeared. The formation of the thiazole ring caused a shift of C=N vibration towards 1610 cm^{-1}, although this shift was less discernible for TTT-TAPB due to overlapping vibrations within its triazolo-triazine core(**Figure 3.4**). The appearance of new peaks around 1380 cm^{-1} and 815 cm^{-1} in the FTIR spectra of the post-modified COFs (Tfpy-PDA-S and TTT-TAPB-S) are assigned to the C-S stretching and breathing vibrations of the thiazole ring, respectively, strongly suggesting their successful formation.

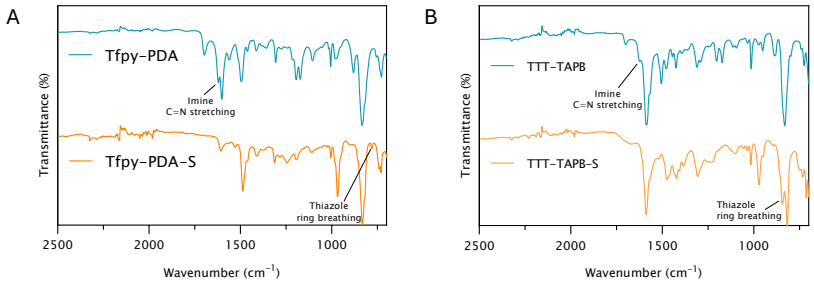

Figure 3.4. Comparison of A) Tfpy-PDA and B) TTT-TAPB before and after post-modification using FTIR.

Nitrogen sorption analysis was performed at 77 K to evaluate the porosity of all COFs (**Figure 3.5**). The Brunauer-Emmet-Teller (BET) surface area of Tfpy-PDA is 2155 m^2/g (R^2 = 0.999 and C (BET constant) = 170), which after post-modification to TFPy-PDA-S COF reduces to 1295 m^2/g (R^2 = 0.998 and C = 523). TTT-TAPB COF and TTT-TAPB-S COFs exhibited both type IV isotherms, indicating their mesoporous nature. The BET surface areas were calculated to be 1384 m^2/g (R^2 = 0.996 and C

= 111) and 1124 m^2/g (R^2 = 0.998 and C = 54), respectively (**Figure 3.5, Figure A.42**). Regarding the shape of the nitrogen sorption isotherms, Tfpy-PDA COF exhibits a type-IV isotherm, which corresponds to a mesoporous type of material, whilst Tfpy-PDA-S COF has a type-I isotherm, which is characteristic of microporous materials (pore size < 2 nm). TTT-TAPB COF and TTT-TAPB-S COF both show Type-IV isotherms coherent with their mesoporous pore size (> 2 nm). After the post-modification step, pore size analysis with quenched-solid density functional theory (QSDFT) (using the cylindrical/sphere pore, adsorption branch kernel) also shows a reduction in pore sizes. Due to the cyclization of the imine linkage in Tfpy-PDA COF into a thiazole linkage in Tfpy-PDA-S, the pore contracts, leading to a decrease in pore size from 2.19 nm to 1.98 nm (**Figure A.43**,**Figure A.44**). This can also be observed for the conversion of TTT-TAPB COF into TTT-TAPB-S COF where the pore sizes are 2.31 nm and 2.18 nm, respectively.

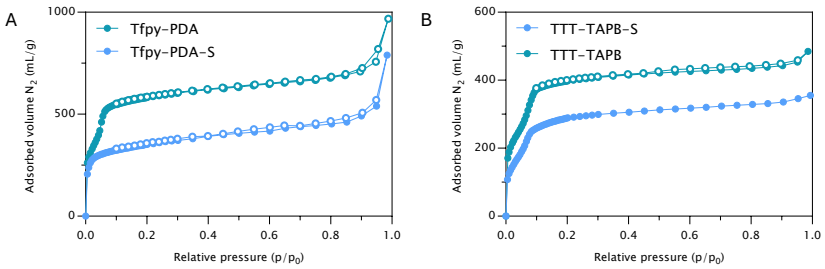

Figure 3.5. Comparison of A) Tfpy-PDA and B) TTT-TAPB before and after post-modification using nitrogen sorption.

X-ray Photoelectron Spectroscopy (XPS) provided additional evidence for the conversion (**Figure 3.6**). For the pyrene system, the N 1s peak assigned to imine nitrogens at 398.3 eV in Tfpy-PDA shifted to a higher binding energy of 399.1 eV in Tfpy-PDA-S. A similar shift from 400.8 eV to 401.3 eV was observed for the TTT-TAPB system. In both cases, the shift indicates a change in the electronic environment of the nitrogen atom consistent with its incorporation into a thiazole ring.

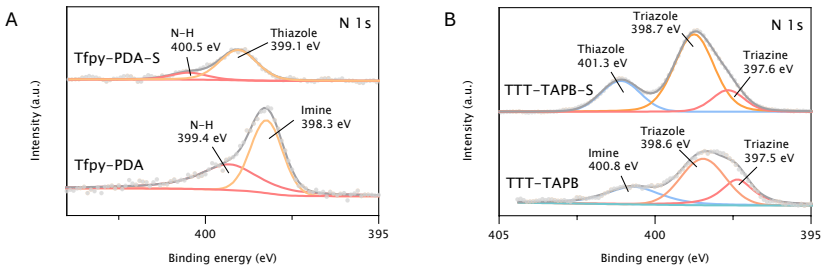

Figure 3.6. Comparison of A) Tfpy-PDA and B) TTT-TAPB before and after post-modification using nitrogen XPS.

Finally, the chemical stability of the frameworks was compared. The thiazole-linked COFs maintained their crystallinity after being immersed in 1 mol L^{-1} HCl for 24 hours, whereas the parent imine COFs showed significant deterioration due to the hydrolysis of the imine bonds under acidic conditions (**Figure 3.7**). This result clearly demonstrates the enhanced robustness imparted by the imine-to-thiazole linkage conversion.

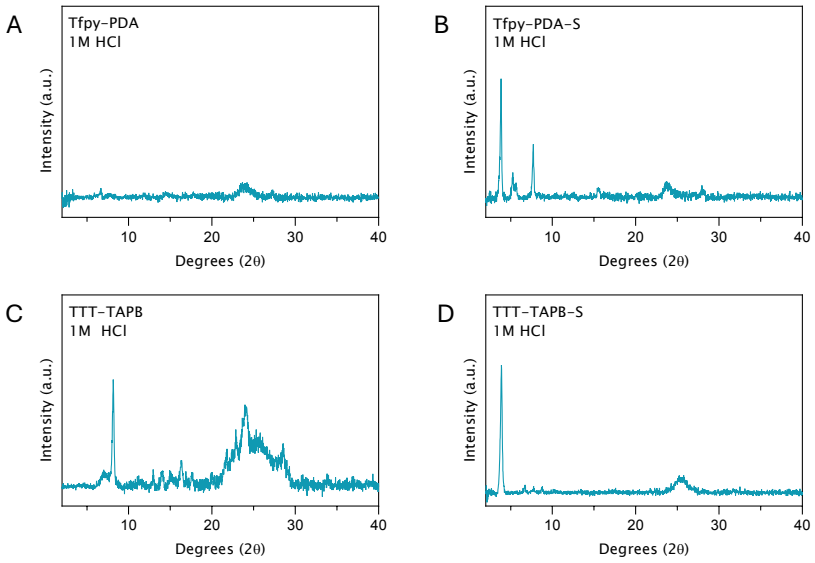

Figure 3.7. PXRD of A) Tfpy-PDA, B) Tfpy-PDA-S, C) TTT-TAPB, D) TTT-TAPB-S after immersing COFs 24h in 1M HCl solution.

3.2.2 Gold Adsorption Performance

Adsorption in Dark vs. Light Conditions

The gold adsorption capabilities of the four COFs were evaluated under both dark and light-irradiated conditions.

Under dark conditions, all materials showed high uptake capacities (**Figure 3.8A**). The parent imine COFs, Tfpy-PDA and TTT-TAPB, achieved capacities of 2322 mg/g and 3088 mg/g, respectively. The post-synthetically modified thiazole COFs exhibited even higher performance, with Tfpy-PDA-S reaching 3106 mg/g and TTT-TAPB-S achieving an impressive 3533 mg/g. This enhancement underscores the positive role of the introduced sulfur sites. Upon irradiation with a 34 W LED white light, the adsorption capacities were enhanced for all materials (**Figure 3.8B**). The capacity of Tfpy-PDA-S surged by 157% to a remarkable 7980 mg/g,

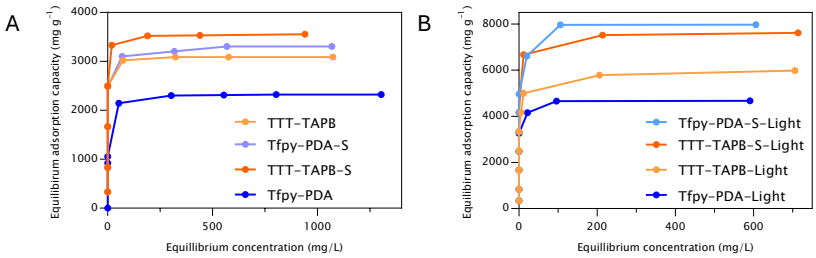

Figure 3.8. A) Adsorption isotherms of Au(III) under dark conditions and B) upon light irradiation, demonstrating the significant photocatalytic enhancement of gold uptake capacity.

while TTT-TAPB-S increased by 115% to 7620 mg/g. These values represent some of the highest ever reported for gold recovery (**Figure A.75**, **Figure A.76**), highlighting the powerful synergy between the COF framework and photocatalysis.

Adsorption Kinetics and pH Influence

The kinetics of gold uptake were exceptionally rapid, particularly for the thiazole-linked COFs. Both Tfpy-PDA-S and TTT-TAPB-S removed over 95% of gold from a 100 ppm solution within the first minutes (**Figure A.65**). The kinetic data fit well with a pseudo-second-order model, which is characteristic of chemisorption processes where electron transfer is the rate-limiting step (**Figure A.66**),(**Figure A.67**).

The influence of pH was also investigated. Adsorption performance remained stable across a wide acidic-to-neutral pH range (**Figure A.69**). However, at pH values above 7, the capacity decreased significantly. This is attributed to the hydrolysis of the negatively charged $[AuCl_4]^-$ anion into neutral or differently charged gold-hydroxo species under alkaline conditions, which hinders the electrostatic attraction to the COF surface.[2]

3.2.3 Mechanistic investigation

A multi-faceted investigation was undertaken to elucidate the mechanism of gold recovery with these COFs, combining spectroscopic, microscopic, electrochemical, and computational methods to understand the process in both dark and light-irradiated conditions.

The Adsorption-Reduction Mechanism in Darkness

In the absence of light, gold capture is governed by a dual-function mechanism involving initial reductive chemisorption followed by autocatalytic growth. XPS and FTIR analyses of the gold-loaded COFs were used to identify the active sites. For the imine COFs, a significant positive shift in the N 1s core level binding energy confirmed that the imine nitrogen atoms act as the primary sites for binding and reducing Au(III) ions (**Figure 3.9A**).[3] This was corroborated by FTIR, where the characteristic imine (C=N) stretching vibration, for example, in TTT-TAPB COF shifted significantly from approximately 1627 cm^{-1} to 1665 cm^{-1} upon interaction with gold ions (**Figure 3.9C**). For the thiazole-linked COFs, XPS analysis revealed shifts in both the N 1s and S 2p core level spectra, including the appearance of an oxidized sulfur peak around 168.0 eV, confirming the synergistic involvement of both nitrogen and sulfur atoms in the redox process(**Figure 3.9B**, **Figure A.53**). For the thiazole COFs, no notable shifts in FTIR were observed, probably due to thiazole ring vibrations being less discernible in FTIR. Additionally, this initial binding is strongly supported by electrostatic interactions. Zeta potential measurements confirmed that the COF surfaces possess a net positive charge within the optimal acidic pH range, facilitating a favorable electrostatic attraction with the negatively charged $[AuCl_4]^-$ anions (**Figure 3.9D**, **Figure A.56**).

The exceptionally high, super-stoichiometric capacities observed cannot be explained solely by direct binding and reduction. This points to a

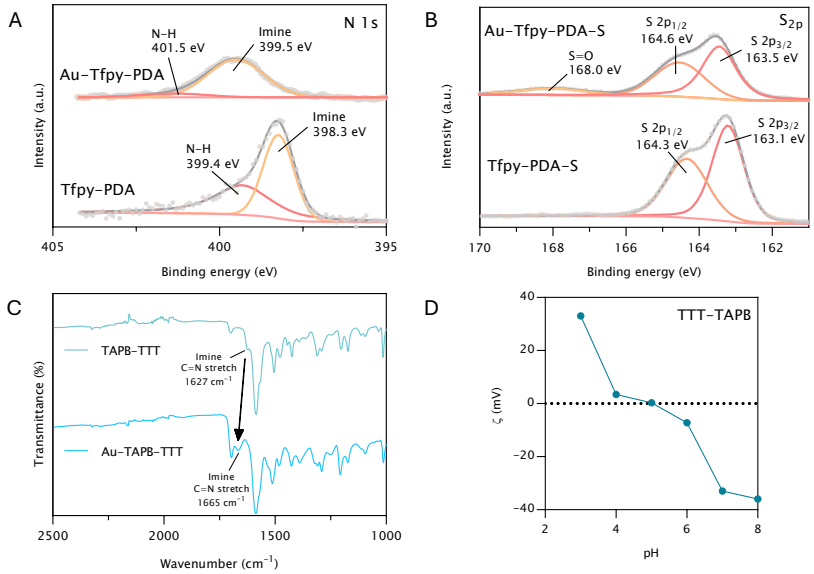

Figure 3.9. A) XPS spectra overlap of N 1s core level of Tfpy-PDA and Au-Tfpy-PDA, B) XPS spectra overlap S 2p core level of Tfpy-PDA and Au-Tfpy-PDA-S, C) FTIR spectrum overlap of the TTT-TAPB before and after gold adsorption, D) Zeta potential vs. pH curve of TTT-TAPB.

secondary, autocatalytic growth mechanism. After initial Au(0) nanoparticles are formed and stabilized on the COF surface, they act as catalytic seeds. These seeds autocatalytically reduce additional $[AuCl_4]^-$ ions from the solution, with water molecules serving as the reductant.[4] This process was experimentally verified by monitoring for the production of hydrogen peroxide (H_2O_2), a byproduct of water oxidation, during the adsorption experiment in an oxygen-free environment (**Figure A.61**). The detection of H_2O_2 provides strong evidence for this seed-mediated growth model, which explains the system's ability to achieve gold loadings that far surpass the stoichiometric limits of the framework's binding sites.

To further elucidate the initial gold adsorption and reduction mechanism, we employed density functional theory (DFT) calculations at the GGA-PW91 level of theory after geometry optimization for different binding sites on their model compounds, which revealed a synergistic multi-step process. Initially, the $[AuCl_4]^-$ anion is drawn to the framework through a combination of physisorption via Au–Cl···H–C hydrogen bonding and strong electrostatic attraction to the protonated nitrogen sites on the COF. The calculated binding energies for this step highlight a stronger interaction in the parent imine-COFs (4.68–5.09 eV for Tfpy-PDA and 2.71–3.24 eV for TTT-TAPB) compared to their thiazole-modified counterparts (1.38–2.08 eV for Tfpy-PDA-S and 1.71–1.82 eV for TTT-TAPB-S) (**Figure A.77-81**). Following this, a crucial chemisorption step occurs through a ligand exchange where the protonated nitrogen directly binds to the gold center by expelling an HCl molecule to form a covalent N–Au bond; a transformation that is highly favorable in an aqueous environment due to the strong solvatation and stabilization of the released chloride anion.[5] DFT confirms that all nitrogen sites are energetically favorable anchors for this initial binding of the Au(III) complex, holding it more strongly than sulfur sites by approximately 0.7 eV (**Figure 3.10**). After the formation of these covalent Au-N and Au-S bonds, electrons from the conjugated framework can be used to further reduce the Au(III) to Au(0) with a sequential ligand exchange mechanism.[6, 7] This pathway involving both nitrogen and sulfur sites are in agreement with the XPS and FTIR observations.

Definitive evidence of the gold reduction was obtained from multiple characterization techniques. Examination of the Au 4f core level XPS spectra for all gold-loaded COFs consistently revealed the presence of gold in two distinct oxidation states: Au(0) (peaks at 84.4 eV and 88.1 eV) and Au(III) (peaks at 85.6 eV and 89.7 eV)(**Figure 3.11A**, **Figure A.55**). This confirms the coexistence of adsorbed Au(III) ions and reduced elemental Au(0) on the COF surface. PXRD analysis of the COFs after gold adsorption showed new diffraction peaks corresponding to the (111), (200), (220), and (311) planes of face-centered cubic (fcc) elemental gold,

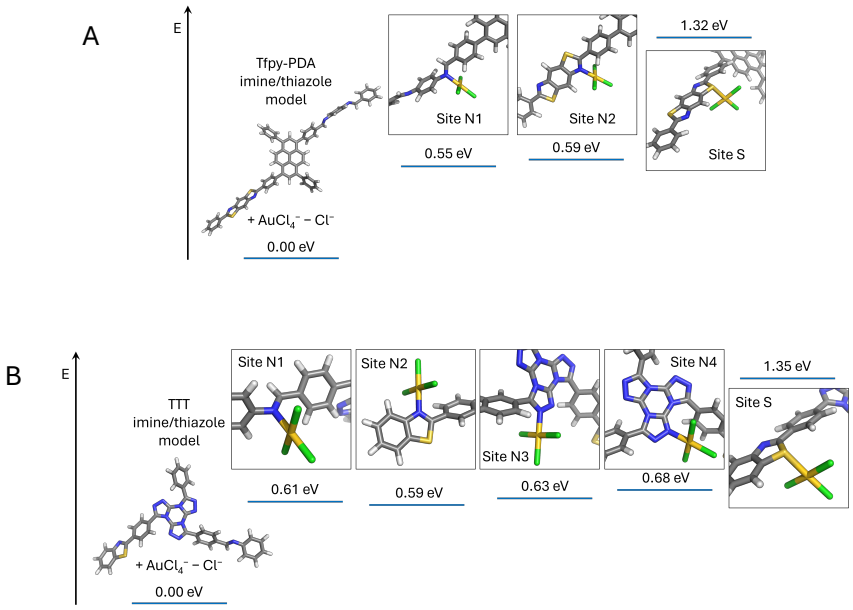

Figure 3.10. Binding energies of the different N and S binding sites for the model compounds of A) Tfpy-PDA and Tfpy-PDA-S and B) TTT-TAPB and TTT-TAPB-S.

further confirming the reduction to metallic nanoparticles (**Figure A.72**). Finally, Transmission Electron Microscopy (TEM) imaging provided direct visual evidence of these gold nanoparticles (AuNPs) within the COF structures, which were generally spherical with sizes ranging from 1 to 20 nm (**Figure 3.11B**, **Figure A.57-60**).

The Enhanced Photocatalytic Pathway

Under light irradiation, the system transitions to a significantly more efficient photocatalytic pathway. The thermodynamic feasibility of this process was first established. The prerequisite for photocatalytic reduction is that the Conduction Band Minimum (CBM) of the COF semiconductor must be at a more negative potential than that of the Au(III)/Au(0) couple (+1.002 V vs. NHE). Mott-Schottky analysis confirmed that all four COFs

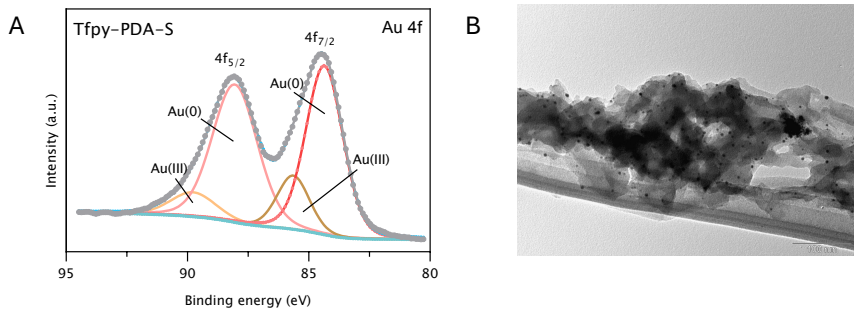

Figure 3.11. A) XPS spectrum of the Au 4f core level after gold adsorption of Tfpy-PDA-S, B) TEM image of gold adsorbed on Tfpy-PDA.

are n-type semiconductors with CBMs substantially more negative than the gold reduction potential (e.g., -0.53 V vs. NHE for Tfpy-PDA-S), providing the necessary thermodynamic driving force for electron transfer (**Figure 3.12A,Figure A.45**).

The superior performance of the thiazole-linked COFs under illumination stems from their enhanced photophysical properties. Solid-state UV-Vis diffuse reflectance spectroscopy (DRS) revealed a notable broadening of the absorption band and a significant red-shift of the absorption edge for the thiazole COFs compared to their imine analogues (e.g., from 536 nm to 660 nm for Tfpy-PDA-S) (**Figure 3.12B**). This indicates a narrowing of the optical band gap, a direct result of the enhanced π-conjugation afforded by the planar thiazole rings. This allows the materials to harvest a larger portion of the visible light spectrum, generating more electron-hole pairs.

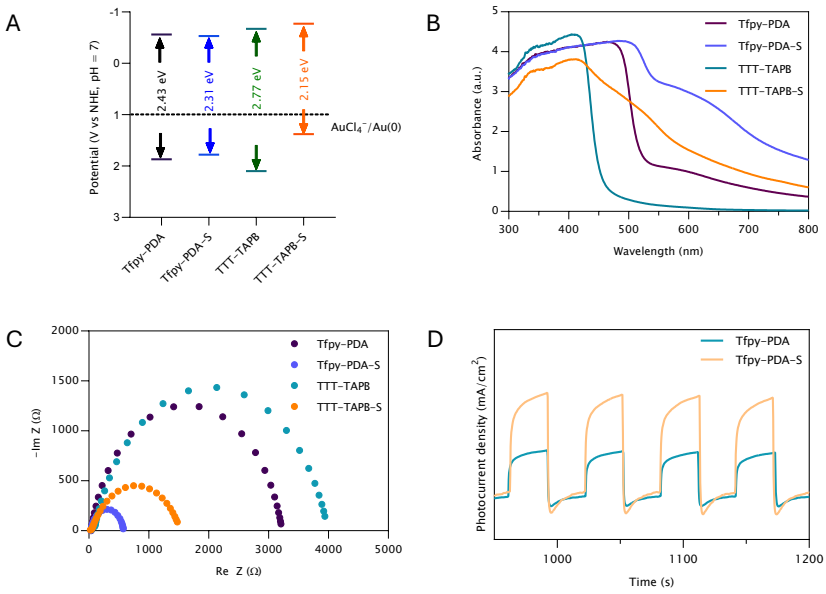

Figure 3.12. A) Band position diagram, B) Solid-state UV-Vis absorption spectra, C) Electrochemical impedance (EIS) Nyquist plots, D) Photocurrent response curves of Tfpy-PDA and Tfpy-PDA-S.

Beyond improved light harvesting, the thiazole modification leads to more efficient charge separation and transfer, which is the core of the photocatalytic enhancement. Electrochemical impedance spectroscopy (EIS) showed that the thiazole-linked COFs possess lower charge transfer resistance, as indicated by smaller semicircles in their Nyquist plots(**Figure 3.12C**). Furthermore, photocurrent response measurements provided direct evidence of superior performance, with Tfpy-PDA-S and TTT-TAPB-S generating significantly higher photocurrent densities than their imine counterparts (**Figure 3.12D**). This confirms a more efficient generation and/or separation of photogenerated charge carriers in the thiazole-based systems.

This evidence culminates in a comprehensive photocatalytic cycle (**Figure 3.13**). Upon illumination, photoexcited electrons are generated within the framework, providing a powerful and readily available source

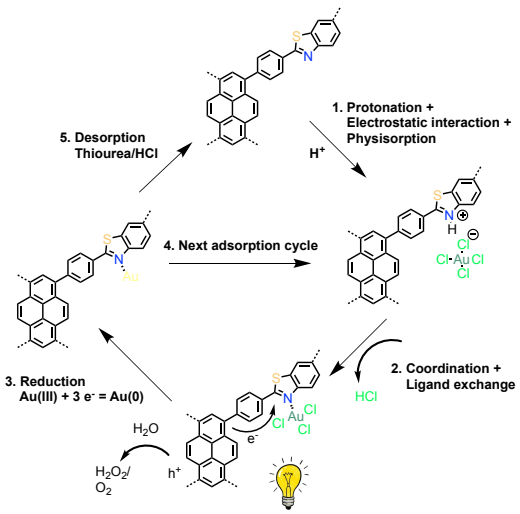

Figure 3.13. Adsorption and photocatalytic redox cycle of a thiazole-linked COF.

of reducing agents that rapidly convert the anchored Au(III) complexes to Au(0). We, therefore, propose a mechanism where the abundant nitrogen and sulfur sites first anchor the Au(III) complex, after which the superior photocatalytic properties of the thiazole-COFs facilitate its reduction to metallic Au(0). Simultaneously, the corresponding holes (h^+) in the valence band are consumed through the oxidation of water to directly produce hydrogen peroxide (H_2O_2) or oxygen (O_2) which can be further utilized to photosynthesize H_2O_2, thus completing the photocatalytic cycle with water acting as a sacrificial electron donor (**Figure A.61**). It was noted that the H_2O_2 production is consistently higher than in the experiments in the dark. Despite this efficient mechanism, the process is ultimately self-limiting due to catalyst passivation. This passivation arises from the system naturally seeking its lowest surface energy state. Nanoparticle growth stops once they reach a size and shape where it is no longer energetically favorable to get bigger, achieving a stable thermodynamic equilibrium on the COF surface.[8]

Selective Gold Recovery from Electronic Waste

To assess the practical utility of these materials, their performance was evaluated under realistic conditions using leachate derived from computer processing unit (CPU) scrap. The leachate, prepared by dissolving CPU scrap in aqua regia, contained a complex mixture of metals, with gold present at a low concentration (5.9 ppm) alongside high concentrations of competing ions, primarily copper (385 ppm), nickel (126 ppm), and zinc (9 ppm).

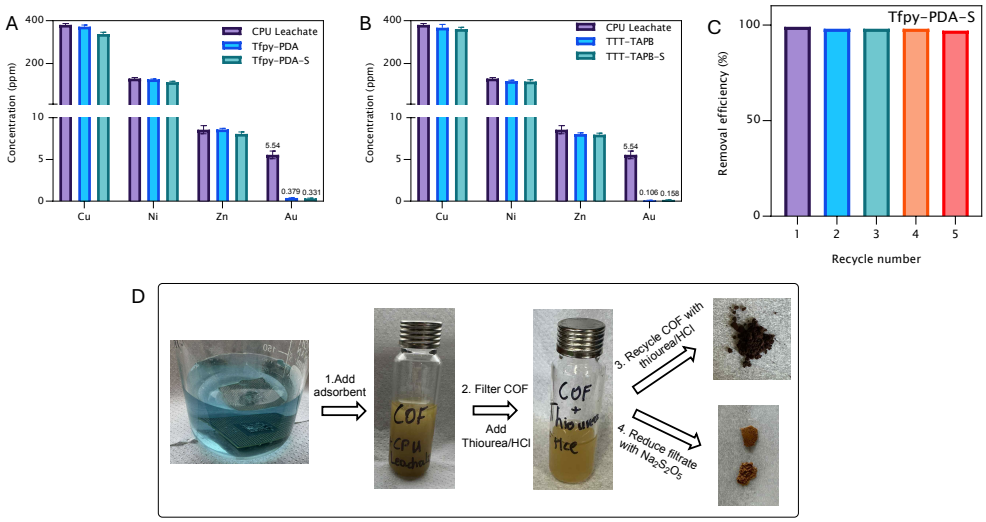

Figure 3.14. Removal efficiency Au, Cu, Ni, Zn in a CPU leaching solution using A) Tfpy-PDA and Tfpy-PDA-S, B) TTT-TAPB and TTT-TAPB-S, C) Recyclability of Tfpy-PDA-S for the removal efficiency of a 100 ppm Au(III) solution, D) Practical routine for the recovery of gold from CPU-waste using COFs.

All four COFs demonstrated outstanding performance in this challenging multi-element matrix. High gold removal efficiencies were achieved even without light irradiation, with TTT-TAPB as the top performer, extracting 98% of the available gold (**Figure 3.14A,B**). Crucially, the uptake of the other major metal ions (Cu, Ni, Zn) was minimal, with removal efficiencies remaining below 10% for all COFs. This confirms the exceptional

selectivity of the materials towards gold in a competitive environment. Interestingly, light irradiation did not lower the final residual gold concentration in the e-waste solution beyond what was achieved in darkness. This high selectivity can be rationalized by HSAB theory: the soft Lewis acid Au(III) exhibits a strong affinity for the soft base sites (N, S) and the (photogenerated) electrons in the COF, while harder Lewis acid competitors like copper, zinc, and nickel show much weaker interaction, making their adsorption and reduction far less favorable.

The reusability of the adsorbents is a critical factor for practical applications. The thiazole-linked COFs exhibited excellent recyclability, maintaining high removal efficiencies over five consecutive cycles of adsorption and regeneration(**Figure 3.14C**, **Figure A.74**). This superior performance is directly linked to the enhanced chemical stability imparted by the linkage conversion. The robust thiazole linkage withstands the acidic thiourea solution used for elution, preserving the framework's integrity. In contrast, the imine-linked COFs showed a gradual decline in performance, which is attributed to the partial hydrolysis of the less stable imine bond during the acidic regeneration step. This provides a clear, practical consequence for the initial linkage engineering strategy, directly connecting enhanced stability to improved reusability.

To complete the recovery cycle and demonstrate the feasibility of obtaining high-purity metal, a final recovery step was performed. After saturating Tfpy-PDA-S with gold from the CPU leachate, the adsorbed metal was eluted using an acidic thiourea solution. The gold in the eluate was then chemically reduced with sodium metabisulfite, precipitating a fine, dark yellow gold powder (**Figure 3.14D**). Analysis of this recovered solid by ICP-MS confirmed a gold purity of 98.35%, equivalent to 23.6 karats. This result validates the efficacy of the complete adsorption-desorption-reduction cycle for selectively capturing and recovering high-purity gold from complex electronic waste streams.

3.2.4 Conclusion

In this work, we demonstrate that a simple post-synthetic conversion of imine-linked covalent organic frameworks (COFs) to their thiazole-linked analogues creates highly efficient adsorbents for gold recovery. This imine-to-thiazole transformation represents a powerful example of synergistic materials design, where a single chemical modification concurrently imparts a threefold advantage crucial for this complex application. Firstly, the inherent robustness of the thiazole linkage provides superior chemical stability, allowing the framework to maintain its structural integrity and performance over multiple adsorption-elution cycles in acidic media. Secondly, the modification strategically introduces soft-base sulfur atoms into the COF backbone to enhance the material's intrinsic adsorption capacity in dark conditions. Finally, the planar thiazole rings enhance the framework's overall π-conjugation, leading to vastly improved photophysical properties, including superior light harvesting and more efficient charge separation that drive the dramatic light-induced enhancement of gold uptake to record-high levels. This photophysical enhancement enables a highly efficient photoreduction of gold ions under light, leading to a remarkable maximum adsorption capacity up to 7980 mg/g. Critically, these materials demonstrated practical utility by selectively recovering up to 98% of gold from real electronic waste leachates over multiple cycles. Our findings establish this strategy as a straightforward and highly effective route for designing next-generation photocatalytic materials for sustainable resource recovery.

3.3 Experimental Section

3.3.1 Monomer Synthesis

The Tfpy(1,3,6,8-Tetrakis(4-formylphenyl)pyrene) linker was synthesized via a Suzuki coupling reaction. 1,3,6,8-tetrabromopyrene (371 mg, 0.72

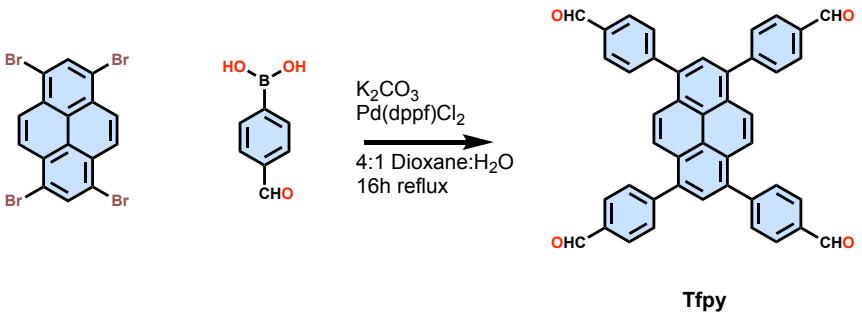

Figure 3.15. Synthesis of 1,3,6,8-Tetrakis(4-formylphenyl)pyrene (Tfpy) linker.

mmol) and 4-formylphenylboronic acid (480 mg, 3.20 mmol) were added to a two-necked round-bottom flask with 8 mL of 1,4-dioxane and 2 mL of H_2O. The mixture was degassed by refluxing under an argon atmosphere for 30 minutes. Subsequently, K_2CO_3 (547 mg, 3.66 mmol) and $Pd(dppf)Cl_2$ (26 mg, 0.036 mmol) were added, and the reflux was continued for 16 hours. After cooling, 20 mL of H_2O was added, and the precipitate was collected by filtration, washed with H_2O and MeOH, and dried under vacuum to yield the product as a yellow powder (404 mg, 91% yield).

^{1}H NMR (300 MHz, $CDCl_3$, 298 K): δ (ppm) = 10.17 (s, 4H), 8.18 (s, 4H), 8.10 (d, 8H), 8.04 (s, 2H), 7.86 (d, 8H).

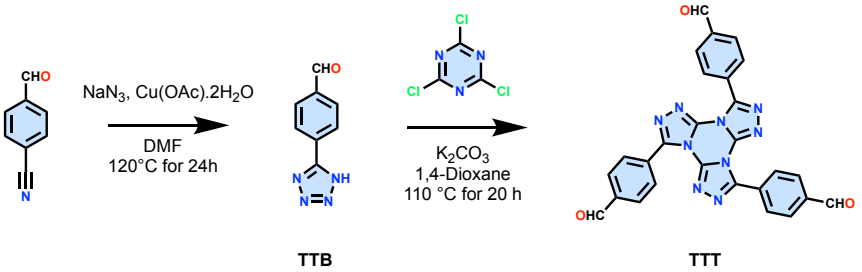

Figure 3.16. Synthesis of 4,4',4"- (tris((1,2,4)triazolo)-(1,3,5)-triazine-tribenzaldehyde (TTT) linker.

The synthesis of TTT (4,4',4"-(tris((1,2,4)triazolo)-(1,3,5)-triazine-tribenzaldehyde) was a two-step process. First, 4-(1H-tetrazol-5-

yl)benzaldehyde (TTB) was prepared by reacting 4-formylbenzonitrile (1.31 g, 10 mmol) with sodium azide (780 mg, 12 mmol) and $Cu(OAc)_2 \cdot H_2O$ (200 mg) in DMF at 120°C for 24 hours. The product was precipitated with 5 mol L^{-1} HCl and washed to yield TTB (1.70 g, 95% yield). Next, TTB (870 mg), cyanuric chloride (275 mg), and K_2CO_3 (2.78 g) were refluxed in dry dioxane at 110°C for 20 hours under argon. The dioxane solvent was removed under reduced pressure and methanol was added to the residue. The off-white precipitate was filtered and washed with water, methanol, then dried under vacuum for 16 hours (0.125 g, 26% yield). Synthesis was adjusted from literature.[9]

^{1}H NMR (300 MHz, DMSO-d_6, 298 K): δ (ppm) = 10.18 (s, 3H), 8.25 (d, 6H), 8.20 (d, 6H).

3.3.2 COF Synthesis

Tfpy-PDA COF

Tfpy (360 mg, 0.501 mmol) and 1,4-phenylenediamine (110 mg, 1.02 mmol) were combined in a 40 mL vial. A solvent mixture (19.4 mL) of n-butanol, glacial acetic acid, and water (67:23:10 v/v) was added. Finally, the vial was closed with a screwcap, and the resulting solution was bubbled for 15 min with Ar through a needle. The mixture was stirred at 70°C and stirred for 16 hours. After cooling to room temperature, the obtained COF was filtered over a nylon filter of 0.45μm pore diameter, washed with 10 mL H_2O, 2x10 mL methanol, then 2x10 mL acetone. The resulting powder was dried under vacuum at 90°C for 16h (0.402 g, 93% yield).

Tfpy-PDA-S COF

In a glass ampule were added 20 mg of Tfpy-PDA COF and 200 mg of elemental sulfur. The ampule was evacuated under vacuum for 15 min

and flame-sealed. The ampule was heated to 150 °C (at 5 °C min^{-1} heating rate) for 3 hours, then the temperature was raised to 310 °C (at 0.89 °C min^{-1} heating rate) and kept for 6 hours at this temperature. After cooling to room temperature, the residue was washed overnight with 50 mL of a 3/2 volume ratio solution of ortho-dichlorobenzene/chlorobenzene at 100 °C to remove the residual sulfur. The solid was collected by filtration and washed with water, methanol, and acetone. The resulting dark yellow powder was dried at 90 °C under vacuum for 16 hours. (19.1 mg, 88% yield)

TTT-TAPB COF

31 mg TTT (0.06 mmol) and 21 mg TAPB (0.09 mmol) were added to a 4 mL glass vial containing an oblong teflon stirring bar with a length of 1 cm. 1.5 mL of a solution consisting of 1 mL n-butanol, 0.150 mL water, and 0.350 mL glacial acetic acid was added. The vial was closed with a plastic screwcap, and stirred at 250 rpm at 70 °C for 16 hours in an aluminium heating block. After cooling to room temperature, the solid from the resulting yellow slurry was collected by filtration over a nylon filter of 0.45 μm pore diameter, washed with 10 mL H_2O, 10 mL DMF, 10 mL acetone, then 10 mL methanol. The powder was soaked in the solvent for 10 minutes each washing step. The resulting bright-yellow powder was dried at 90°C under vacuum for 16 hours (36 mg, 94% yield).

TTT-TAPB-S COF

For the post-synthetic modification of the imine linkage to the thiazole linkage, 20 mg of TAPB-TTT was thoroughly ground with elemental sulfur for 5 minutes in a pestle and mortar. The resulting mixture was transferred to a glass ampoule, evacuated to 0.40 mbar for 5 minutes, and flame-sealed under vacuum. The ampoule was heated in a muffle furnace. The temperature was first increased to 155 °C over a period of

two hours, then held at 155 °C for 3 hours. Then, the temperature was increased to 320 °C over 3 hours and held at this temperature for 5 hours, before cooling down to room temperature. The ampoule was opened, and the obtained brown monolith was soaked in 20 mL of chlorobenzene/o-dichlorobenzene in a 2:3 volume ratio at 120 °C while stirring overnight. The material was filtered over a nylon filter of 0.45 μm pore diameter, washed with methanol and acetone, and dried under vacuum for 16 hours. (19.3 mg, 85%)

3.3.3 Materials Characterization

For spectroscopic and structural analysis, several methods were employed. Nuclear Magnetic Resonance (NMR) spectra were recorded on a Bruker Avance I spectrometer at 7.0 Tesla. Powder X-Ray Diffraction (PXRD) patterns were collected on a Bruker D8 Advance diffractometer using a Cu-Kα source. Fourier Transform Infrared (FTIR) Spectroscopy was performed on a Perkin Elmer FTIR SPECTRUM 1000 with an Attenuated Total Reflection (ATR) unit. Ultraviolet/Visible (UV-Vis) Spectroscopy was conducted on a Shimadzu UV 2600 Scanning Spectrophotometer. The material's morphology was examined with Scanning Electron Microscopy (SEM) using a JCM-7000 NeoScopeTM Benchtop SEM. The surface chemical composition was analyzed by X-Ray Photoelectron Spectroscopy (XPS) on a PHI 5000 VersaProbe II spectrometer. Thermogravimetric Analysis (TGA) was performed on a Perkin-Elmer STA6000 analyzer. Elemental concentrations in solution were determined by Inductively Coupled Plasma Mass Spectrometry (ICP-MS) on a NexION 300 (for Au) and ICP-OES on a Thermo Fisher iCap 7000 (for other metals). Nitrogen Sorption isotherms were measured at 77 K using an Anton Paar Autosorb 6100 after samples were activated overnight under vacuum at 120°C. For electrochemical measurements, 3 mg of the photocatalysts were dispersed in a mixture containing 300 μL EtOH, and 30 μL Nafion. The mixture was sonicated for 4 hours to form a homogenous catalyst ink. 100 μL of this catalyst ink was drop-casted on a polished 1 cm × 2 cm area

of an FTO glass and dried in air. These measurements were conducted on a CHI 660E electrochemical workstation in a three-electrode cell system under irradiation of with 300 W Xe lamp (Perfect Light PLS-SXE 300+) with a ≥420 nm cutoff filter. A Pt wire and a calomel electrode were used as the working electrode and the reference electrode, respectively. A 0.1 M Na_2SO_4 solution was utilized as electrolyte. Electrochemical impedance spectroscopy (EIS) was carried out at a bias potential of +1.5 V in the dark. Impedance spectra were fitted using the equivalent Randle circuit R_s+ (Q_{Bulk}/R_{Bulk}) + (Q_{CT}/R_{CT}), where R_s is the solvent resistance, R_{Bulk} is the bulk resistance, and R_{CT} is the charge transfer resistance. The Mott-Schottky measurement was performed at frequency of 1000, 2000, and 3000 Hz respectively in dark conditions. ICP-MS measurements were performed on a NexION 300 (Perkin Elmer) apparatus, with gold analysis on mass 197 Dalton. The calibration was done with standards which are 0 – 1 – 5 – 20 – 100 μg/L prepared from a single 1000 mg/L stock solution (Chemlab, CL01.0731.0100). The calibration was verified with an independant standard of 20 μg/L prepared from a multi-element stock standard of 10 mg/L (TraceCERT 41135-100 mL). Internal standard correction was by inline adding 10 μg/L Thorium.

3.3.4 Gold Sorption Methodology

Adsorption Isotherms: 3 mg of COF was immersed in 10 mL aqueous solutions of $KAuCl_4$ with varying concentrations (100-2000 ppm) and stirred overnight. For photo-assisted experiments, the setup was irradiated with a 34 W white LED light. The final gold concentration in the filtrate was analyzed by ICP-MS.

Adsorption Kinetics: 3 mg of COF was added to 100 mL of a 100 ppm Au(III) solution. Aliquots were taken at predetermined time intervals, filtered, and analyzed by ICP-MS.

Selectivity Tests: 3 mg of COF was added to 10 mL of a solution containing 10 ppm Au(III) and 100 ppm each of several competing metal ions

(Cu^{2+}, Ni^{2+}, etc.) by using their nitrate salts, respectively. The mixture was stirred for 10 minutes before filtration and analysis by ICP-MS/OES.

CPU Leachate Preparation and Testing: For the recovery of the Au(III) from electronic waste an end-of-life CPU was immersed in an aqua regia solution consisting of 75 mL concentrated HCl and 25 mL of concentrated HNO_3 over 3 days. This aqua regia solution was further dilluted to pH 4. 10 mg of COF was added to 10 mL of the CPU solution, and this solution was stirred for 1 hour at room temperature. After the adsorption, the mixture was filtered to separate the COF from the supernatant. The elemental composition of the supernatant was analyzed with ICP-MS and compared with the original CPU solution.

Regeneration: After the adsorption of gold with 100 ppm solution of Au(III) solution, the COFs were filtered. 10mg of gold-loaded COF were eluted in a 40 mL aqueous solution containing a 1:1 (V/V) ratio of 1M thiourea and 0.1 mol L^{-1} HCl and put in an ultrasonic bath for 30 min. The COF was filtered, washed with water, and subsequently dried under vacuum. The gold ions in the resulting eluate was then chemically reduced with sodium metabisulfite ($Na_2S_2O_5$), which precipitated a fine, dark yellow gold powder.

Photocatalytic H_2O_2 production 5 mg of the COF was dispersed in 10 mL of degassed deionized water (degassed by bubbling 30 min of Ar) in a glass vial of 20 mL. Prior to the photocatalysis, the suspension was dispersed in a sonication bath for 10 min. Subsequently, the vial was irradiated by white LED (34 W) lights for 3 hours, and the reaction temperature was kept at 25°C. After certain time periods, an aliquot of the reaction mixture was filtered through a 0.22 μm syringe filter to remove the photocatalysts. The concentration of H_2O_2 was determined by using an UV-Vis spectrophotometer colorometric method. An aliquot of the reaction mixture was filtered through a 0.22 μm syringe filter to remove the photocatalyst. The concentration of H_2O_2 was determined by using a UV-Vis spectrophotometer. The sample was mixed with a prepared $[Ti(OH)_3(H_2O)_3]^+_{(aq.)}$ solution. The UV spectrophotometry

$[Ti(O_2)OH(H_2O)_3]^+_{(aq.)}$ color method follows the reaction, in which the colorless $[Ti(OH)_3(H_2O)_3]^+_{(aq.)}$ reacts with H_2O_2 to generate a yellow peroxotitanium complex $[Ti(O_2)OH(H_2O)_3]^+_{(aq.)}$ whose absorbance (A) can be measured at 410 nm.

3.3.5 Computational Modelling

Initial geometry optimizations of the COF structures were performed using the Forcite module of BIOVIA Materials Studio 2017 with the Universal Force Field (UFF). Pawley refinement of the experimental PXRD patterns was carried out using the Reflex module to determine unit cell parameters. DFT calculations were performed with the Dmol3 module to model the binding of $AuCl_4^-$ within the COF unit cells. For $AuCl_3$ binding, a model compound was optimized at the ωB97xD/def2-SV(P) level of theory using Gaussian16 to compare the relative binding energies at different N and S sites.

References

1. Kinik, F. P., Ortega-Guerrero, A., Ongari, D., Ireland, C. P. & Smit, B. Pyrene-based metal organic frameworks: from synthesis to applications. *Chemical Society Reviews* **50,** 3143–3177 (2021).
2. Wojnicki, M., Rudnik, E., Luty-Błocho, M., Pacławski, K. & Fitzner, K. Kinetic studies of gold(III) chloride complex reduction and solid phase precipitation in acidic aqueous system using dimethylamine borane as reducing agent. *Hydrometallurgy* **127-128,** 43–53 (2012).
3. Li, Z., Zhao, W., Li, C., *et al.* Electronegative Strategic Positions in Covalent Organic Frameworks: Unlocking High-Efficiency Gold Recovery. *Angewandte Chemie International Edition* **64,** e202502199 (May 2025).
4. Eatoo, M. A., Wehbe, N., Kharbatia, N., Guo, X. & Mishra, H. Why do some metal ions spontaneously form nanoparticles in water microdroplets? Disentangling the contributions of the air–water interface and bulk redox chemistry. *Chemical Science* **16,** 1115–1125 (2025).
5. Glišić, B. Đ., Warżajtis, B., Hoffmann, M., Rychlewska, U. & Djuran, M. I. Mononuclear gold(iii) complexes with diazanaphthalenes: the influence of the position of nitrogen atoms in the aromatic rings on the complex crystalline properties. *RSC Advances* **10,** 44481–44493 (2020).
6. Yang, X., Jiang, D., Fu, Y., *et al.* Synergistic Linker and Linkage of Covalent Organic Frameworks for Enhancing Gold Capture. *Small* **20,** 2404192 (Nov. 2024).
7. Li, K., Mei, D., Liu, Y.-s. & Yan, B. Three-Dimensional Covalent Organic Frameworks Containing Diverse Nitrogen Sites for Gold Adsorption. *Chemistry of Materials* **37,** 2535–2545 (Apr. 2025).
8. Thanh, N. T. K., Maclean, N. & Mahiddine, S. Mechanisms of Nucleation and Growth of Nanoparticles in Solution. *Chemical Reviews* **114,** 7610–7630 (Aug. 2014).

9. Laemont, A., Matthys, G., Lavendomme, R. & Van Der Voort, P. Mild and Scalable Conditions for the Solvothermal Synthesis of Imine-Linked Covalent Organic Frameworks. *published on ChemRXiv - under review at Angewandte Chemie* (2024).

Conclusions

4

4.1 Conclusions

This doctoral thesis has centered on advancing the utility of Covalent Organic Frameworks (COFs) for challenging adsorption applications. While imine-linked COFs offer a versatile synthetic platform, their inherent chemical instability can limit their deployment in harsh industrial environments. We have addressed this limitation not by modifying the peripheral linkers, but by re-engineering the covalent linkages themselves through post-synthetic modification (PSM). This work has demonstrated that transforming the imine bond into more robust heterocyclic systems is a powerful strategy to create exceptionally stable and highly functional materials tailored for specific, demanding separation processes: the capture of radioactive iodine and the recovery of precious gold.

In **chapter 2**, we successfully converted a crystalline, picolinaldehyde-based imine COF into a novel imidazopyridinium-linked framework. This transformation not only provided superior chemical and thermal stability but also introduced permanent positive charges and halide counter-anions into the structure. These new features enabled a powerful and synergistic capture mechanism, combining strong halogen bonding, electrostatic attraction, and hydrogen bonding. The resulting materials demonstrated exceptional performance for iodine sequestration, exhibiting ultra-fast adsorption kinetics and high gravimetric capacities in the gas phase. Critically, under industrially relevant dynamic conditions (150°C, 50% RH), the framework's performance surpassed the current

industrial benchmark. Furthermore, its efficacy in aqueous environments was equally impressive, achieving rapid removal of triiodide from solution and purifying spiked seawater to natural background levels, highlighting its potential for both nuclear waste remediation and water purification.

In **chapter 3**, we have established a potent linkage engineering strategy, demonstrating that the post-synthetic conversion of imine-based covalent organic frameworks to their thiazole-linked analogues yields exceptionally effective adsorbents for the selective recovery of gold. This structural transformation confers a suite of synergistic benefits. The introduction of thiazole linkages not only imparts superior chemical stability, which is directly correlated with enhanced recyclability, but also strategically incorporates sulfur atoms into the framework. In accordance with Hard-Soft Acid-Base (HSAB) principles, these sites act as additional binding sites for gold(III), leading to a marked increase in adsorption capacity under dark conditions.

Furthermore, the conversion significantly augments the frameworks' photophysical properties by narrowing the optical band gap and improving charge-carrier separation. This enables a highly efficient photocatalytic reduction pathway upon irradiation, culminating in a record-high gold uptake capacity of 7980 mg g^{-1} for the Tfpy-PDA-S framework. Crucially, the practical viability of this approach was validated through the treatment of complex, real-world CPU waste leachates, from which these materials selectively recovered up to 98% of the available gold over multiple cycles. Collectively, these findings establish the post-synthetic thionation of imine COFs as a straightforward and highly effective strategy for the rational design of robust, next-generation photocatalytic adsorbents for sustainable resource recovery and urban mining.

4.2 Outlook

Looking forward, the success of the linkage modification strategies detailed in this thesis opens up numerous avenues for future research. The work presented herein serves as a robust proof-of-concept, demonstrating that post-synthetic modification is a powerful tool for overcoming the inherent stability-crystallinity dilemma in COF chemistry. While the academic potential of COFs in areas from catalysis to electronics is vast, it is my firm belief that adsorption-based applications will be at the forefront transitioning into the industrial landscape. A direct parallel can be drawn to the trajectory of Metal-Organic Frameworks (MOFs), which, after years of foundational research, are now being deployed commercially for industrial-scale CO_2 capture. We anticipate that the demonstrable, high-impact performance of COFs in critical separation processes will pave a similar path toward their real-world implementation.

In the short term, a deeper investigation into the long-term operational stability of these modified materials is necessary. This includes extensive cycling studies and performance evaluation under more complex, realistic conditions, such as the presence of NO_x gases in nuclear off-gas streams or a broader range of competing metals in real e-waste leachates and extensive flow-through experiments. Building on the success demonstrated here, the versatility of the PSM approach should be applied to a wider library of imine COF precursors with different topologies and functionalities. This could lead to new cationic or sulfur-rich materials tailored for capturing other critical environmental contaminants. The principles of anion capture shown to be effective for iodide could be translated to the sequestration of persistent organic pollutants like per- and polyfluoroalkyl substances (PFAS), while the selective chelation and reduction mechanisms could be adapted for the extraction of other strategic elements, such as uranium from seawater or platinum-group metals from industrial waste.

A longer-term vision involves transitioning beyond powdered materials to more advanced and process-ready systems. A significant hurdle for all COF materials remains their processability. Future work must focus on integrating these high-performance powders into practical device architectures, such as shaping them into pellets, extrudates, or fabricating COF-based membranes and fiber composites suitable for industrial-scale column or flow-through applications.

Finally, by combining these experimental strategies with computational screening, we can accelerate the discovery of ideal imine COF platforms for targeted linkage conversions, moving toward a rational, predictive design of next-generation adsorbents. Ultimately, this work serves as a foundation for the continued development of robust, precisely engineered COFs, bringing them a step closer to providing sustainable solutions for critical environmental and resource challenges.

To address the future of the field, one must critically evaluate the position of COFs within the broader spectrum of porous materials. The primary strength of COFs lies in their "reticular chemistry", the ability to atomistically design pore environments for specific interactions. However, this strength is counterbalanced by significant weaknesses: the high cost of monomer synthesis and the difficulty of scaling up production while maintaining crystallinity.

A vision for commercialization is needed. While academic research heavily favours gas storage and carbon capture, I believe that the first large-scale commercial applications of COFs will not be in these commodity gas sectors. The economic competition with incredibly cheap materials like activated carbon or zeolites is too steep for bulk applications. Instead, the "killer application" for COFs will likely be found in high-value separations where selectivity is paramount and the recovered material justifies the cost of the adsorbent. Applications in nuclear safety (Chapter 2) or pharmaceutical purification, where the cost of failure is high and regulatory standards are strict, offer another pathway. In these scenarios, the superior performance and stability of COFs justify their premium price

over traditional sorbents. As demonstrated in Chapter 3, the recovery of precious metals (Gold, Palladium, Platinum) from e-waste represents an economically viable entry point. The value of the recovered gold can offset the higher cost of the COF material, provided the adsorbent is recyclable.

For COFs to transition from academic curiosity to industrial reality, research must pivot from synthesizing new structures to solving engineering challenges. The "powder problem" remains a significant hurdle; industrial columns cannot operate with fine powders due to pressure drops. Future success depends on developing robust shaping technologies, such as pelletization, extrusion, or membrane integration, that do not compromise the accessibility of the active sites. Furthermore, the field must move toward continuous flow processes rather than batch testing to prove long-term stability and diverse recyclability.

In conclusion, the future of COFs lies in "precision engineering" for high-stakes separation problems. By focusing on niche, high-value applications and solving the macroscopic processability issues, COFs can secure a vital role in the next generation of sustainable industrial processes.

Appendix

A

A.1 Supporting information of Chapter 1

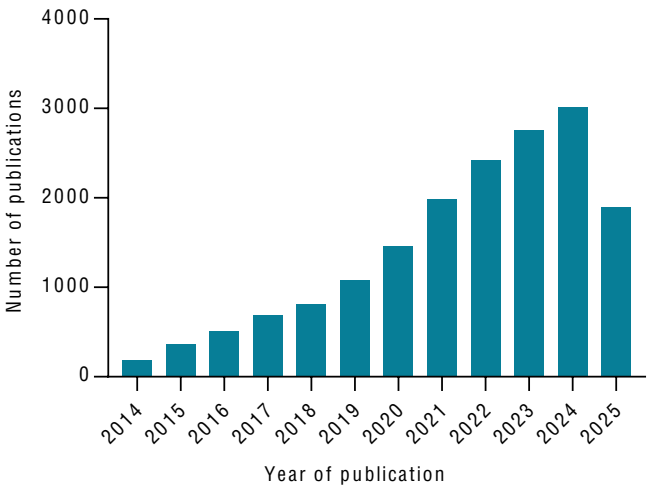

Figure A.1. The number of publications containing the keywords 'Covalent Organic Framework' or 'COF' according to Web Of Science, consulted August 2025.

A.2 Supporting information of Chapter 2

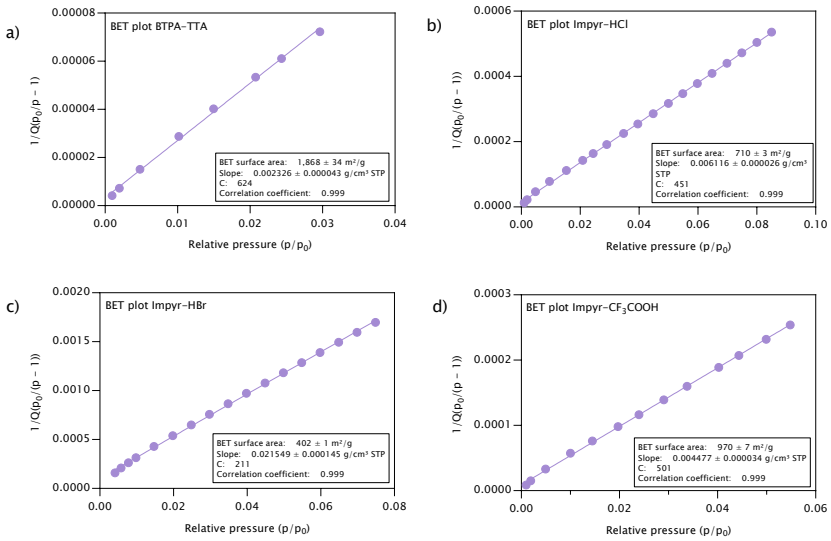

Figure A.2. BET plots of a) BTPA-TTA COF and b-d) the imidazopyridinium-HX COFs.

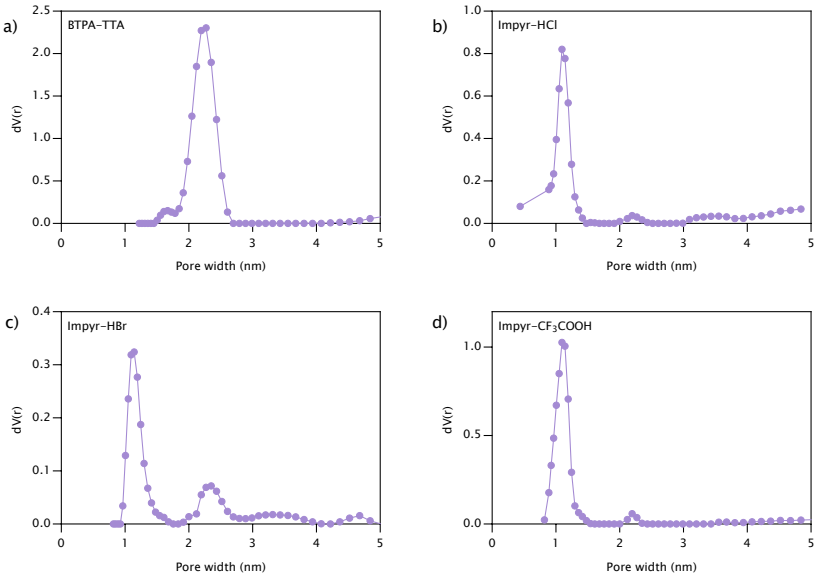

Figure A.3. Pore size distribution (PSD): a) BTPA-TTA, b) Impyr-HCl, c) Impyr-HBr, d) Impyr-CF_3COOH.

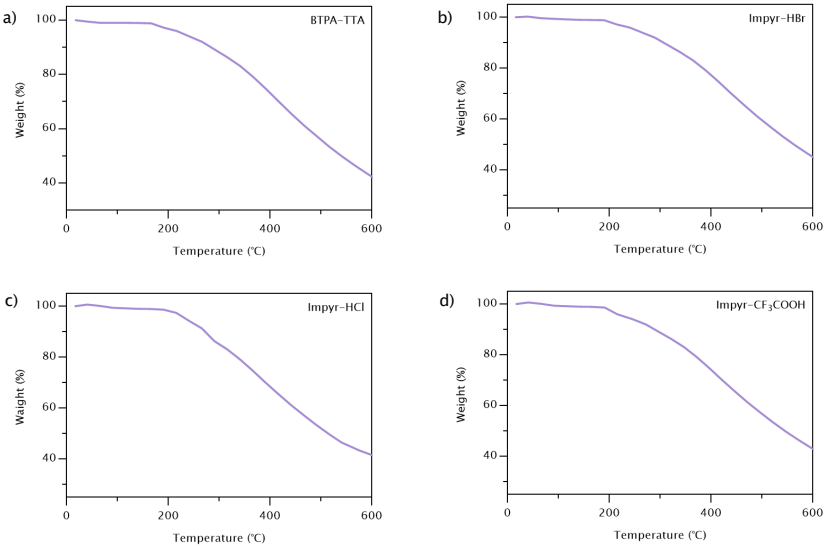

Figure A.4. Thermogravimetrical analysis (TGA) of a) BTPA-TTA, b) Impyr-HBr, c) Impyr-HCl, d) Impyr-CF_3COOH.

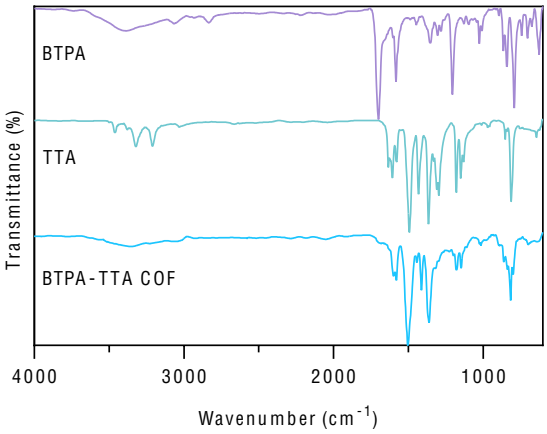

Figure A.5. FTIR spectra of the transformation of TTA (amine) and BTPA (aldehyde) linkers into BTPA-TTA Imine COF.

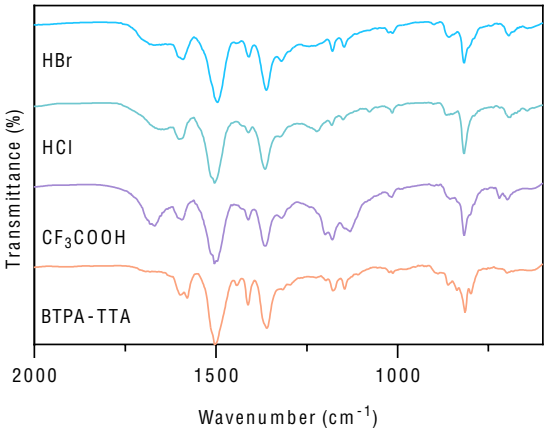

Figure A.6. FTIR spectra of the post-modification of BTPA-TTA COF into different imidazopyridinium COFs treated with different acids.

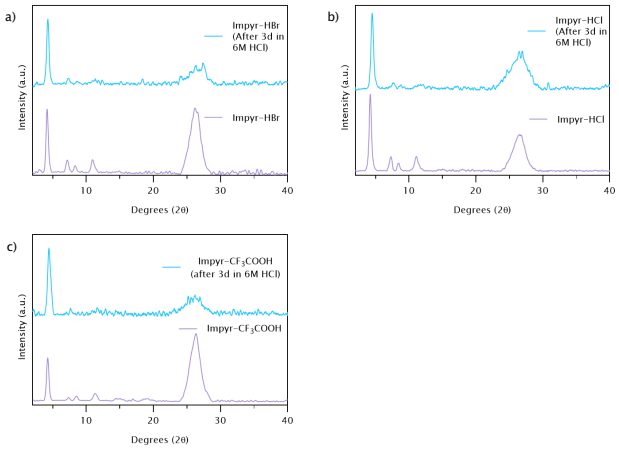

Figure A.7. PXRD of a) Impyr-HBr, b) Impyr-HCl, c) Impyr-CF_3COOH after treatment with 6M $HCl_{(aq.)}$ for 3 days.

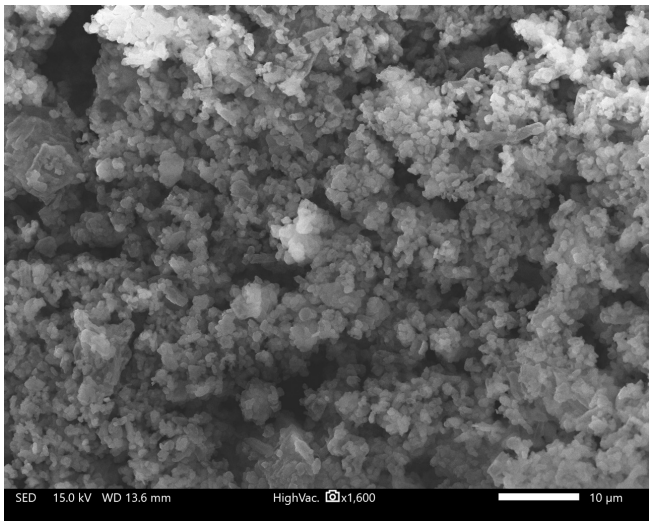

Figure A.8. SEM image of BTPA-TTA COF.

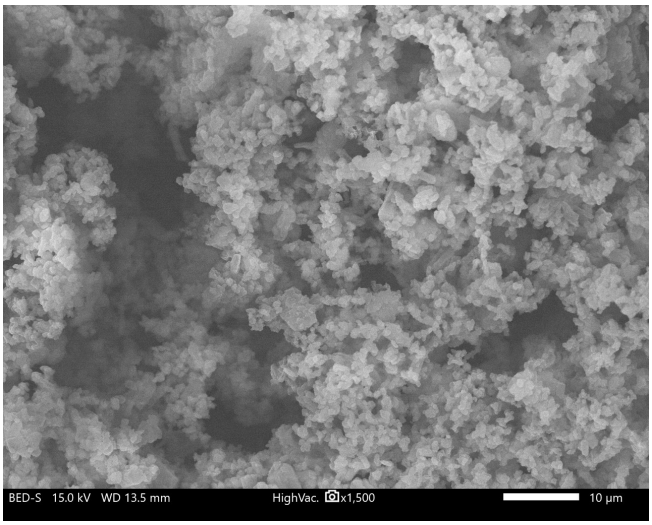

Figure A.9. SEM image of Impyr-HCl COF.

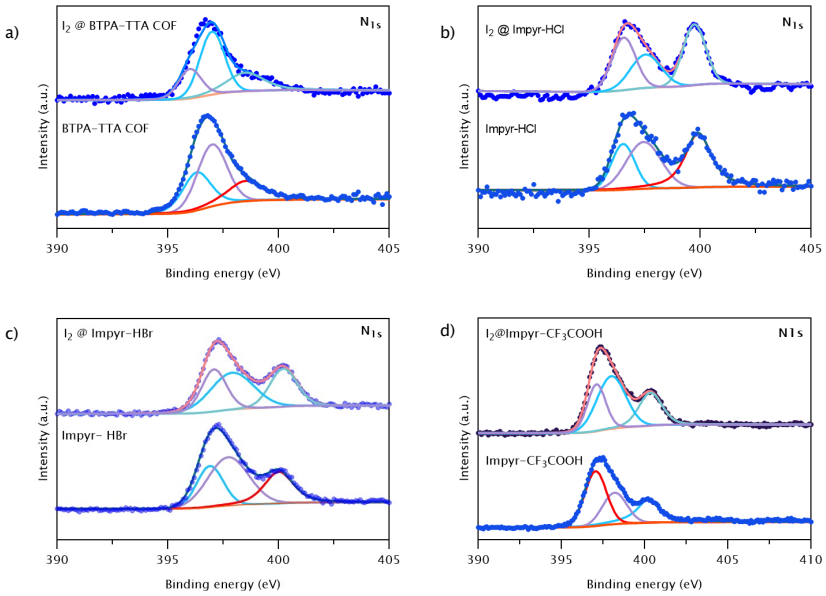

Figure A.10. Nitrogen XPS of the pristine and iodine adsorbed a) BTPA-TTA, b) Impyr-HCl, c) Impyr- HBr, d) Impyr-CF_3COOH.

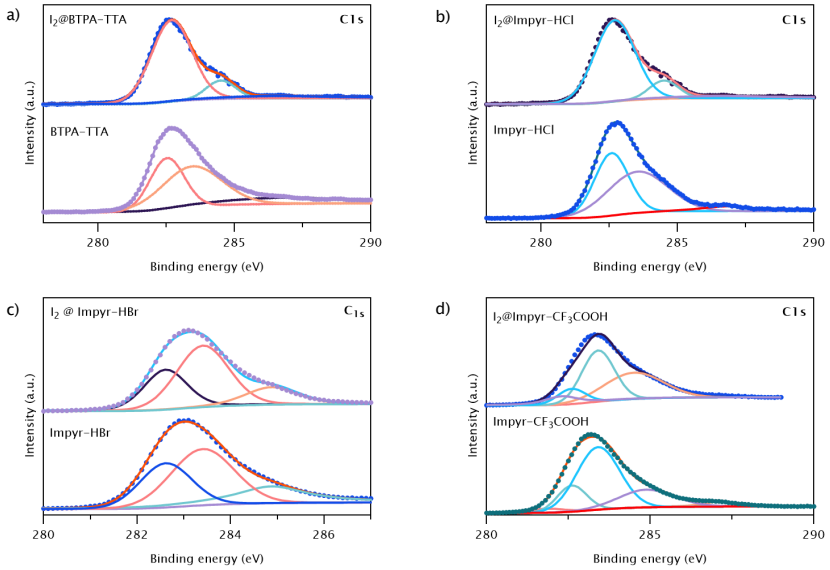

Figure A.11. Carbon XPS of the pristine and iodine adsorbed a) BTPA-TTA, b) Impyr-HCl, c) Impyr- HBr, d) Impyr-CF_3COOH.

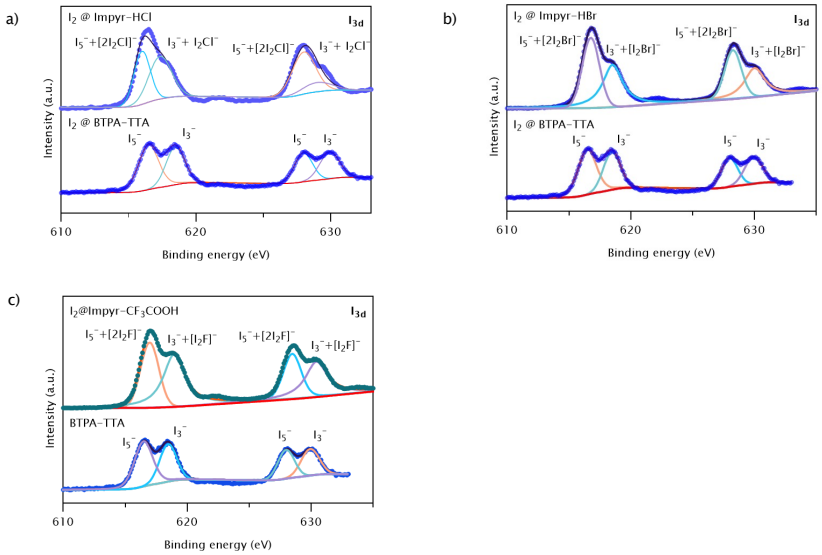

Figure A.12. Iodine XPS of the pristine and iodine adsorbed a) Impyr-HCl, b) Impyr-HBr, c) Impyr- CF_3COOH.

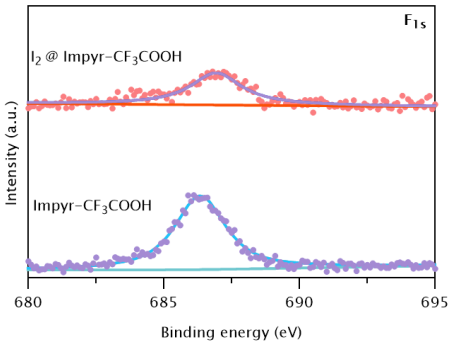

Figure A.13. Fluorine XPS of the pristine and iodine adsorbed Impyr-CF_3COOH.

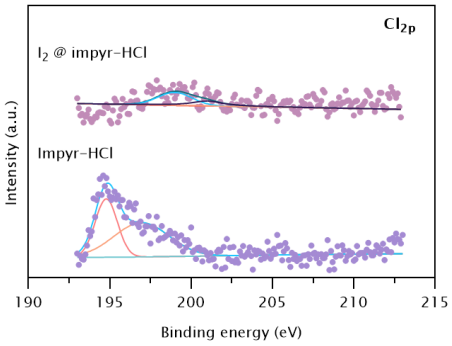

Figure A.14. Chlorine XPS of the pristine and iodine adsorbed Impyr-HCl.

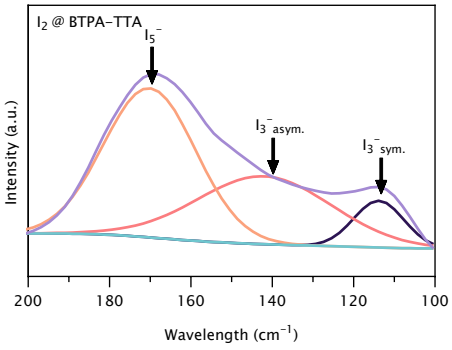

Figure A.15. Raman spectrum of iodine adsorbed BTPA-TTA COF.

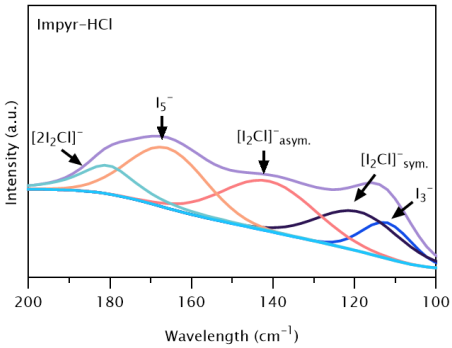

Figure A.16. Raman spectrum of iodine adsorbed Impyr-HCl COF.

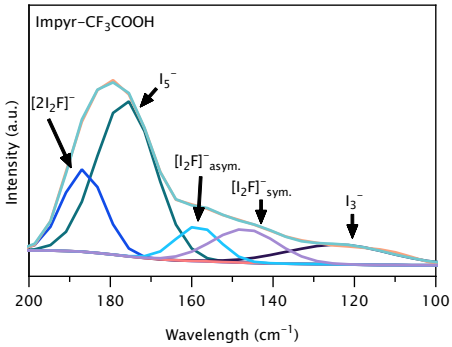

Figure A.17. Raman spectrum of iodine adsorbed Impyr-CF_3COOH COF.

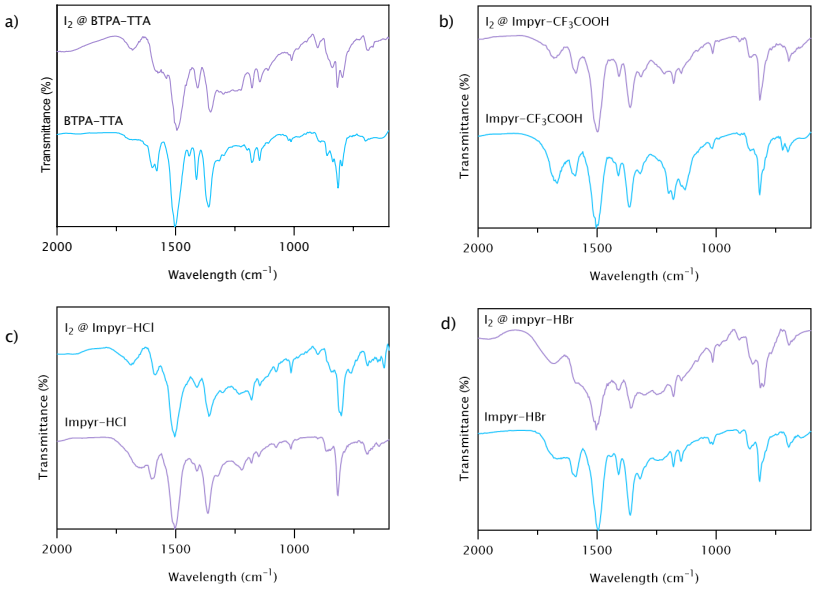

Figure A.18. FTIR spectra of the pristine and iodine adsorbed a) BTPA-TTA, b) Impyr-CF_3COOH, c) Impyr-HCl, d) Impyr-HBr.

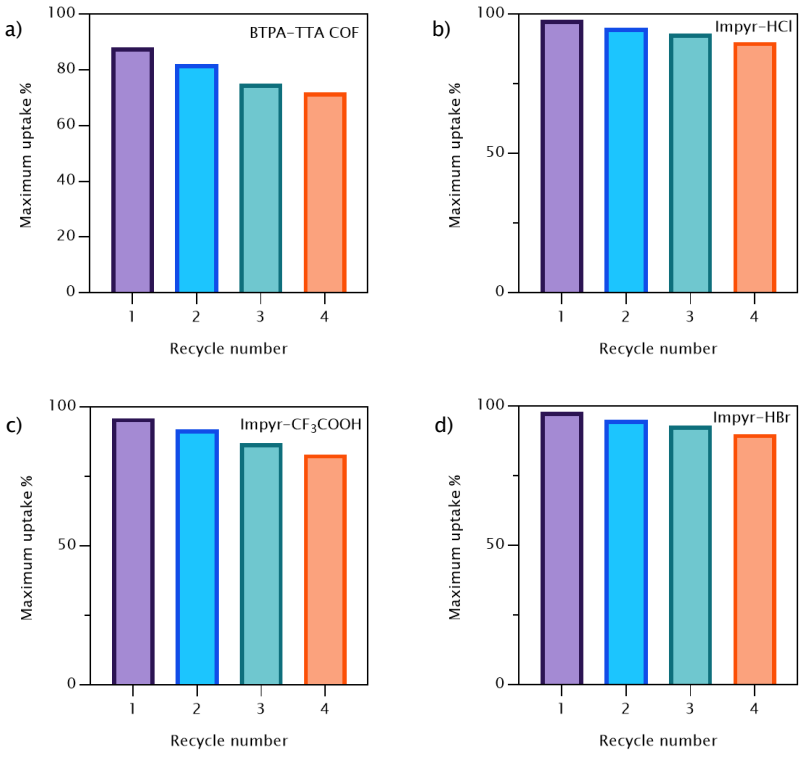

Figure A.19. Percentage of static maximum iodine adsorption capacity of the recycled a) BTPA-TTA, b) Impyr-HCl, c) Impyr-CF_3COOH, d) Impyr-HBr in comparison with the first adsorption experiment.

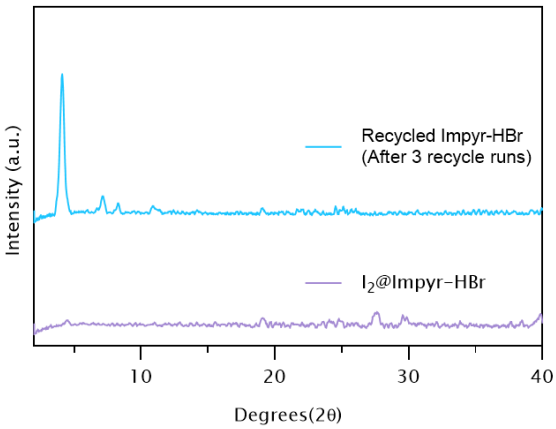

Figure A.20. PXRD of static I_2 doped Impyr-HBr and after 3 recycle runs.

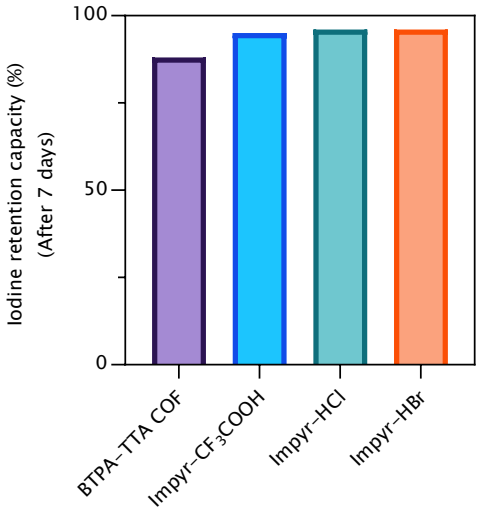

Figure A.21. Retention (in weight percentage (wt%)) of iodine onto BTPA-TTA, Impyr-CF_3COOH, Impyr-HCl, Impyr-HBr COFs after 7 days in open air at room temperature.

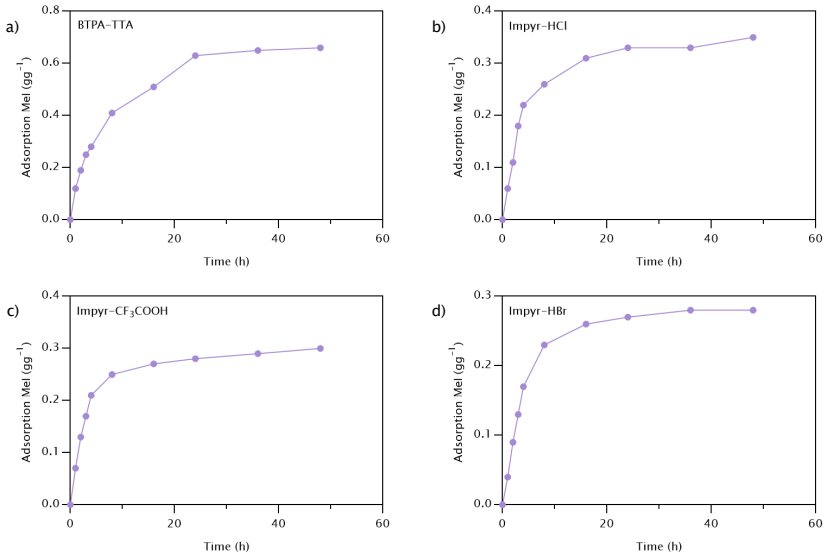

Figure A.22. Static methyliodide adsorption of a) BTPA-TTA, b) Impyr-HCl, c) Impyr-CF_3COOH, d) Impyr-HBr.

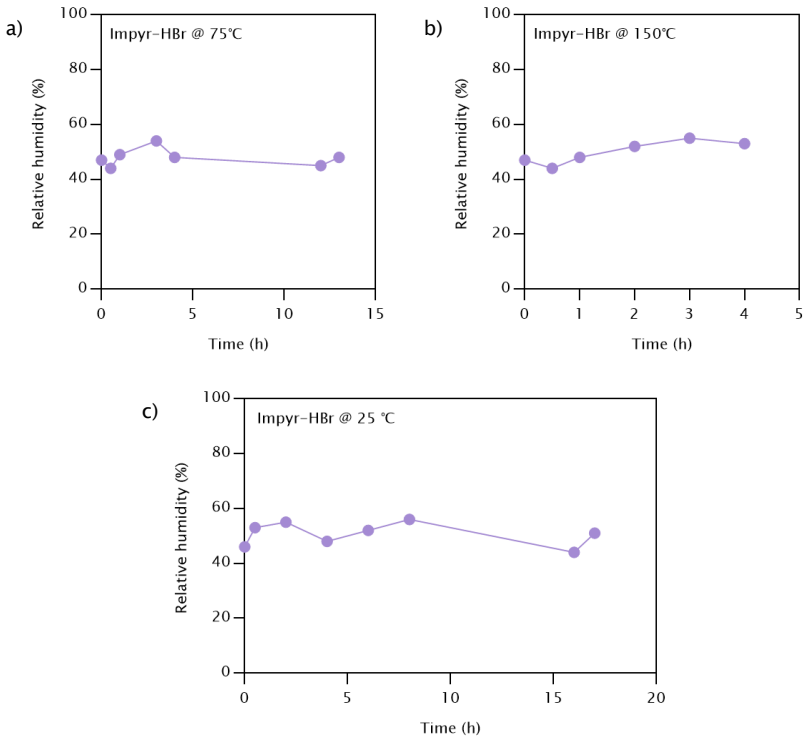

Figure A.23. Relative humidity measurement after certain amounts of time of dynamic adsorption experiment of Impyr-HBr at a) 75 °C, b) 150 °C, c) 25 °C.

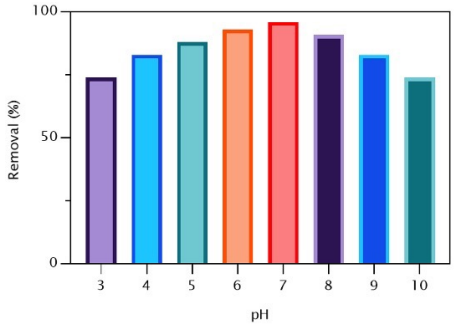

Figure A.24. Influence of pH on the removal of triiodide (I_3^-) ions with BTPA-TTA COF.

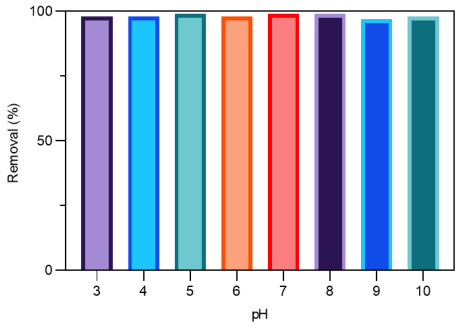

Figure A.25. Influence of pH on the removal of triiodide (I_3^-) ions with Impyr-HCl COF.

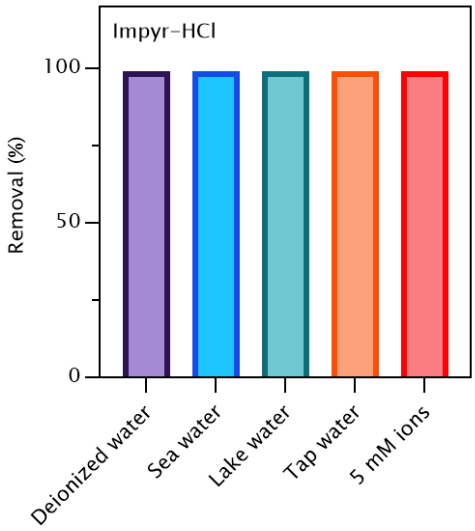

Figure A.26. Static adsorption selectivity study with different types of water containing 1.5 mM I_3^- and 5 mM of possible competing ions and Impyr-HCl as adsorbent measured after 24 h.

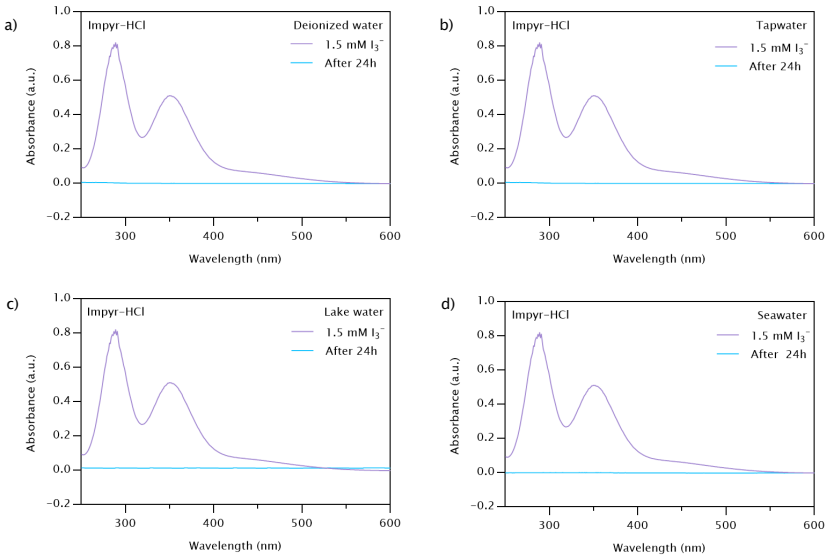

Figure A.27. UV-Vis spectra of the adsorption of I_3^- using a) deionized, b) tap, c) lake, d) sea water with Impyr-HCl.

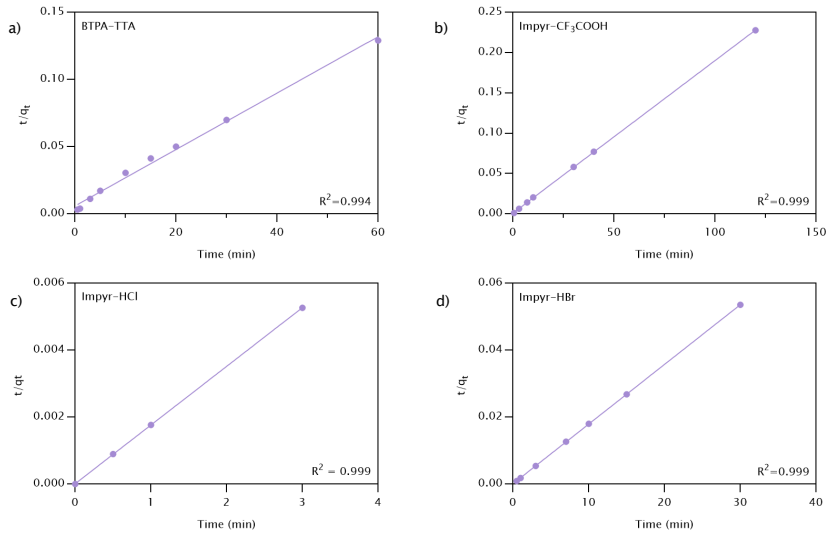

Figure A.28. Pseudo-second order kinetics fit for the adsorption of triiodide (I_3^-) for a) BTPA-TTA, b) Impyr-CF_3COOH, c) Impyr-HCl, d) Impyr-HBr.

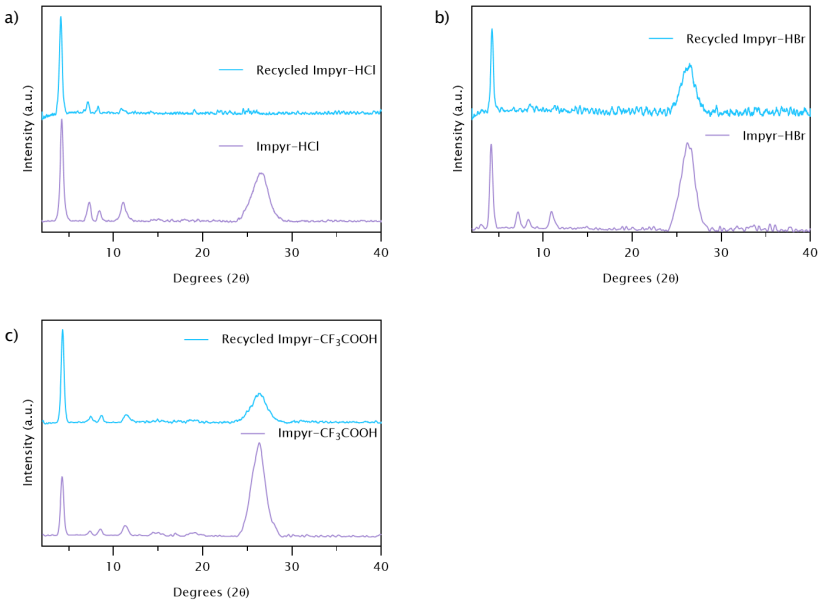

Figure A.29. PXRD of recycled a) Impyr-HCl, b) Impyr-HBr, c) Impyr-CF_3COOH after 4 recycle runs.

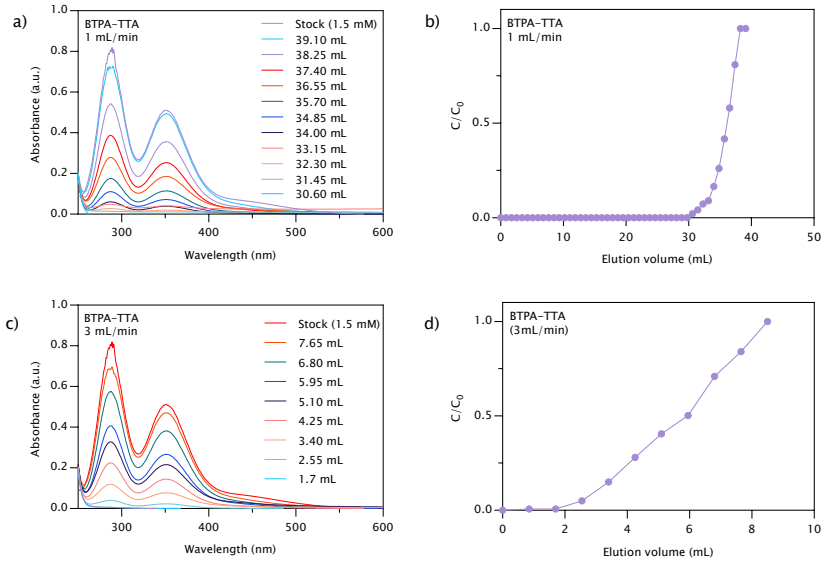

Figure A.30. UV-Vis spectra after breakthrough of a) BTPA-TTA after breakthrough at 1 mL/min and c) at 3mL/min with b) and d) corresponding breakthrough profiles.

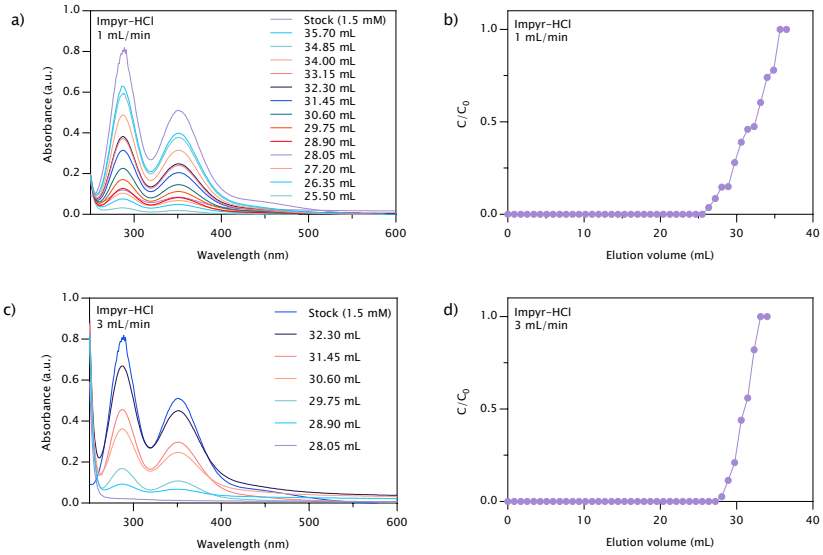

Figure A.31. UV-Vis spectra after breakthrough of a) Impyr-HCl after breakthrough at 1 mL/min and c) at 3mL/min with b) and d) corresponding breakthrough profiles.

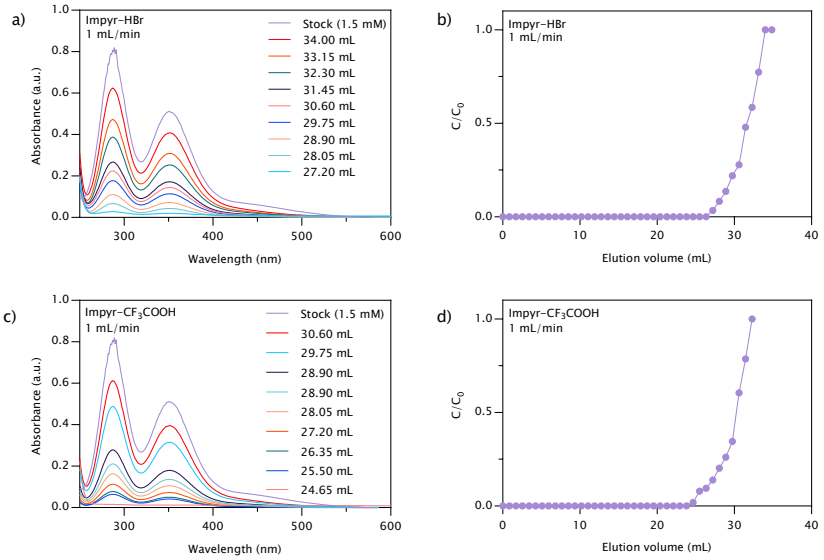

Figure A.32. UV-Vis spectra after breakthrough of a) impyr-HBr after breakthrough at 1 mL/min and c) impyr-CF_3COOH after breakthrough at 1 mL/min with b) and d) corresponding breakthrough profiles.

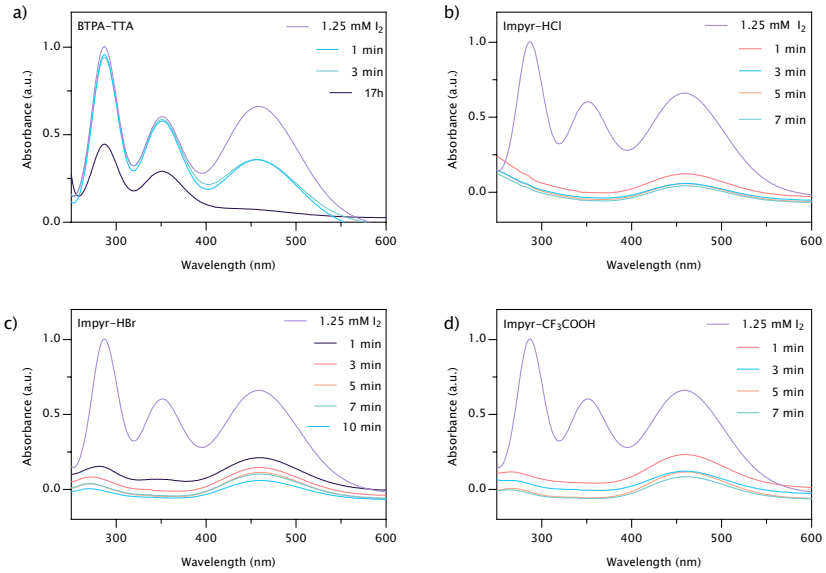

Figure A.33. UV-Vis spectra of the kinetic adsorption study of 1.25 mM saturated I_2 aqueous solution with 10 mg a) BTPA-TTA, b) Impyr-HCl, c) Impyr-HBr, d) Impyr-CF_3COOH.

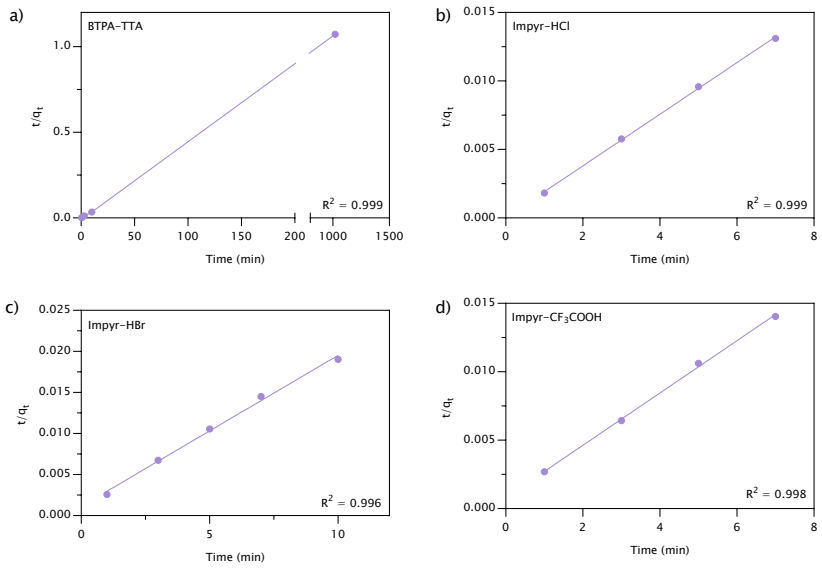

Figure A.34. Pseudo-second order kinetics fit of I_2 adsorption with a) BTPA-TTA, b) Impyr-HCl, c) Impyr-HBr, d) Impyr-CF_3COOH.

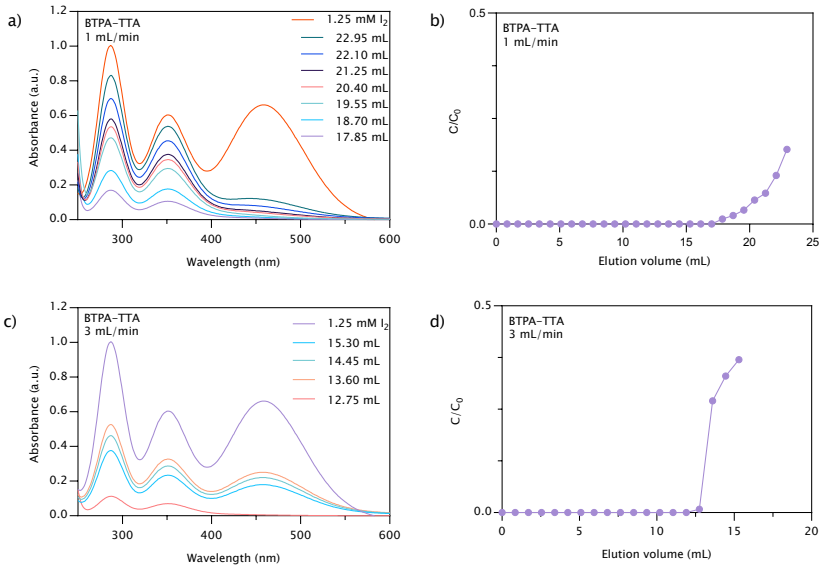

Figure A.35. UV-Vis spectra of I_2 adsorption a) BTPA-TTA after breakthrough at 1 mL/min and c) BTPA-TTA after breakthrough at 3 mL/min with b) and d) corresponding breakthrough profiles.

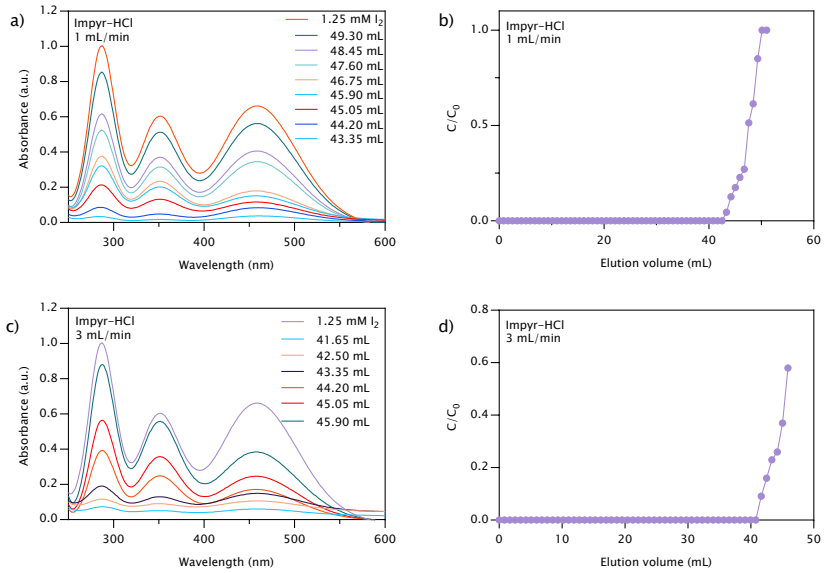

Figure A.36. UV-Vis spectrum of I_2 adsorption a) Impyr-HCl after breakthrough at 1 mL/min and c) Impyr-HCl after breakthrough at 3 mL/min with b) and d) corresponding breakthrough profiles.

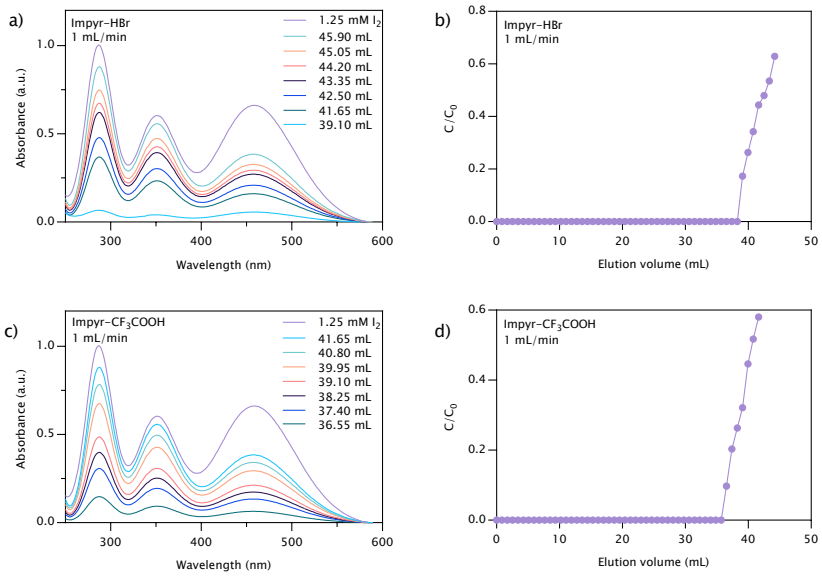

Figure A.37. UV-Vis spectrum of I_2 adsorption a) impyr-HBr after breakthrough at 1 mL/min and c) impyr-CF_3COOH after breakthrough at 1 mL/min with b) and d) corresponding breakthrough profiles.

A.3 Supporting information of Chapter 3

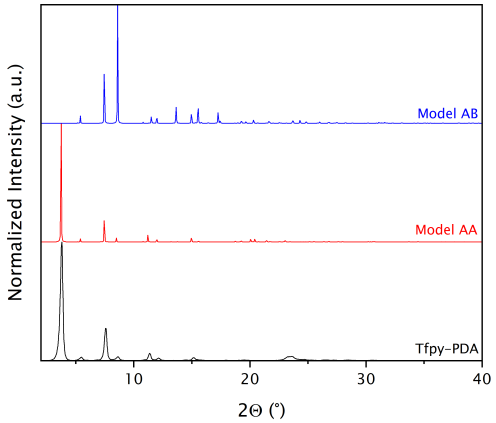

Figure A.38. AB and AA stacking models of Tfpy-PDA COF

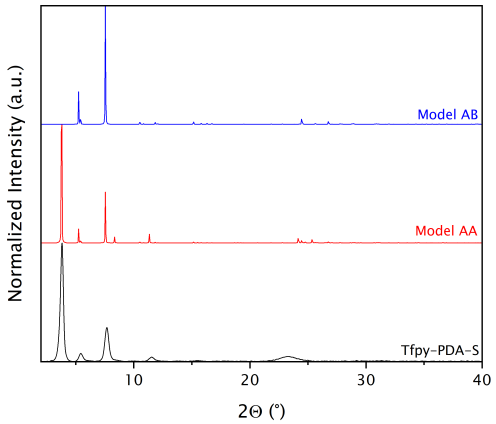

Figure A.39. AB and AA stacking models of Tfpy-PDA-S COF

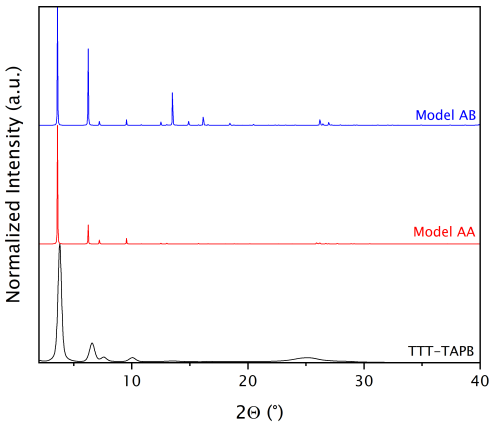

Figure A.40. AB and AA stacking models of TTT-TAPB COF

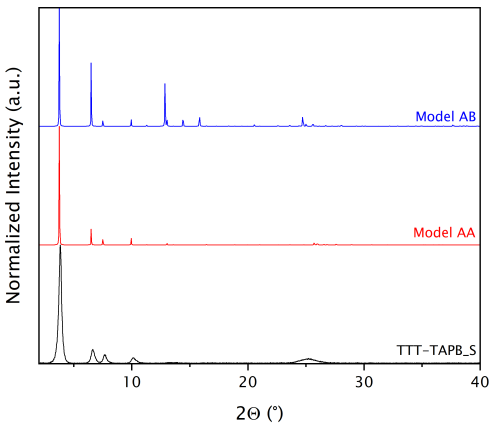

Figure A.41. AB and AA stacking models of TTT-TAPB-S COF

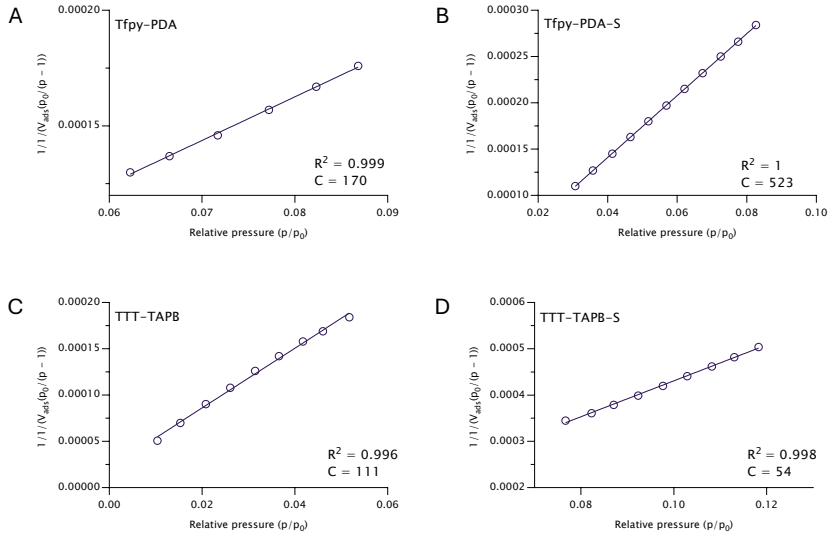

Figure A.42. BET plots of A) Tfpy-PDA, B) Tfpy-PDA-S, C) TTT-TAPB, D) TTT-TAPB-S

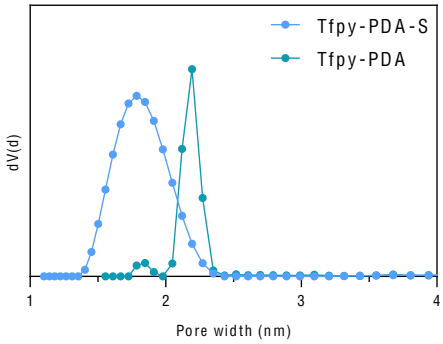

Figure A.43. Pore size distribution of Tfpy-PDA(-S)

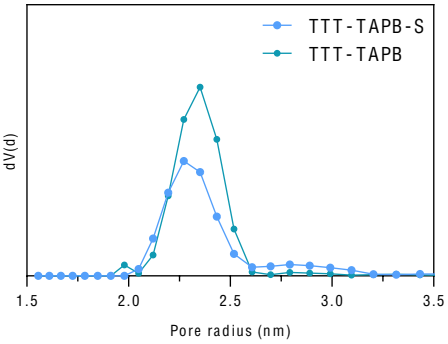

Figure A.44. Pore size distribution of TTT-TAPB(-S).

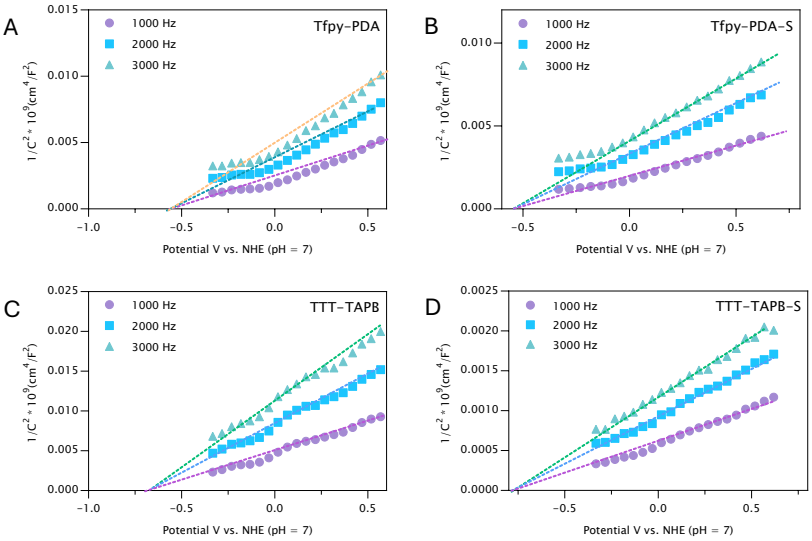

Figure A.45. Mott-Shottky curves (vs. NHE, pH = 7) of A) Tfpy-PDA, B) Tfpy-PDA-S, C) TTT-TAPB, D) TTT-TAPB-S.

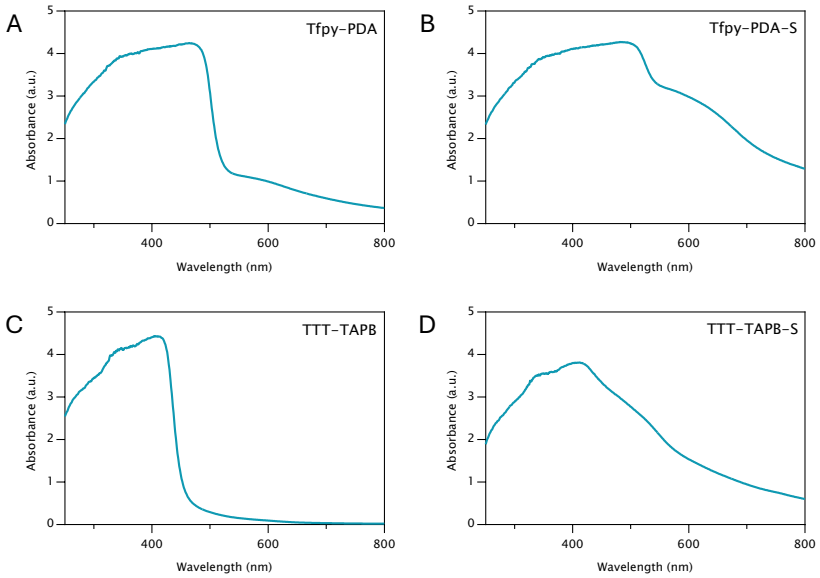

Figure A.46. Solid-state UV-Vis absorption spectra of A) Tfpy-PDA, B) Tfpy-PDA-S, C) TTT-TAPB, D) TTT-TAPB-S.

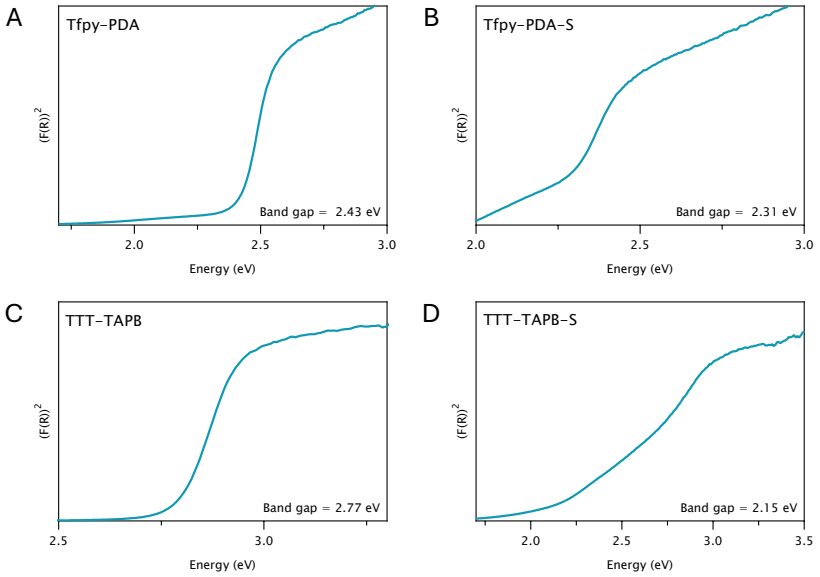

Figure A.47. Tauc plot of A) Tfpy-PDA, B) Tfpy-PDA-S, C) TTT-TAPB, D) TTT-TAPB-S.

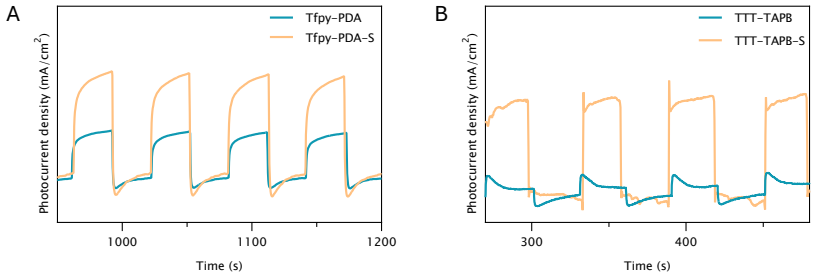

Figure A.48. Photocurrent response curves of A) Tfpy-PDA(-S) and B) TTT-TAPB(-S).

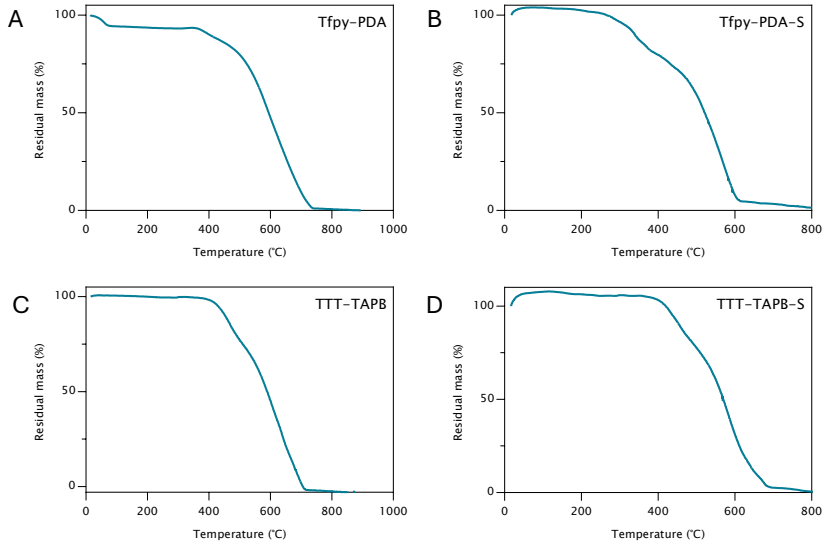

Figure A.49. TGA of A) Tfpy-PDA, B) Tfpy-PDA-S, C) TTT-TAPB, D) TTT-TAPB-S.

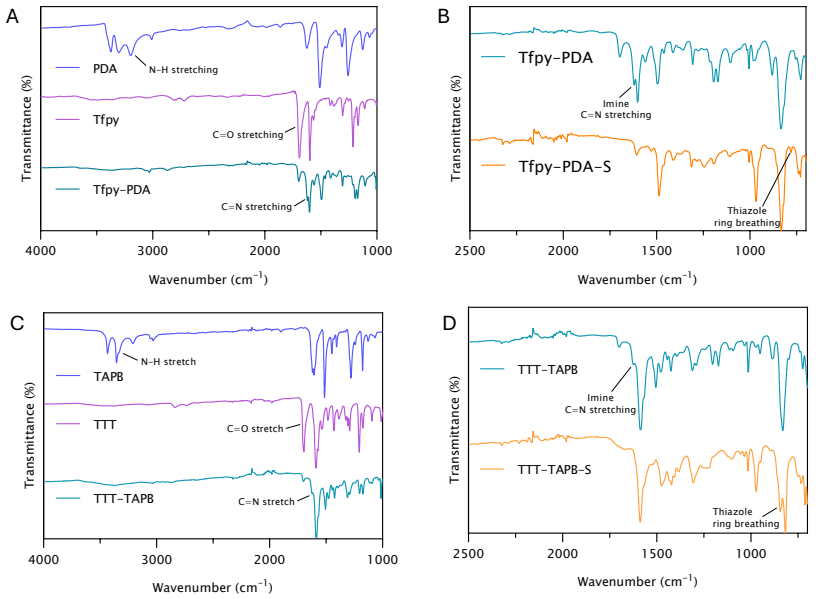

Figure A.50. FTIR spectra of synthesis A) Tfpy-PDA, B) Tfpy-PDA-S, C) TTT-TAPB, D) TTT-TAPB-S.

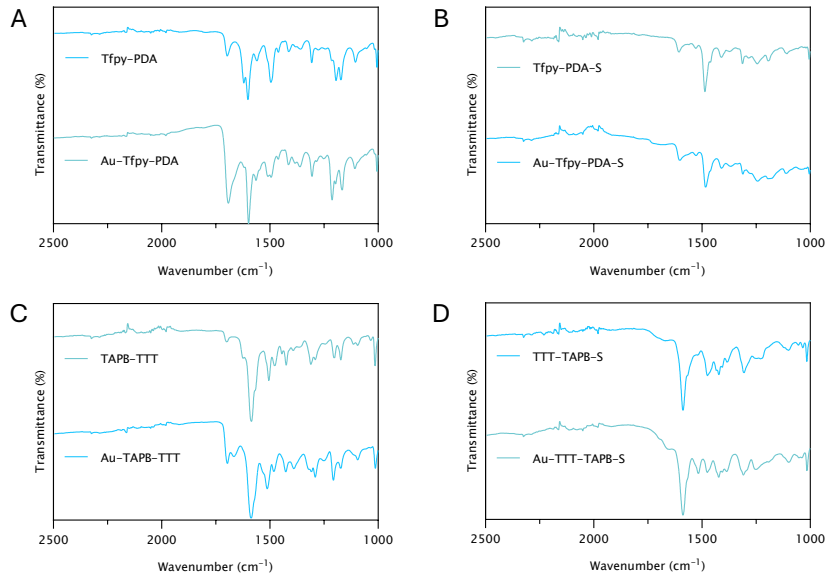

Figure A.51. FTIR spectra overlap of pristine COFs and gold-loaded COFs.

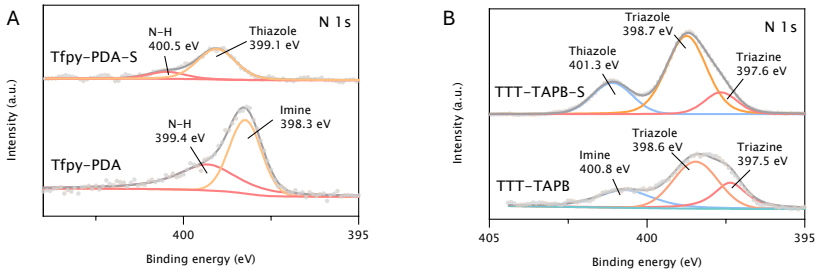

Figure A.52. Nitrogen (N 1s) XPS spectra of A) Tfpy-PDA and Tfpy-PDA-S and B) TTT-TAPB and TTT-TAPB-S.

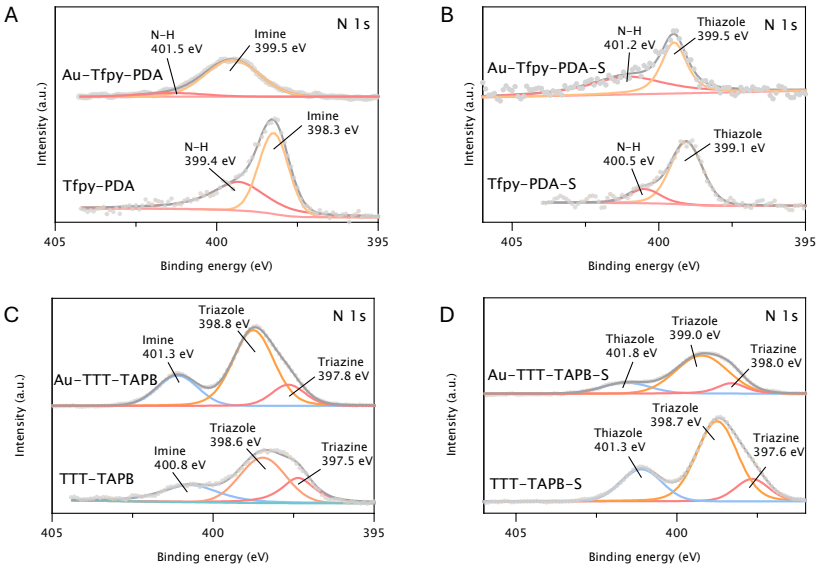

Figure A.53. Nitrogen (N 1s) XPS spectra of A) Tfpy-PDA and Au-Tfpy-PDA, B) Tfpy-PDA-S and Au-Tfpy-PDA-S, C) TTT-TAPB and Au-TTT-TAPB, D) TTT-TAPB-S and Au-TTT-TAPB-S.

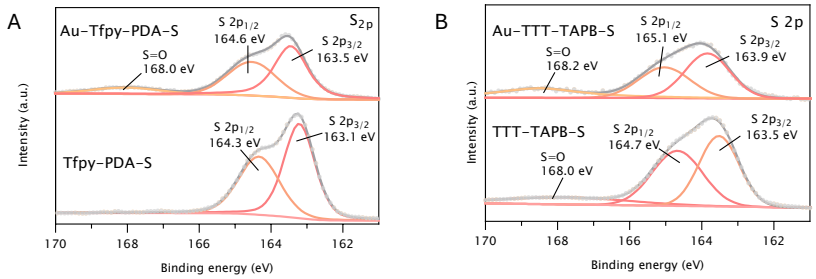

Figure A.54. Sulfur (S 2p) XPS spectra of A) Tfpy-PDA and Au-Tfpy-PDA-S, B) Tfpy-PDA-S and Au-Tfpy-PDA-S.

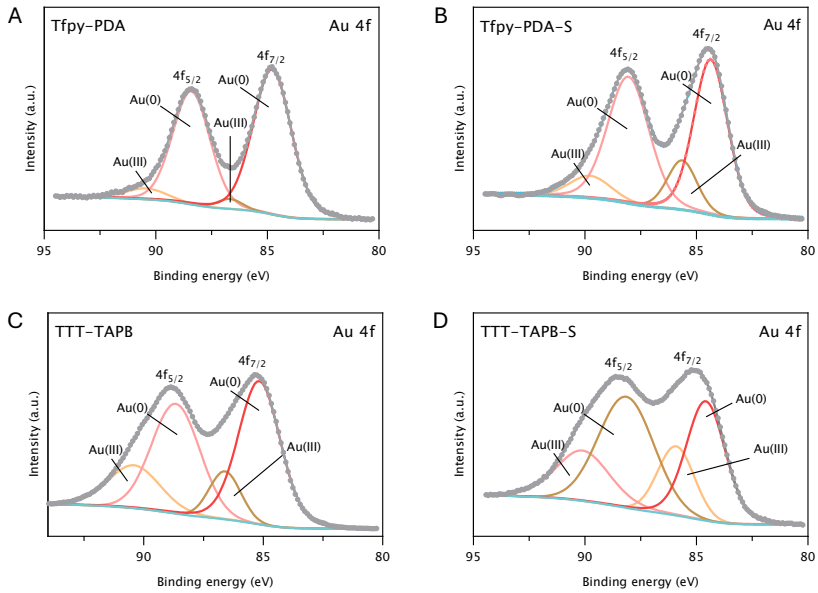

Figure A.55. Gold (Au 4f) XPS spectra after gold adsorption onto A) Tfpy-PDA, B) Tfpy-PDA-S, C) TTT-TAPB, D) TTT-TAPB-S.

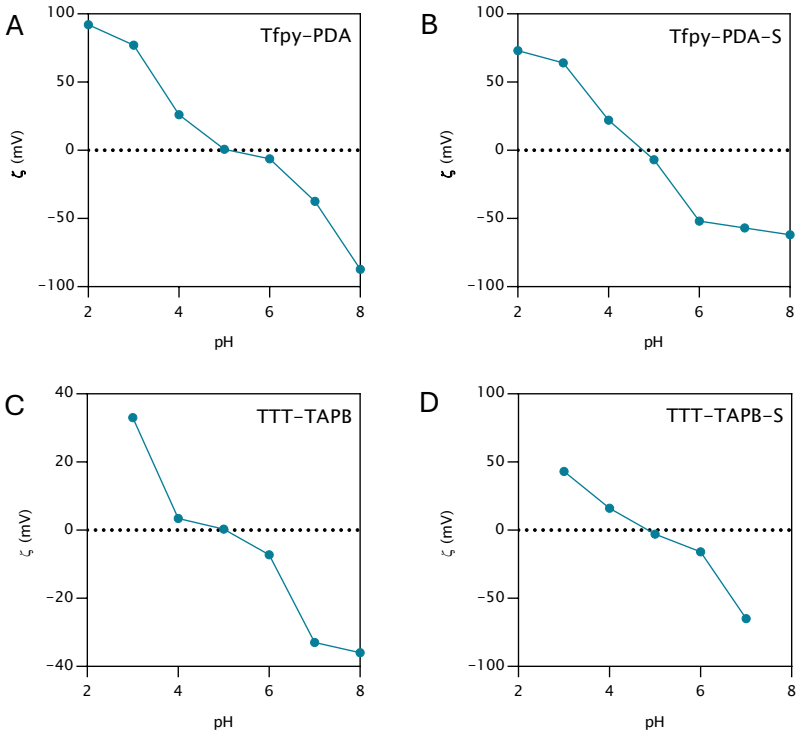

Figure A.56. Zeta potential in function of pH of A) Tfpy-PDA, B) Tfpy-PDA-S, C) TTT-TAPB, D) TTT-TAPB-S.

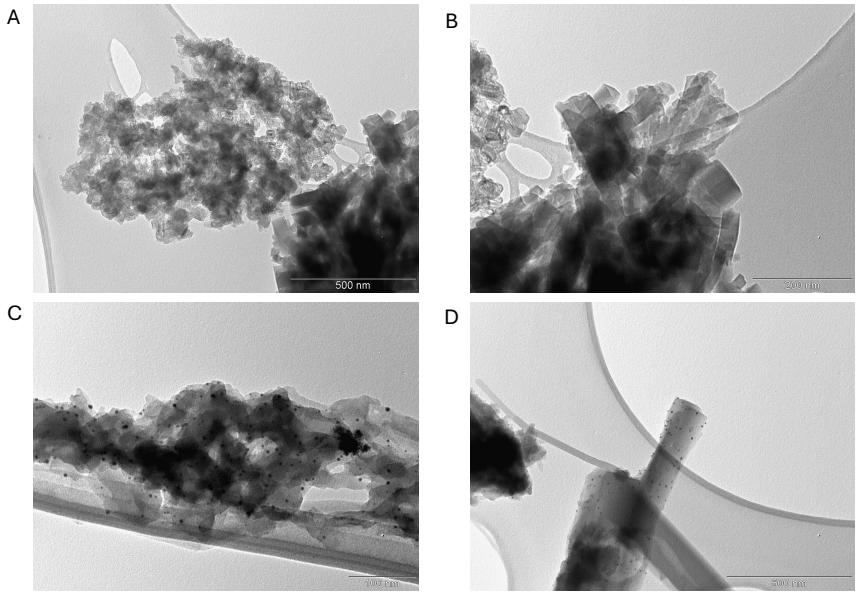

Figure A.57. TEM images of A,B) Tfpy-PDA and C,D) Au-Tfpy-PDA.

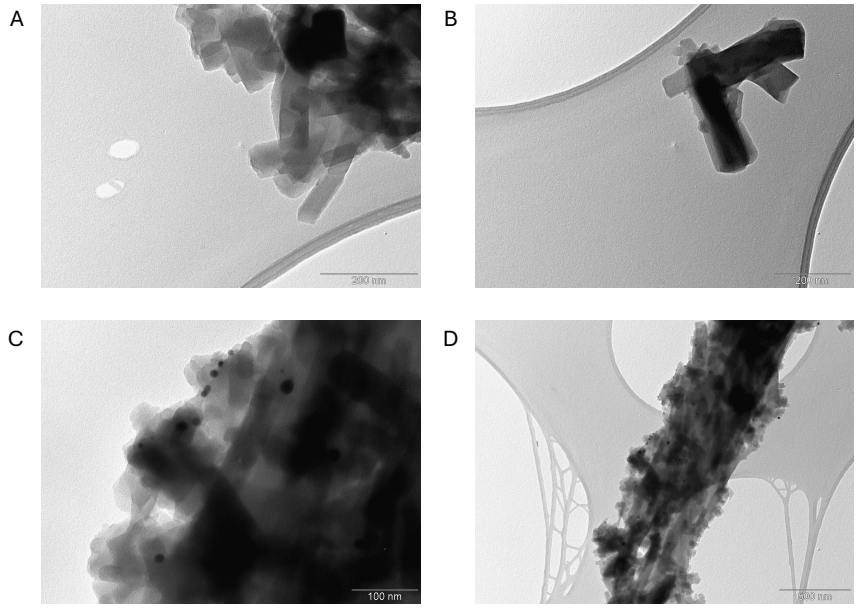

Figure A.58. TEM images of A,B) Tfpy-PDA-S and C,D) Au-Tfpy-PDA-S.

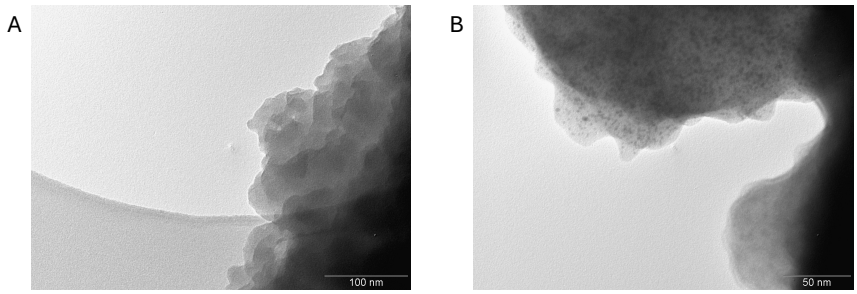

Figure A.59. TEM images of A) TTT-TAPB and B) Au-TTT-TAPB.

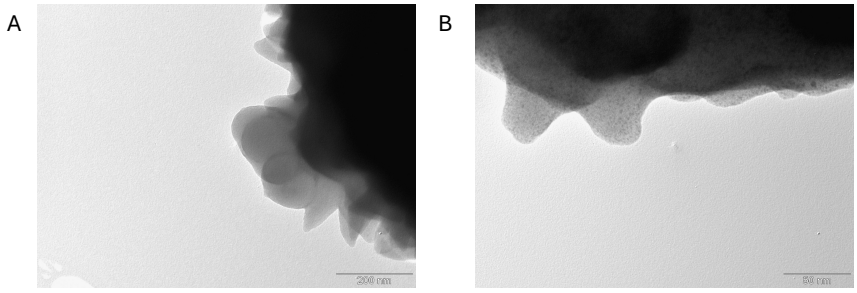

Figure A.60. TEM images of A) TTT-TAPB-S and B) Au-TTT-TAPB-S.

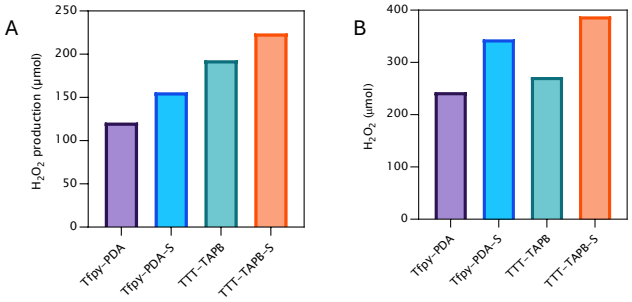

Figure A.61. A) H_2O_2 production amount under dark conditions after one hour (under Ar atmosphere), B) Photocatalytic H_2O_2 production of each COF in water under light irradiation (under Ar atmosphere).

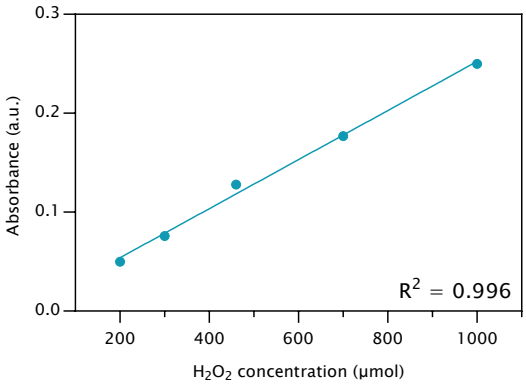

Figure A.62. Calibration curve of the UV-Vis measurements for H_2O_2 production.

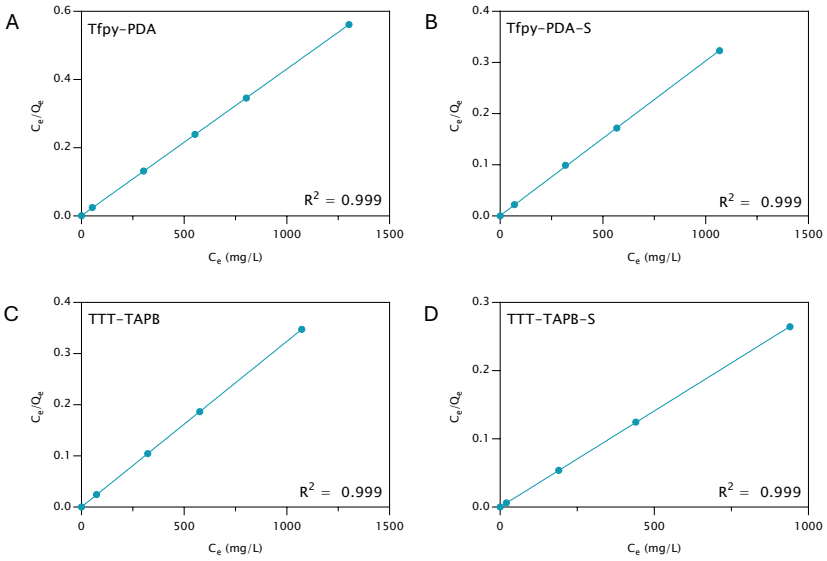

Figure A.63. Langmuir adsorption isotherm fitting curves for A) Tfpy-PDA, B) Tfpy-PDA-S, C) TTT-TAPB, D) TTT-TAPB-S.

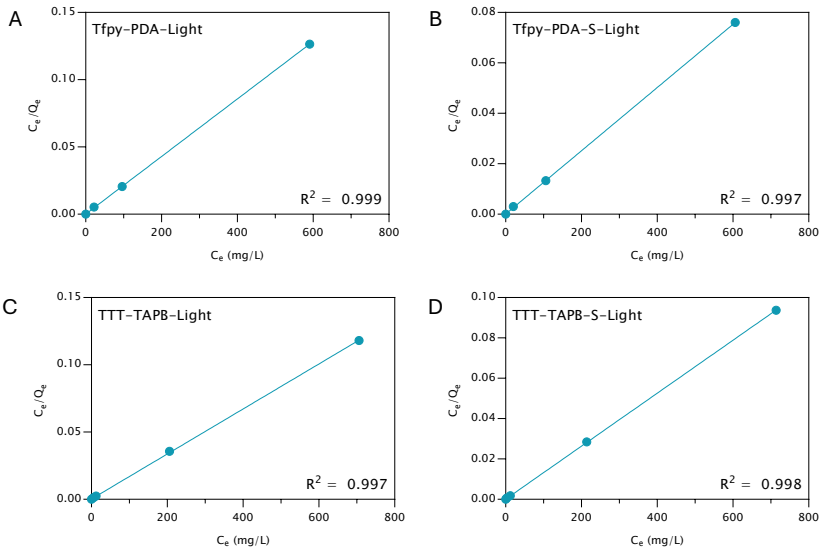

Figure A.64. Langmuir adsorption fitting curves for A) Tfpy-PDA, B) Tfpy-PDA-S, C) TTT-TAPB, D) TTT-TAPB-S under light irradiation.

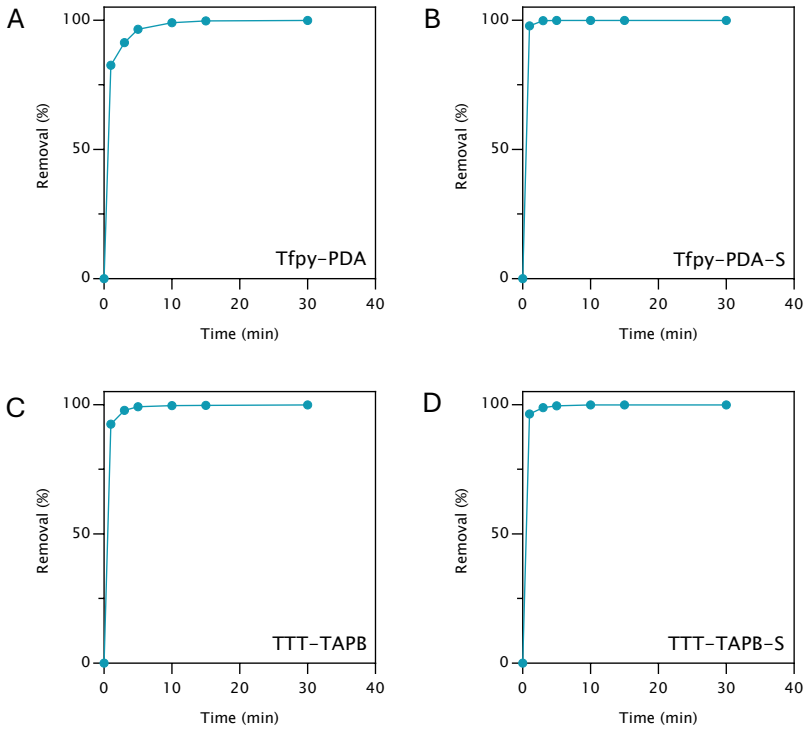

Figure A.65. Removal of 100 ppm of Au(III) in function of time on A) Tfpy-PDA, B) Tfpy-PDA-S, C) TTT-TAPB, D) TTT-TAPB-S.

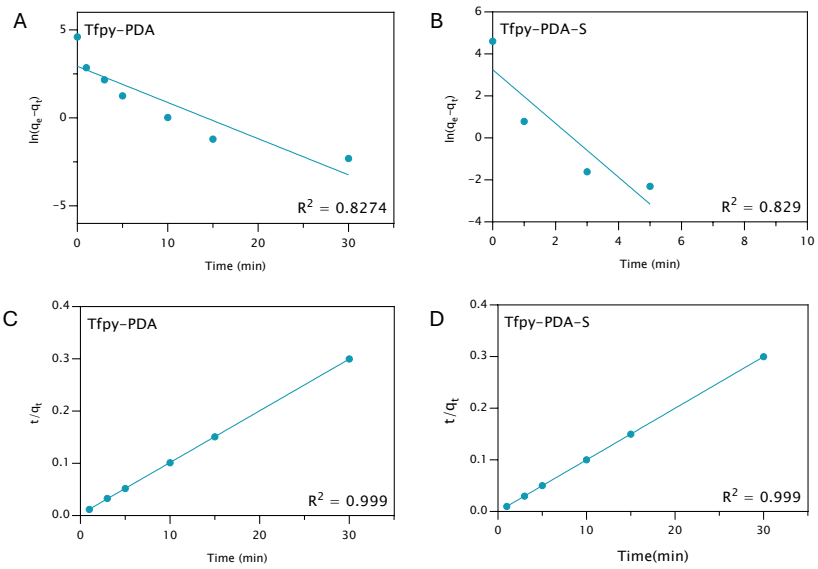

Figure A.66. Kinetic modelling of Au(III) adsorption with pseudo-first order model for A) Tfpy-PDA , B) Tfpy-PDA-S and pseudo-second-order model for C) Tfpy-PDA, D) Tfpy-PDA-S.

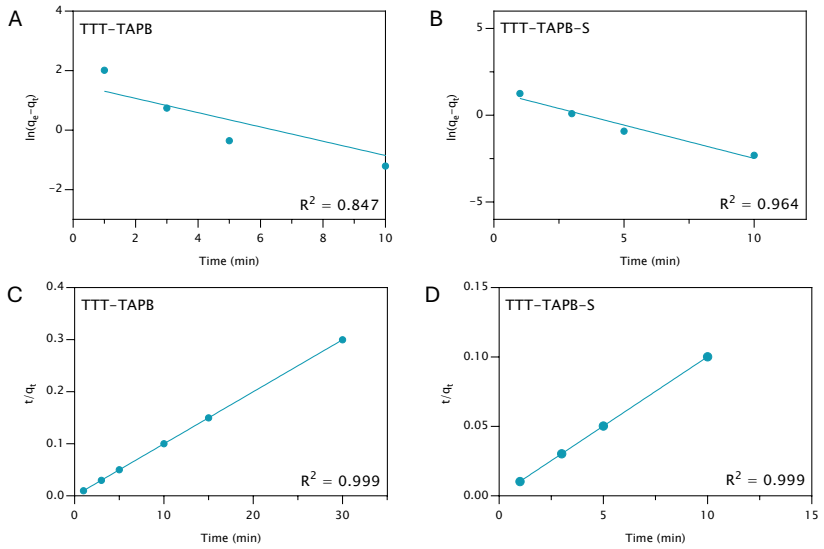

Figure A.67. Kinetic modelling of Au(III) adsorption with pseudo-first-order of A) TTT-TAPB, B) TTT-TAPB-S and pseudo-second-order of C) TTT-TAPB and D) TTT-TAPB-S.

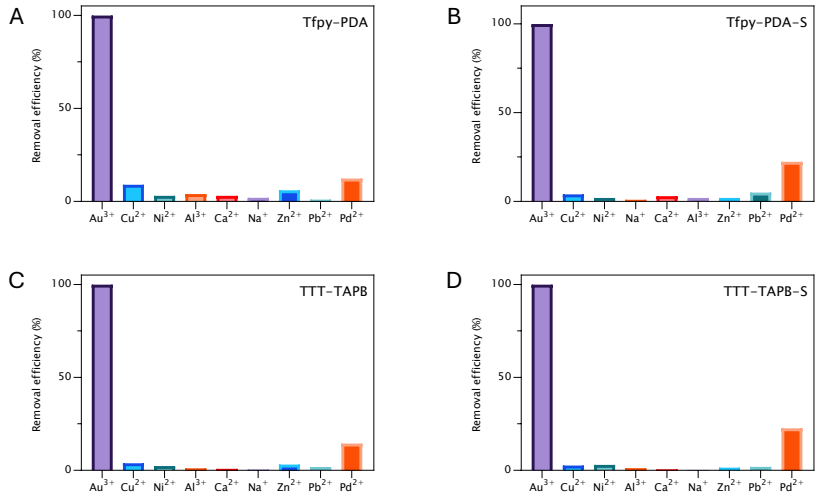

Figure A.68. : Selectivity test by assessing the removal efficiency of different competing ions at 100 ppm and gold(III) ions at 10 ppm onto A) Tfpy-PDA, B) Tfpy-PDA-S, C) TTT-TAPB, D) TTT-TAPB-S.

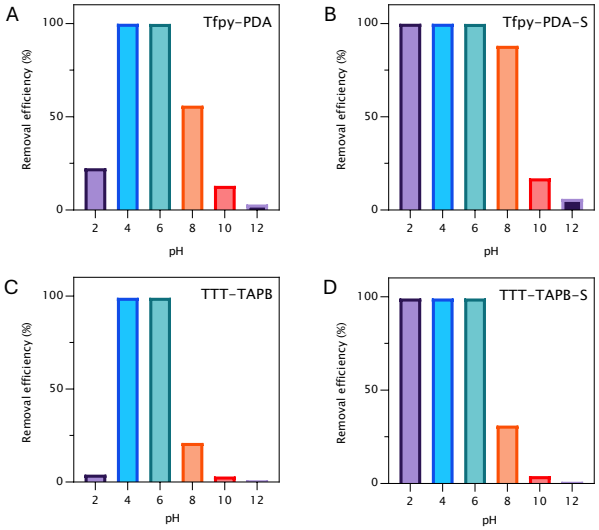

Figure A.69. Removal efficiency in function of pH in a 100 ppm Au(III) solution on A) Tfpy-PDA, B) Tfpy-PDA-S, C) TTT-TAPB , D) TTT-TAPB-S.

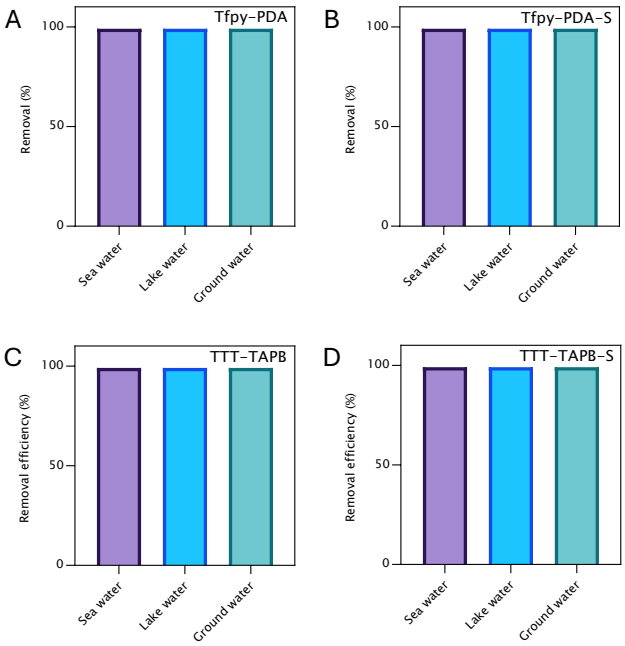

Figure A.70. Removal of 10 ppm Au(III) in different water matrices spiked with 100 ppm of Cu(II) and Ni(II) on A) Tfpy-PDA, B) Tfpy-PDA-S, C) TTT-TAPB, D) TTT-TAPB-S.

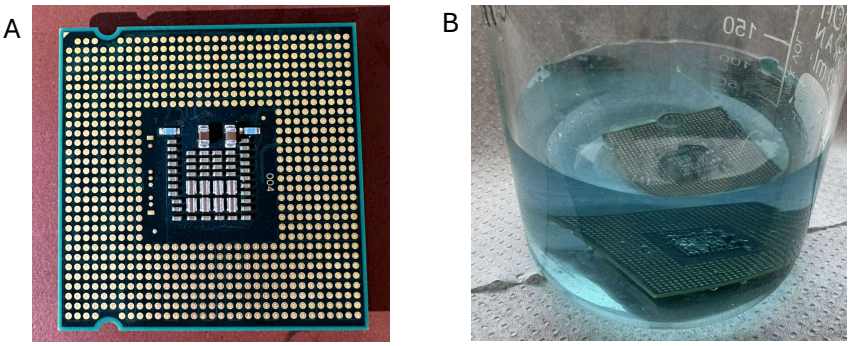

Figure A.71. A) Intel CPU processor, B) Leachate solution of CPU consisting of diluted aqua regia (pH= 4).

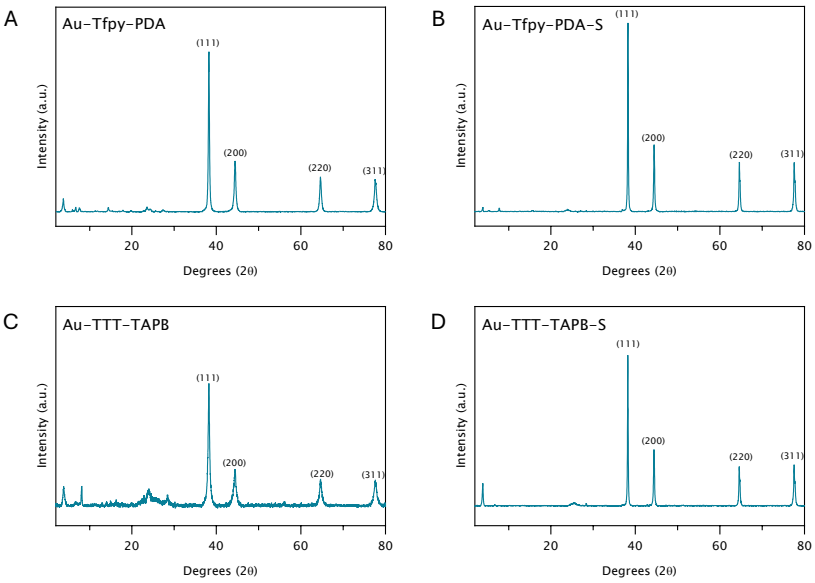

Figure A.72. PXRD after gold adsorption of A) Au-Tfpy-PDA, B) Au-Tfpy-PDA-S, C) Au-TTT-TAPB, D) Au-TTT-TAPB-S.

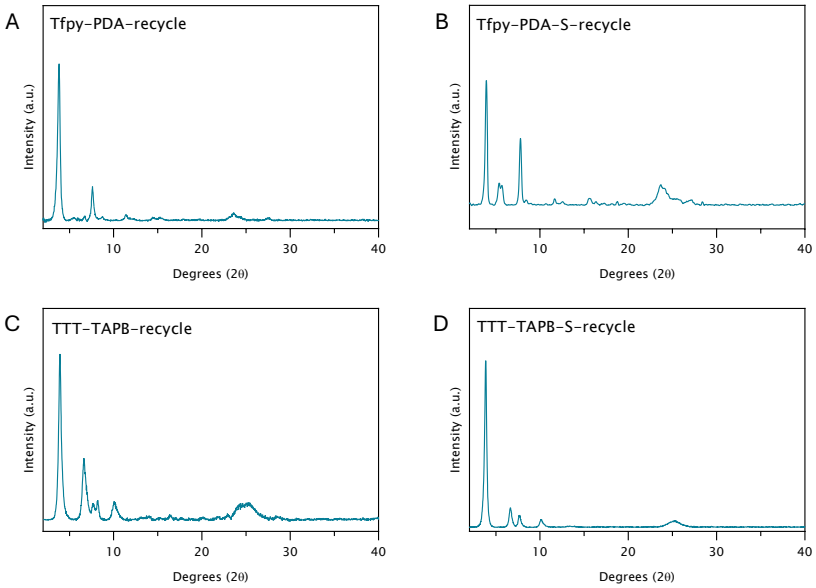

Figure A.73. PXRD of the recycled COFs after the first adsorption/recycle run with a 100 mg/L solution $AuCl_4^-$: A) Tfpy-PDA, B) Tfpy-PDA-S, C) TTT-TAPB, D) TTT-TAPB-S.

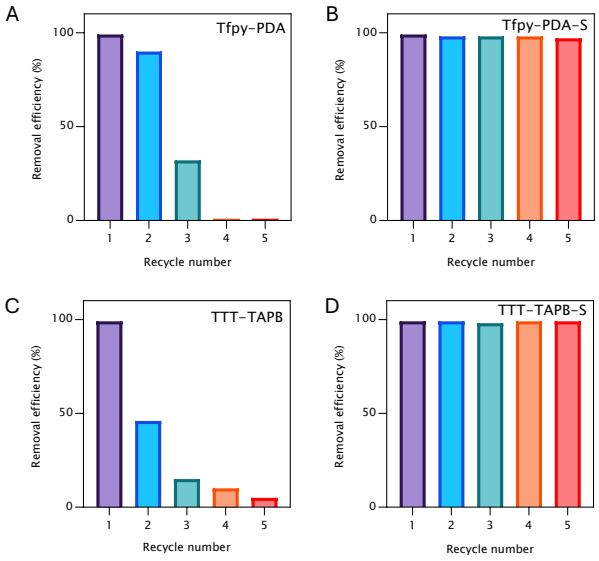

Figure A.74. Removal efficiency of 100 ppm $AuCl_4^-$ in function of recycle numbers with light irradiation of A) Tfpy-PDA, B) Tfpy-PDA-S, C) TTT-TAPB, D) TTT-TAPB-S.

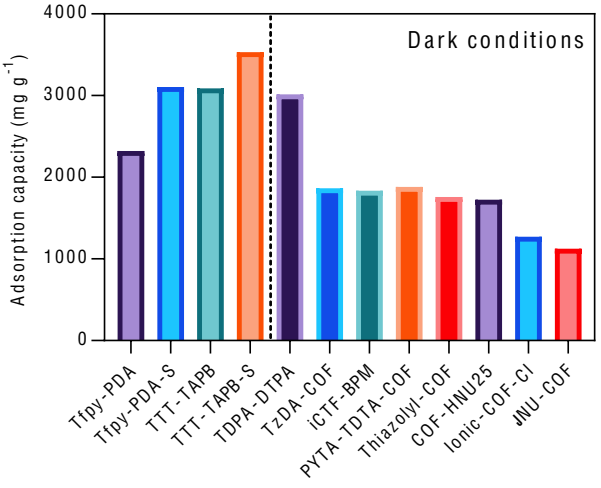

Figure A.75. Literature comparison of adsorption capacity onto COFs.

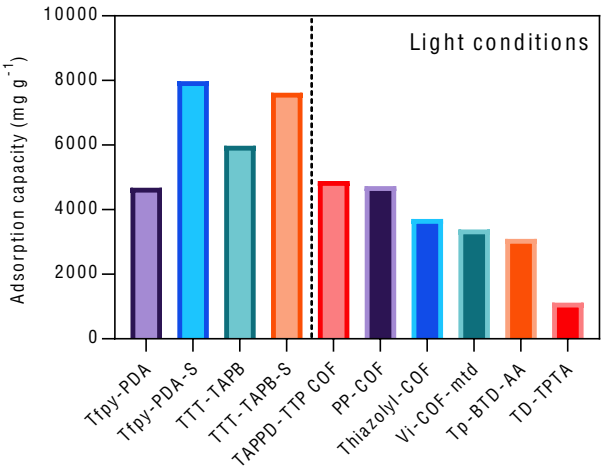

Figure A.76. Literature comparison of adsorption capacity onto COFs under light irradiation.

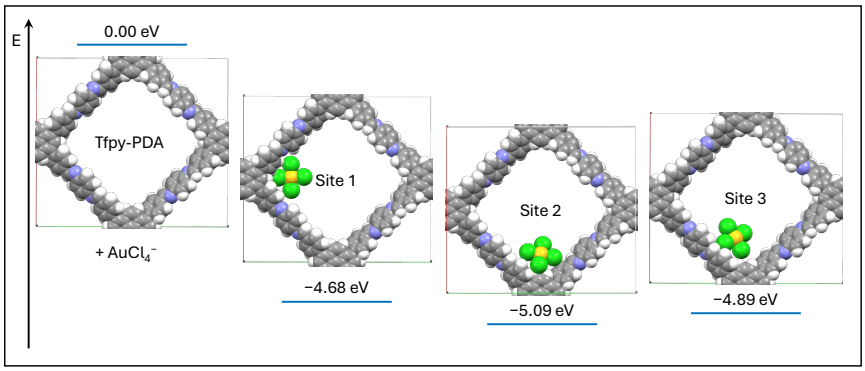

Figure A.77. Binding energies between $AuCl_4^-$ and Tfpy-PDA COF.

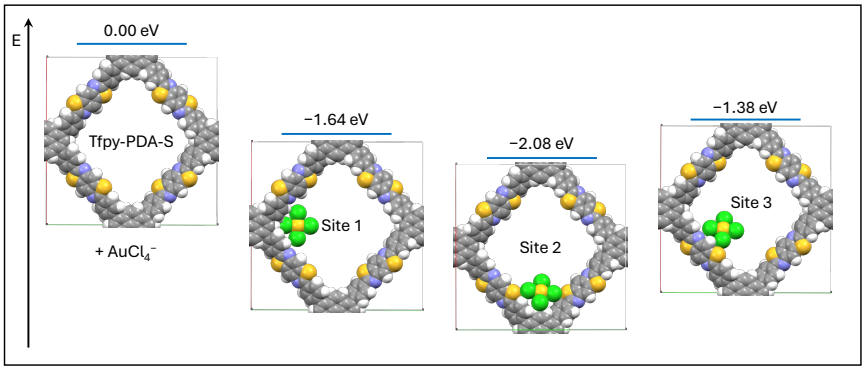

Figure A.78. Binding energies between $AuCl_4^-$ and Tfpy-PDA-S COF.

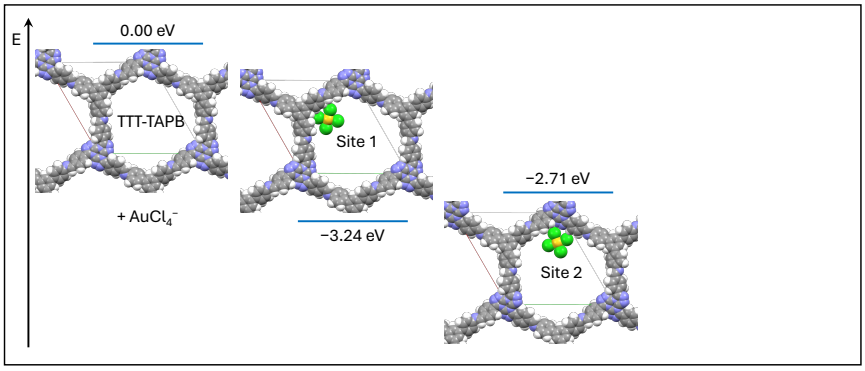

Figure A.79. Binding energies between $AuCl_4^-$ and TTT-TAPB COF

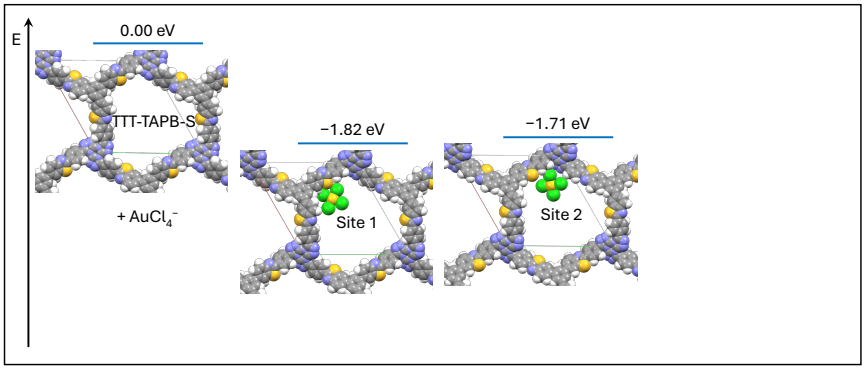

Figure A.80. Binding energies between $AuCl_4^-$ and TTT-TAPB-S COF.

A.4 Scientific Publications

- Laemont, A., Matthys, G., Lavendomme, R. & Van Der Voort, P. Mild and Scalable Conditions for the Solvothermal Synthesis of Imine-Linked Covalent Organic Frameworks. *Angewandte Chemie - International Edition* (2024)
- Matthys, G., Laemont, A., De Geyter, N., Morent, R., Lavendomme, R. & Van Der Voort, P. Robust Imidazopyridinium Covalent Organic Framework as Efficient Iodine Capturing Materials in Gaseous and Aqueous Environment. *Small*, 2404994 (2024).
- Matthys, G., Laemont, A., Bourda, L., Van Hamme, D., Wang, R., Mohamed, A. W., Leus, K., De Geyter, N., Morent, R., Lavendomme, R. & Van Der Voort, P. Thiazole-Linked Covalent Organic Frameworks for Enhanced Photoreductive Gold Recovery from E-Waste. *Submitted to Green Chemistry* (2025).